Fall 2019

Enhanced Heat Transfer in Spray Cooling Through Surface Modifications: An Experimental and Computational Study

Azzam Saadi Salman

ENHANCED HEAT TRANSFER IN SPRAY COOLING THROUGH SURFACE MODIFICATIONS: AN EXPERIMENTAL AND COMPUTATIONAL STUDY

By

Azzam Saadi Salman

Bachelor of Science
Mosul University, 2006

Master of Science
Mosul University, 2009

Submitted in Partial Fulfillment of the Requirements

For the Degree of Doctor of Philosophy in

Mechanical Engineering

College of Engineering and Computing

University of South Carolina

2019

Accepted by:

Jamil A. Khan, Major Professor

Chen Li, Committee Member

Tanvir I. Farouk, Committee Member

Jasim Imran, Committee Member

Titan C. Paul, Committee Member

Cheryl L. Addy, Vice Provost and Dean of the Graduate School

DEDICATION

This dissertation is dedicated to the memory of my beloved father Engineer. Saadi Salman. Even though he passed away before I started my graduate studies, he still is the force behind my success.

ACKNOWLEDGMENT

First and foremost, I would like to express my sincere appreciation and deepest gratitude to my advisor, Dr. Jamil Khan, for his inspiration, encouragement, and outstanding mentorship throughout all phases of my Ph.D. study. It has been a great opportunity and honor for me to work with him. Also, I would like to acknowledge Dr. Chen Li, Dr. Tanvir I. Farouk, Dr. Jasim Imran, and Dr. Titan C. Paul for serving as my committee members and for their invaluable comments and suggestions.

I would like to extend my sincere gratitude to all my beloved family members, especially my mother, brothers (Mohanad, Layth, and Mahmood), and sister and her family. Also, to my wife and sons (Yaman and Banan) without their love, encouragement, and support, I could not have completed this journey. Additionally, I would like to thank my wife's father, mother, and sisters, as well as my uncles, aunts, and all relatives for their encouragement.

Especial thanks to my Enhanced Heat Transfer Lab colleagues, Dr. Noble Anumbe, Mr. Ahmed Musafi Abir, Dr. Saad K. Oudah, Dr. Nabeel M. Abdulrazzaq, Mr. Amitav Tikadar, Dr. Abdulwahab Alhashem, and Mrs. Sowmya Raghu, for their help, support, and friendship. Also, I would like to thank Mr. Bill Bradley and Mr. David Westbury for their technical assistance.

Finally, I would like to acknowledge the Higher Committee for Education Development in Iraq (HCED) for offering me a fully funded scholarship and for their continuous support.

ABSTRACT

Today, dissipating high heat flux safely is one of the greatest challenges for thermal engineers in thermal management systems, and it becomes a critical barrier to technological developments for many engineering applications. Due to technological advances and aggressive micro-miniaturization of electronic components, the surface area of most devices has shrunk while the computational power increased exponentially. Therefore, the amount of heat dissipated from surfaces has increased significantly. Numerous cooling techniques have been introduced to replace the traditional air cooling systems and to maintain the efficiency and reliability of electronic components. Microelectronics work efficiently and safely at surface temperatures of < 100 ℃ and 125 ℃ for general and defense applications, respectively. One of the proposed alternative schemes is spray cooling, which is considered one of the most advanced cooling methods. It is used for high and ultra-high heat flux dissipation, as it can dissipate 150-200 W/cm^2 while maintaining the surface temperature within this range. Also, spray cooling removes a large amount of energy at a lower liquid flow rate compared to other cooling techniques, such as jet impingement and microchannel heat sink. The thermal performance of spray cooling systems can be enhanced either actively or passively. Active enhancement is a very efficient technique; however, it adds more pumping power. The present work focuses on three main objectives: evaluating and analyzing spray cooling performance, developing a three-dimensional numerical multi-phase model for heat transfer process in spray cooling and enhancing the thermal performance of spray cooling passively.

First, to evaluate and analyze the spray cooling performance of a flat surface, an experimental investigation was conducted in a closed-loop spray cooling system, utilizing deionized water as a cooling medium. A flat copper surface with a diameter of 15 mm was tested at volumetric flow rates that ranged 115 - 180 mL/min, a nozzle-to-surface distance of 8-12 mm, coolant inlet temperature, surface temperature, and chamber pressure, $\sim 22℃$, $< 100℃$, and atmospheric pressure, respectively. However, the results showed that increasing volumetric flow rate enhances the thermal performance of the spray cooling system at all nozzle-to surface distances, but at the same time increases the required pumping power. Therefore, a new criterion, " Performance Evaluation Criterion of Spray Cooling" (PEC_{SC}), was introduced to evaluate the spray cooling performance precisely, based on the combination of the amount of heat removed and the corresponding pumping power consumed. Using this criterion showed that increasing the nozzle differential pressure minimizes the overall spray cooling performance, and the maximum PEC_{SC} was 2022, which was achieved at a volumetric flow rate and nozzle-to-surface distance of 115 mL/min and 10 mm, respectively. Moreover, enhancing the thermal performance of a spray cooling system by increasing nozzle differential pressure is not an economical enhancement option.

Second, a three-dimensional multi-phase numerical model was developed to simulate the heat transfer process and understand the underlying physics in the spray cooling system. STAR-CCM+, 12.04.010-R8 was utilized as a computational fluid dynamics solver. A Lagrangian-Eulerian and Eulerian - Eulerian modeling approaches were adopted to simulate the fluid flow and heat transfer in spray cooling. The predicted and experimental heat transfer coefficients were compared at same operating conditions.

The comparison showed a satisfactory agreement; the maximum absolute deviation was $< 15\%$. The results illustrated that spraying parameters, such as volumetric flow rate, nozzle-to-surface distance, and surface temperature have a significant effect on liquid film characteristics, such as spatial heat transfer coefficient, liquid film thickness, and liquid film velocity. Results showed that the heat transfer coefficient in the spray impingement zone is highly affected by the volumetric flow rate and nozzle-to-surface distance, compared to the film zone. Also, more insights are provided about the heat flow mechanisms that are involved on the target surface. The volumetric flow rate has a dominant effect on the spatial distribution of heat transfer coefficient, liquid film thickness, and surface temperature. Moreover, decreasing the distance between the nozzle and the target surface increases the heat transfer coefficient in the spray impingement zone meaningfully.

Third, inorder to focus on enhancing the spray cooling system passively, the target surface was modified geometrically to increase the surface contact area and change the flow pattern on the surface. Geometrical surface modification is one of the most stable and durable among other enhancement methods. Three surfaces were modified with circular and radial grooves and examined at different operating conditions. The first surface M1 was modified with four circular grooves, each having 0.5 mm width, 0.5 mm depth with 1.5 mm pitch, to increase the surface contact area and the turbulence on the surface. The data analysis of (M1) showed that it had good thermal performance at a high volumetric flow rate but had low thermal performance at a low nozzle differential pressure. At low volumetric flow rate, the water replacement rate is low, and some of the water stagnates in channels and consequently increases the thermal resistance and negatively affects the heat

transfer process. In other words, the performance of this surface depends on the pumping power, because the water replacement rate increases with increasing the nozzle differential pressure. Therefore, the second surface (M2) was modified with four radial grooves having widths and heights of 0.5 mm, in addition to the circular grooves, to increase the water replacement rate. The results showed that M2 had better heat transfer performance than M1 due to the decrease in water thermal resistance and the activation of the radial momentum. This means radial flow has a significant effect on the spray cooling heat transfer performance. For further passive heat transfer enhancement, a third surface (M3) was modified with eight radial grooves in addition to the four circular grooves to take advantage of the flow in the radial direction, by increasing the wet surface area and accelarating the drainage rate. The results indicated that M3 had the highest heat transfer performance when compared to the other surfaces, at both low and high volumetric flow rates. The experimental results demonstrated that volumetric flow rate has a significant effect on the spray cooling thermal performance for all surfaces; thus, increasing the volumetric flow rate enhances the thermal performance of enhanced surfaces with different enhancement ratios. The effect of nozzle-to-surface distance depends mainly on both surface geometry, volumetric flow rate, and surface temperature. Furthermore, M3 has the highest heat transfer enhancement ratio at all operating conditions, followed by M2 and M1, where the maximum heat transfer enhancements were 80%, 36.3%, and 28.7%, respectively. Thus, using surfaces modified with a combination of circular and radial grooves can enhance spray cooling heat transfer performance significantly. Moreover, M3 has better thermal performance than a surface modified with only straight grooves by 34% at the same operating conditions.

TABLE OF CONTENTS

DEDICATION iii

ACKNOWLEDGMENT iv

ABSTRACT v

LIST OF TABLES xii

LIST OF FIGURES xiii

LIST OF SYMBOLS xix

CHAPTER 1 INTRODUCTION 1

1.1 MOTIVATION 1

1.2 BACKGROUND 3

1.3 RESEARCH OBJECTIVES 5

CHAPTER 2 REVIEW OF PREVIOUS WORK 9

2.1 EXPERIMENTAL PARAMETRIC STUDIES 9

2.2 NUMERICAL PARAMETRIC STUDIES 14

2.3 PASSIVE HEAT TRANSFER ENHANCEMENT TECHNIQUES 15

2.4 SUMMARY OF PREVIOUS WORK 22

CHAPTER 3 THEORETICAL BACKGROUND OF SPRAY COOLING AND HEAT TRANSFER MECHANISMS 24

3.1 SPRAY COOLING MECHANISM 24

3.2 Droplet interaction with a solid surface 28
3.3 Heat transfer mechanisms in spray cooling 31
CHAPTER 4 EXPERIMENTAL FACILITY AND METHODOLOGY 35
4.1 Experimental facility 35
4.2 Test parameters and procedure 44
4.3 Data reduction 46
4.4 Uncertainty Analysis 47
4.5 Experimental setup validation 48
CHAPTER 5 EVALUATION OF SPRAY COOLING PERFORMANCE 50
5.1 the influence OF VOLUMETRIC flow rate 50
5.2 the influence of Nozzle-to-surface distance 57
5.3 Performance evaluation criterion of spray cooling 63
5.4 Summary 65
CHAPTER 6 NUMERICAL MODELING OF SPRAY COOLING 67
6.1 Numerical methods and computational domain 67
6.2 Governing equations 68
6.3 Boundary and Initial Conditions 71
6.4 Numerical solving procedure and convergence criteria 73
6.5 Grid generation and grid independence test. 74
6.6 Numerical model validation 76
6.7 influence of Volumetric flow rate 78
6.8 influence of Nozzle-to-surface distance 83

6.9 INFLUENCE OF SURFACE TEMPERATURE 92

6.10 SUMMARY 97

CHAPTER 7 IMPACTS OF GEOMETRICAL SURFACE MODIFICATION ON HEAT TRANSFER ENHANCEMENT 98

7.1 GEOMETRICAL SURFACE MODIFICATIONS 98

7.2 EFFECT OF VOLUMETRIC FLOW RATE 100

7.3 EFFECT OF NOZZLE-TO-SURFACE DISTANCE 107

7.4 ENHANCEMENT RATIO 120

7.5 SUMMARY 128

CHAPTER 8 CONCLUSIONS, CONTRIBUTIONS, AND FUTURE WORK 129

8.1 CONCLUSIONS 129

8.2 CONTRIBUTIONS TO THE STATE OF THE ART 130

8.3 SUGGESTIONS FOR FUTURE WORK 132

REFERENCES 133

LIST OF TABLES

Table 6.1 Dimensions of the computational domain. 68

Table 6.2 Experimental operating conditions used to validate the numerical model. 72

Table 6.3 Comparison between experimental and numerical average heat transfer coefficients. 78

Table 7.1 Summary of the geometrical parameters of enhanced surfaces. 100

Table 7.2 Average enhancement ratios of modified surfaces at different operating conditions. 126

LIST OF FIGURES

Figure 1.1 Schematic of a UniJet full cone nozzle [18]. 4

Figure 3.1 Droplets break-up physics [15]. 25

Figure 3.2 Schematic of forces acting on a single droplet. 26

Figure 3.3 Schematic of a droplet behavior on a solid surface [60]. 29

Figure 3.4 Diagram of droplet behavior on a surface [61]. 30

Figure 3.5 Schematic of nucleate boiling process on a solid surface[66]. 33

Figure 3.6 Schematic of secondary nucleate boiling [66]. 34

Figure 4.1 Schematic diagram of the experimental setup. 36

Figure 4.2 Actual picture of the experimental facility. 37

Figure 4.3 Schematic of the spray chamber 39

Figure 4.4 CAD view of the heater assembly. 40

Figure 4.5 CAD view of the thermocouple positions (all dimensions in mm). 40

Figure 4.6 Screenshot of the LabVIEW for monitoring and recording data. 41

Figure 4.7 Flow meter calibration. 43

Figure 4.8 Thermocouples calibration. 43

Figure 4.9 Steady state level of surface temperature. 45

Figure 4.10 Steady state level of nozzle differential pressure. 45

Figure 4.11 Steady state level of volumetric flow rate. 46

Figure 4.12 Comparison of the experimental results with Oliphant et. al [72]. 49

Figure 4.13 Comparison of the experimental results with Rybiki and Mudawar [21]. ... 49

Figure 5.1 Effect of volumetric flow rate on heat flux at nozzle-to-surface distance of 10 mm. 51

Figure 5.2 Effect of volumetric flow rate on average heat transfer coefficient at nozzle-to-surface distance of 10 mm. 51

Figure 5.3 Nozzle differential pressure versus volumetric flow rate. 53

Figure 5.4 Flow visualization at volumetric flow rates. 53

Figure 5.5 Effect of volumetric flow rate on droplet flux (N), Sauter mean diameter (SMD), and break-up velocity (v). 54

Figure 5.6 Relation between forces acting on a droplet before impacting the target surface at different volumetric flow rates. 55

Figure 5.7 Effect of chamber temperature on droplet diameter. 56

Figure 5.8 Effect of chamber temperature on droplet break-up velocity. 56

Figure 5.9 Schematic of spraying over a surface. 57

Figure 5.10 Effect of nozzle-to-surface distance on heat flux at a volumetric flow rate of 115 mL/min. 58

Figure 5.11 Effect of nozzle-to-surface distance on average heat transfer coefficient at a volumetric flow rate of 115 mL/min. 59

Figure 5.12 Effect of nozzle-to-surface distance on heat flux at a volumetric flow rate of 153 mL/min. 60

Figure 5.13 Effect of nozzle-to-surface distance on average heat transfer coefficient at a volumetric flow rate of 153 mL/min. 60

Figure 5.14 Effect of nozzle-to-surface distance on heat flux at a volumetric flow rate of 180 mL/min. 61

Figure 5.15 Effect of nozzle-to-surface distance on average heat transfer coefficient at a volumetric flow rate of 180 mL/min. 61

Figure 5.16 Local droplet velocity at volumetric flow rates. 62

Figure 5.17 Performance evaluation criterion of spray cooling at different volumetric flow rates and a nozzle-to-surface distance of 8 mm. 64

Figure 5.18 Performance evaluation criterion of spray cooling at different volumetric flow rates and a nozzle-to-surface distance of 10 mm. 64

Figure 5.19 Performance evaluation criterion of spray cooling at different volumetric flow rates and a nozzle-to-surface distance of 12 mm. 65

Figure 6.1 3D CAD view of the computational domain. 68

Figure 6.2 Computational boundary conditions..... 71

Figure 6.3 Views of meshes of the computational domain..... 75

Figure 6.4 Average heat transfer coefficient for three different mesh sizes; 90k, 180k, and 360k..... 76

Figure 6.5 Three-dimensional simulation of spray-liquid film formation. 77

Figure 6.6 Average transient heat transfer coefficient. 77

Figure 6.7 Spatial heat transfer coefficient at different volumetric flow rates and a nozzle-to-surface distance of 10 mm. 80

Figure 6.8 Spatial liquid film thickness at different volumetric flow rates and a nozzle-to-surface distance of 10 mm. 81

Figure 6.9 Velocity vector and magnitude at different volumetric flow rates and a nozzle-to-surface distance of 10 mm. 82

Figure 6.10 Velocity flow field of spray at a volumetric flow rate and nozzle-to-surface distance of 115 mL/min and 10 mm. 83

Figure 6.11 Spatial heat transfer coefficient at different nozzle-to-surface distances and a volumetric flow rate of 115 mL/min. 85

Figure 6.12 Spatial heat transfer coefficient at different nozzle-to-surface distances and a volumetric flow rate of 153 mL/min. 86

Figure 6.13 Spatial heat transfer coefficient at different nozzle-to-surface distances and a volumetric flow rate of 180 mL/min. 87

Figure 6.14 Spatial distribution of liquid film at different nozzle-to-surface distances and a volumetric flow rate of 115 mL/min. 88

Figure 6.15 Spatial distribution of liquid film at different nozzle-to-surface distances and a volumetric flow rate of 153 mL/min. 89

Figure 6.16 Spatial distribution of liquid film at different nozzle-to-surface distances and a volumetric flow rate of 180 mL/min. 90

Figure 6.17 Average surface temperature at different nozzle-to-surface distances and a volumetric flow rate 115 mL/min. 91

Figure 6.18 Average surface temperature at different nozzle-to-surface distances and a volumetric flow rate 153 mL/min. 91

Figure 6.19 Average surface temperature at different nozzle-to-surface distances and a volumetric flow rate 180 mL/min. 92

Figure 6.20 Influence of surface temperature on average heat transfer at a volumetric flow rate of 153 mL/min, and nozzle-to-surface distance of 10 mm. 93

Figure 6.21 Influence of surface temperature on average heat transfer coefficient at a volumetric flow rate of 153 mL/min, and nozzle-to-surface distance of 10 mm. 94

Figure 6.22 Spatial heat transfer coefficient at different surface temperatures, a nozzle-to-surface distance of 10 mm, and a volumetric flow rate of 153 mL/min. 95

Figure 6.23 Spatial liquid film thickness at different surface temperatures, a nozzle-to-surface distance of 10 mm, and a volumetric flow rate of 153 mL/min. 96

Figure 7.1 CAD view of the enhanced surfaces. 99

Figure 7.2 Heat flux curves at a volumetric flow rate of 115 mL/min. 101

Figure 7.3 Heat flux curves at a volumetric flow rate of 153 mL/min. 101

Figure 7.4 Heat flux curves at a volumetric flow rate of 180 mL/min. 102

Figure 7.5 Average heat transfer coefficient of enhanced surfaces at a volumetric flow rate of 115 mL/min. 105

Figure 7.6 Average heat transfer coefficient of enhanced surfaces at a volumetric flow rate of 153 mL/min. 106

Figure 7.7 Average heat transfer coefficient of enhanced surfaces at a volumetric flow rate of 180 mL/min. 106

Figure 7.8 Effect of nozzle-to-surface distance on the thermal performance of M1 at a volumetric flow rate of 115 mL/min. 108

Figure 7.9 Effect of nozzle-to-surface distance on the thermal performance of M1 at a volumetric flow rate of 153 mL/min. 109

Figure 7.10 Effect of nozzle-to-surface distance on the thermal performance of M1 at a volumetric flow rate of 180 mL/min. 109

Figure 7.11 Effect of nozzle-to-surface distance on the thermal performance of M2 at a volumetric flow rate of 115 mL/min. 110

Figure 7.12 Effect of nozzle-to-surface distance on the thermal performance of M2 at a volumetric flow rate of 153 mL/min. 111

Figure 7.13 Effect of nozzle-to-surface distance on the thermal performance of M2 at a volumetric flow rate of 180 mL/min. 111

Figure 7.14 Effect of nozzle-to-surface distance on the thermal performance of M3 at a volumetric flow rate of 115 mL/min. 112

Figure 7.15 Effect of nozzle-to-surface distance on the thermal performance of M3 at a volumetric flow rate of 153 mL/min. 113

Figure 7.16 Effect of nozzle-to-surface distance on the thermal performance of M3 at a volumetric flow rate of 180 mL/min. 113

Figure 7.17 Effect of nozzle-to-surface distance on average heat transfer coefficient of M1 at a volumetric flow rate of 115 mL/min. 114

Figure 7.18 Effect of nozzle-to-surface distance on average heat transfer coefficient of M1 at a volumetric flow rate of 153 mL/min. 115

Figure 7.19 Effect of nozzle-to-surface distance on average heat transfer coefficient of M1 at a volumetric flow rate of 180 mL/min. 115

Figure 7.20 Effect of nozzle-to-surface distance on average heat transfer coefficient of M2 at a volumetric flow rate of 115 mL/min. 116

Figure 7.21 Effect of nozzle-to-surface distance on average heat transfer coefficient of M2 at a volumetric flow rate of 153 mL/min. 117

Figure 7.22 Effect of nozzle-to-surface distance on average heat transfer coefficient of M2 at a volumetric flow rate of 180 mL/min. 117

Figure 7.23 Effect of nozzle-to-surface distance on average heat transfer coefficient of M3 at a volumetric flow rate of 115 mL/min. 118

Figure 7.24 Effect of nozzle-to-surface distance on average heat transfer coefficient of M3 at a volumetric flow rate of 153 mL/min. 118

Figure 7.25 Effect of nozzle-to-surface distance on average heat transfer coefficient of M3 at a volumetric flow rate of 180 mL/min. 119

Figure 7.26 Enhancement ratio versus temperature difference for surface M1 at a volumetric flow rate of 115 mL/min and different nozzle-to-surface distances. 121

Figure 7.27 Enhancement ratio versus temperature difference for surface M1 at a volumetric flow rate of 153 mL/min and different nozzle-to-surface distances. 121

Figure 7.28 Enhancement ratio versus temperature difference for surface M1 at a volumetric flow rate of 180 mL/min and different nozzle-to-surface distances..... 122

Figure 7.29 Enhancement ratio versus temperature difference for surface M2 at a volumetric flow rate of 115 mL/min and different nozzle-to-surface distances..... 123

Figure 7.30 Enhancement ratio versus temperature difference for surface M2 at a volumetric flow rate of 153 mL/min and different nozzle-to-surface distances..... 123

Figure 7.31 Enhancement ratio versus temperature difference for surface M2 at a volumetric flow rate of 180 mL/min and different nozzle-to-surface distances..... 124

Figure 7.32 Enhancement ratio versus temperature difference for surface M3 at a volumetric flow rate of 115 mL/min and different nozzle-to-surface distances..... 125

Figure 7.33 Enhancement ratio versus temperature difference for surface M3 at a volumetric flow rate of 153 mL/min and different nozzle-to-surface distances..... 125

Figure 7.34 Enhancement ratio versus temperature difference for surface M3 at a volumetric flow rate of 180 mL/min and different nozzle-to-surface distances..... 126

Figure 7.35 Comparison between the thermal performance of surface modified with a combination of circular and radial grooves (M3) and surface modified with only straight grooves (No.5). 127

LIST OF SYMBOLS

$\vec{a}$	Acceleration
A	Surface area
C_D	Drag coefficient
Cp	Specific heat
D	Surface diameter
d	Diameter
d_{32}	Sauter mean diameter
E_f	Film total energy
ER	Enhancement ratio
F_B	Buoyancy force
f_b	Body force
F_D	Drag force
g	Gravity
F_G	Gravity force
H	Nozzle-to-surface distance
h	Heat transfer coefficient
H_f	Total film enthalpy
h_f	Film thickness
HL	Heat loss

I	Current
k	Thermal conductivity
L	Normal distance between thermocouples
La	Laplace number
m	Mass
$\dot{m}$	Mass flow rate
$\dot{N}$	Droplet flux
Nu	Nusselt number
p	Pressure
PEC_{SC}	Performance evaluation criterion of spray cooling
Pr	Prandtl Number
Q	Heat flow
q''	Heat flux
Re	Reynolds number
S	Droplet path
S_h	Energy Sources
$S_{m,i}$	Mass source or since for species i
S_e	Energy source/sink term per unit film area
T	Temperature
t	Time
T_f	Viscous stress tensor within the film
u	Local droplet velocity
v	Velocity

V	Voltage
$\dot{V}$	Volumetric flow rate
We	Weber number
$Y_{i,f}$	Mass fraction of species i

Greek symbols:

Δ	Difference
μ	Dynamic viscosity
ρ	Density
σ	Surface tension
ϑ	Kinematic Viscosity
$\mu\Phi$	Heat dissipation
λ_eff	Effective heat conductivity

Subscripts:

a	Air
Ch	Channel
d	Droplet
d_{32}	Based on Sauter mean diameter
E	Effective
F	Fin
f	Fluid film
g	Grid

in	Inlet
L	Liquid
M	Modified
o	Orifice
out	Outlet
P	Plain

CHAPTER 1

INTRODUCTION

This dissertation was developed to evaluate and analyze the thermal performance of a flat surface in a spray cooling system at different operating conditions, as well as to develop a three-dimensional multi-phase numerical model to simulate the spray cooling heat transfer process in order to predict the thermo-hydraulic characteristics. Furthermore, this dissertation aims to enhance the overall thermal performance of spray cooling passively by modifying the target surface geometrically to increase the wetted surface area and change the flow pattern. The motivation, brief background, and the objectives of this work are discussed in this chapter.

1.1 MOTIVATION

The exponential growth of the nuclear industry, diode lasers, and electronic components have led to increased heat density [1]. Also, the rapid miniaturization and integration of electronic components used in industry have increased the power density sharply [2]. As such, dissipating large heat fluxes safely is considered one of the greatest challenges in thermal management. Moreover, achieving this process efficiently has become a crucial barrier to technology roadmaps and the main inhibitor of technological development for many engineering applications [3,4]. These developments have created a vital demand for efficient cooling schemes that are capable of fulfilling the desired thermal control requirements.

For instance, most microelectronics work efficiently at a surface temperature below 85 ℃ for general applications and below125℃ for defense applications [5, 6]. The performance, reliability, and lifetime of electronic devices depend highly upon its surface temperature. In order to meet the requirements of the electronic industry, many efficient cooling schemes have been introduced to thermal management systems to replace traditional air cooling systems which more efficient and compact cooling systems[7]. Although air cooling systems are the simplest and most affordable cooling method, they require a large surface area, and have a limited cooling capacity due to the poor thermo-physical properties of air [1, 8]. The maximum heat transfer coefficient of a standard air fan is 150 $W/m^2.K$; thus, it is appropriate for low how heat flux applications. In order to resolve this issue, thermal engineers have proposed liquid cooling techniques for thermal management systems as a sustainable and reliable solution in terms of cooling energy [7,8]. Liquid cooling schemes are recognized to be efficient coolers for high heat flux applications.

Generally, liquid cooling schemes are divided into two categories: direct and indirect cooling schemes. In the direct cooling techniques, the working fluid makes direct contact with the target surface. Typical examples include spray cooling, jet impingement, and pool boiling. In the indirect cooling techniques, the working fluid does not come in contact with the target surface. Examples include heat pipes, microchannels, and phase change materials [10]. Selecting a suitable cooling methodology has become a major challenge for thermal engineers because each cooling scheme has potential benefits and application limitations. For example, microchannels are compact and efficient cooling systems but have higher-pressure drop and temperature difference between the inlet and the outlet [11, 12].

Alternatively, jet impingements are very efficient cooling techniques for high-flux devices but have large spatial temperature gradients [13]. Spray cooling is one of the most efficient and advanced direct cooling techniques used for high and ultra-high heat flux dissipation, according to the heat dissipation categorization shown below [14]:

- High Heat Flux (HHF): 10^2 –10^3 W/cm^2.
- Ultra-High Heat Flux (UHF): 10^3-10^4 W/cm^2.
- Extreme Heat Flux (EHF): >10^4 W/cm^2.

Additionally, spray cooling provides many significant advantages, such as high heat transfer coefficients, high critical heat flux (CHF), and superior surface temperature uniformity. Furthermore, in the spray cooling scheme, a better temperature spatial uniformity and higher heat flux can be achieved with a lower working fluid consumption compared to other cooling techniques [15]. Spray cooling can dissipate 150–200 W/cm^2 while maintaining the surface temperature below 125℃. Therefore, it has been identified as a potential solution for thermal management [16].

Even though spray cooling is considered an efficient high heat flux removal scheme, it is still very complicated, and its physics and mechanisms are not well understood. The complexity of spray cooling systems results from the number of influential parameters on spray cooling thermal performance, in addition to the thermo-physical properties of the working fluid, which are an essential part of the spray cooling performance [12, 14,15].

1.2 BACKGROUND

Despite spray cooling being considered a very complicated cooling technique, it is still one of the most efficient and advanced techniques and is used for high and ultra-high heat flux dissipation. Spray cooling has been widely used in a variety of engineering

applications, such as “computers and data centers, X-ray medical devices, hybrid vehicle power electronics, heat exchangers for hydrogen storage, fusion reactor blankets, particle accelerator targets, magnetohydrodynamic (MHD) electrode walls, rocket nozzles, satellite and spacecraft electronics, laser and microwave directed energy weapons, advanced radars, turbine engines, air-fuel heat exchangers in high-Mach aircraft, and quenching of metal alloy parts”[19].

Generally, spraying systems are divided into two main types: pressure and atomized sprays, depending on the droplet formation method. In pressure sprays, droplets are formed by pumping liquid at high pressure through a small orifice, while in atomized sprays, droplets are generated with the aid of a high-pressure gas stream, like air or inert gas to break up the liquid into droplets [3]. In this study, a pressure spray was used to avoid the side effects of the aided gases on the heat transfer process. Also, the pressure spray nozzle is preferred for spray cooling because of its reliance on the momentum of the liquid alone to achieve the droplet breakup [20]. A UniJet full cone nozzle with a round impact area (TG0.3, Spraying Systems Co.) was used to generate uniform droplet distribution across the impact’s entire circle. Figure 1.1 shows a schematic of a UniJet full cone nozzle.

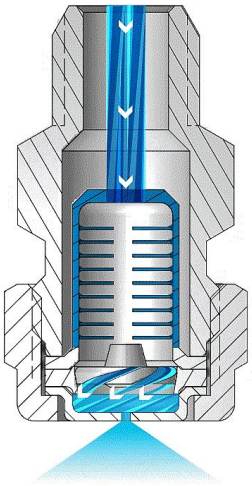

Figure 1.1 Schematic of a UniJet full cone nozzle [21].

When the generated droplets impact the heated surface with enough momentum, a thin liquid film forms on the surface. In general, several heat transfer mechanisms, such as convection, boiling, and evaporation, are involved in spray cooling systems. The existence of heat transfer mechanisms in the liquid film depends on the operating conditions, such as surface temperature and chamber pressure. The heat transfer mechanisms and droplet behavior on the surface will be discussed in detail in chapter 3.

1.3 RESEARCH OBJECTIVES

This work focuses on the fundamental mechanisms of spray cooling and on enhancing its thermal performance passively. The primary objectives of this work are as follows:

1. Evaluating and analyzing the overall spray cooling performance of a flat surface at different operating conditions, based on a criterion that takes into account the combined influence of removed heat and consumed pumping power. Also, analyzing the forces acting on a droplet before impacting the target surface at different droplet velocities and chamber temperatures.
2. Proposing a three-dimensional multi-phase numerical model to simulate the spray cooling heat transfer process in order to understand and provide more insight regarding the effect of spraying conditions on the liquid film thermo-hydraulic characteristics.
3. Enhancing the spray cooling thermal performance passively by modifying the surface geometrically and testing it under different conditions. Various types of surfaces modified with a combination of circular and radial grooves, these surfaces have not been studied before in spray cooling systems.

The objectives of this dissertation were met through systematic experimental and numerical investigations that examined the fundamentals and enhancements of heat transfer in spray cooling systems.

First, the experimental set-up was designed and built with a high level of accuracy to perform spray cooling heat transfer experiments at different operating conditions and to test different surfaces. The validation and reliability of the results were verified with published correlations, and the deviation between several repeated experiments was within the acceptable range. Several experiments were conducted on a plain surface at different operating conditions. In these experiments, the target surface was tested at volumetric flow rates of 115,153, and 180 mL/min, and nozzle-to-surface distances of 8, 10, and 12 mm. The coolant inlet temperature and chamber pressure were maintained at $\sim 22℃$, and at atmospheric pressure, respectively. In fact, one goal of this study was to evaluate the performance of a spray cooling system by using a criterion that combines the removed heat and the consumed pumping power. The effect of spraying parameters on overall spray cooling performance is analyzed and discussed in detail in chapter 5.

Second, a numerical three-dimensional multi-phase model was developed to simulate the heat transfer process in the spray cooling system. Simulation of the spray cooling heat transfer process was performed in a commercial computational fluid dynamics package (STAR-CCM+, 12.04.010-R8). When the predicted results were compared with experimental results, the comparison showed a good agreement between heat transfer coefficients; the maximum absolute deviation was $< 15\%$. The results of the numerical model illustrated that spraying parameters, such as volumetric flow rate, nozzle-to-surface distance, and surface temperature, have a significant effect on liquid film characteristics,

such as heat transfer coefficient, liquid film thickness, and liquid film velocity. It was shown that the heat transfer coefficient in the spray impingement zone is highly affected by volumetric flow rate and nozzle-to-surface distance when compared to the film zone. Also, the model provides more insights into the heat-flow mechanisms that are involved on the target surface. The volumetric flow rate has a significant effect on the spatial distribution of the heat transfer coefficient, liquid film thickness, and film velocity. Moreover, decreasing the distance between the nozzle and the target surface meaningfully increases the heat transfer coefficient in the spray impingement zone but decreases it in the film zone. The numerical results were compared with experimental data, and the characteristics of liquid film are discussed in detail in chapter 6.

Third, the thermal performance of the spray cooling system was enhanced passively by modifying the surface geometry. Since spray cooling is used in many diverse applications, geometrical surface modification is the most reliable and stable enhancement method compared to other enhancements, such as chemical coatings and nanofluids. Enhancing spray cooling performance by forming a chemical coating on the surface is complicated because of the mechanical and thermal stabilities of this layer. Generated droplets can have enough momentum to eventually degrade and remove the chemical coating. In addition, using nanofluids is not a good option for high-heat flux applications because nanoparticles may stick on the target surface and increase the thermal resistance between the target surface and the working fluid. Nanoparticles may partially block the nozzle's orifice and increase the required pumping power and ultimately cause the cooling process to fail.

Therefore, in this study, the target surface was modified geometrically with circular and radial grooves to increase the contact surface areas and the turbulence intensity on the surface. Enhanced surfaces were examined and compared with a plain surface at volumetric flow rates and nozzle-to-surface distances ranging from 115-180 mL/min, and 8-12 mm, respectively. The impact of geometrical surface modification at different operating conditions is discussed in detail in chapter 7.

CHAPTER 2

REVIEW OF PREVIOUS WORK

In order to understand the fundamentals of spray cooling systems and heat transfer enhancement approaches in these systems, a comprehensive survey of both experimental and numerical previous investigations was performed and will be discussed in detail. The review of literature is divided into three main sections, as explained in this chapter. The first section focuses on parametric experimental investigations, which have been conducted to determine the influential parameters on spray cooling heat transfer performance. The second section reviews the parametric numerical studies, which have been conducted to quantify the influence of operating parameters. The third section reviews the geometrical surface modifications, which have been performed to enhance the thermal performance of spray cooling systems passively. These sections are discussed in detail to provide the necessary background information:

2.1 EXPERIMENTAL PARAMETRIC STUDIES

Spray cooling has gained significant attention due to its capability of removing high heat flux at a relatively low volumetric flow rate, and it is used widely in numerous engineering fields. Therefore, many experimental and theoretical parametric investigations have been conducted to understand and improve the thermal performance of spray cooling systems. Many operating parameters, such as flow rate, nozzle height, spray angle, inlet pressure, chamber pressure, and inclination angle were studied to quantify their influence on the thermal performance of a plain surface in spray cooling systems.

For instance, Ghodbane and Holman [22] investigated the effects of mass flux, spray droplet velocity, droplet diameter, and nozzle to surface distance. The surfaces were tested at constant heat flux in a closed-loop spray cooling system utilizing Freon-113 as the working fluid. Full cone circular and hydraulic square nozzles were used to cool a vertical heated surface with a flow rate ranging from 50.47 to 126.18 $cm^3\ s^{-1}$. The distance between the nozzle and the heated surface was varied between 18.42, 27.3, and 34.92 cm, and the subcooled temperature ranged from 5 to 10℃. The results showed that heat transfer increases with increasing mass flux. Also, it was found that the Weber number has a strong effect on the overall heat transfer characteristics. Increasing the subcooling temperature delays the burnout phenomenon and the onset nucleate boiling. Mudawar et al. [15,21,22] studied the effects of Sauter mean diameter (SMD, d_{32}), upward and downward nozzle orientation, and volumetric flux of different working fluids, such as PF-5052, FC-72, and FC-87. The results showed that the orientation of the nozzle (downward or upward) has no impact on the thermal performance of spray cooling. Only volumetric flux and SMD had a substantial effect on spray cooling heat transfer performance. Also, Chen et al. [23,24] experimentally studied the effects of mean droplet size, droplet flux, and droplet velocity on critical heat flux (CHF) in a spray cooling system. The results showed that the mean droplet velocity (V) had the dominant effect on CHF and the heat transfer coefficient, followed by the mean droplet flux (N). Moreover, Sauter mean diameter (d_{32}) did not affect CHF. Increasing the droplet velocity increases both the CHF and the heat transfer coefficient. Additionally, Cheng et al. [27] experimentally studied the effects of the spray characteristics on the thermal performance of a spray cooling system, utilizing distilled water as a working fluid.

The influences of the spray flow rate, spray height, and coolant inlet temperature on spray cooling performance in the single-phase region was investigated to visualize and correlate the spray cooling characteristics under various operating conditions. The results demonstrated that the axial droplet velocity, Sauter mean diameter (SMD), and the droplet numbers density were greater in the main flow stream than in the other regions. Additionally, the heat transfer characteristics are enhanced by increasing the flow rate, reducing the nozzle height, and increasing the inlet working fluid temperature. Huai et al. [28] also investigated the influences of the volumetric flow rate, the nozzle height, and the coolant inlet temperature on the spray cooling heat transfer performance in the single-phase region. The experiments were conducted in an open-loop test system working with deionized water as a cooling medium. The results indicated that increasing the volumetric flow rate or reducing the coolant inlet temperature improves the heat transfer performance. In addition, adding surfactants to working fluid with an appropriate concentration enhances the heat transfer performance, which changes the thermos-physical properties of the cooling medium, such as density, viscosity, and surface tension.

Moreover, Xie et al. [29] used Particle Image Velocimetry (PVI) and Phase Doppler Interferometry (PDI) to examine the thermal effects on the spray cone formation of water, which plays a significant role in spray cooling heat transfer performance. The nozzle inlet pressure and the surface temperature were varied to study its influences on the spray cone formation and spray characteristics. The experimental results showed that the surface temperature had a significant effect on the spray cone formation, where the spray cone expands at high surface temperature, which changes the surface temperature uniformity and reduces the heat transfer coefficient.

Also, increasing the surface temperature increases the diameter of the droplets near the surface as well as secondary droplets, but decreases its velocity. Hou et al. [30] investigated the spray cooling characteristics of R134a under a series of different volumetric flow rates; the experiments were conducted in a vapor compression system. The results showed that increasing the volumetric flow rate enhances the critical heat flux because it maintains the surface wettability and delays the dry out phenomenon. The maximum achieved critical heat flux was 117.2 W/cm^2 at a surface temperature of 319 K and a volumetric flow rate of 0.356 L/min. Recently, Zhou et al. [31] experimentally studied the influences of the spraying parameters, such as spray height, heat flux, inlet pressure, and gravitational angle on spray cooling performance in order to find the most influential parameter. The results indicated that the mass flow rate was the main influential parameter on spray cooling performance, where increasing flow rate improves heat transfer characteristics. Also, it was found that the best heat transfer performance was when the gravitational angle was between 30° and 120°, whereas the worst was 180°. Gao and Li [32] experimentally, investigated the effects of nozzle height and inclination angle on the thermal performance of the spray cooling system. A full cone nozzle was used to generate droplets of water to cool the target surface. The results showed that the optimal spray height, which provides the best thermal performance, occurred at a nozzle-to-surface distance smaller than the height required for covering the entire heater area. Also, their results illustrate that the optimal height decreases as the spray flow rate increases. The inclination angle was varied while maintaining a constant impact length, which was equal to the target surface length; it was found that the effect of nozzle height is negligible at small inclination angles, while it has a significant impact at large inclination angle.

Salman and Khan [33] investigated the effect of spraying parameters on the thermal performance of a spray cooling system. The experiments were conducted in a closed-loop system, utilizing deionized water as a working fluid, under different nozzle inlet pressures and at a nozzle-to-surface of 10 mm. The results demonstrated that increasing the nozzle inlet pressure has the dominant effect on spray cooling thermal performance for both surfaces, resulting from the increase of the droplets momentum. Moreover, surface and chamber temperatures are had a negligible impact on droplets size and impact velocity because they do not affect forces exerted on a droplet. Another study was conducted by Salman et al. [34] to investigate the effects of the nozzle-to-surface distance on spray cooling performance, with distances ranging from 10 to 16 mm, and a mass flux of 15.5 $kg/s.m^2$. This study showed that decreasing the surface-to-nozzle distance improves the spray cooling thermal performance due to the change in the ratio of sprayed to liquid film areas, and as a result of the increase of Weber number and turbulence on the surface, especially within the liquid film.

In summary, previous studies showed that spray cooling is a complex system and not well understood because it is affected by many operating parameters, such as volumetric flow rate, droplet size, droplet flux, and nozzle-to-surface distance. Moreover, the results of most studies demonstrated that the coolant volumetric flow rate has the dominant influence on spray cooling heat transfer performance, and nozzle-to-surface distance has a slight effect on spray cooling thermal performance. Decreasing the distance between a nozzle and a heated surface enhances the heat transfer characteristics of a spray cooling system.

2.2 NUMERICAL PARAMETRIC STUDIES

Due to the complexity and the cost of spray cooling experiments, several numerical studies have been carried out to investigate the influential parameters that affect the spray cooling process. For example, a computational fluid dynamics investigation was performed by Yan et al. [35] to study the effect of nozzle-to-surface distance on heat transfer characteristics. The results illustrated that the wall temperature increases with increasing the nozzle-to-surface distance. Therefore, both the heat flux and heat transfer coefficient decrease as a sequence of the increase in the nozzle-to-surface distance. Also, the effects of mass flux, the number of nozzles, and nozzles-to-surface distance were investigated numerically by Hou et al. [36]. In this study different spray mass fluxes, as well as a different number of nozzles (4, 6, 8, and 10) were used, with nozzle heights of 1, 1.2, 1.4, 1.6, 1.8, and 2 cm. The results showed that the heat flux and heat transfer coefficient increase as the surface temperature and spray mass flux increase. Moreover, they found that increasing nozzle-to-surface distance increases the heat flux at first, but then causes it to decrease. Their results indicate that the optimal number of nozzles was 8, where as the number of nozzles increases, so does the heat flux.

Furthermore, a numerical investigation was conducted by Liu et al. [37] to study the effect of droplet diameter on spray cooling heat transfer characteristics in the single-phase region. The results showed that droplet size is an influential factor in spray cooling performance, especially at low heat flux. Also, smaller droplets form a thicker liquid film, increase the heat transfer coefficient, and reduce the wall temperature at the same heat flux. Another numerical study was carried out by Langari et al. [38] to determine the dominant factor in the spray cooling heat transfer process. Three different spray mass fluxes ranged

between 3.5 and 9.43 kg/m^{2}s, and were used to cool a surface has a diameter of 20 mm. The results showed that spray mass flux, not the droplet velocity, is the dominant factor on spray cooling heat transfer. Chen et al. [39] numerically investigated the effect of different parameters, such as spray pressures, different spray heights, different water temperatures, and different wall temperatures, on the thermal performance of a spray cooling system. The model was used to simulate the spraying process on a heated drum wall, using ANSYS Fluent package. The results showed that heat transfer is enhanced by increasing both wall temperature and spray pressure. Additionally, it is enhanced by reducing the coolant inlet temperature and the distance between the nozzle and the surface. Furthermore, it was found that wall temperature has the highest degree of influence among other parameters followed by spray pressure, water temperature, and spray height, respectively.

In summary, a few numerical investigations have been conducted to study the influence of spray cooling parameters due to the complexity and cost of spray cooling modeling. Therefore, the available results of numerical studies show that spray cooling thermal performance improves as the coolant's volumetric flow rate increases and as nozzle-to-surface distance decreases.

2.3 PASSIVE HEAT TRANSFER ENHANCEMENT TECHNIQUES

Even though active heat transfer enhancement is an efficient enhancing method, it requires additional pumping power, or in other words additional cost. Numerous studies have been conducted on geometrical surface modifications to improve the thermal performance of spray cooling passively. Passive heat transfer enhancement is achieved by enhancing the thermo-physical properties of the working fluid, forming a thin film of a chemical coating over the target surface, and modifying the target surface geometry. The

thermo-physical properties of a working fluid is enhanced by adding conductive particles or surfactants. Even though changing the thermal properties of a coolant improves the spray cooling thermal performance, it has application limitations because at high-temperature applications particles may stick on the target surface and represent an additional thermal resistance between the target surface and the coolant. Also, these particles may clog the nozzle's orifice partially and ultimately lead to failing the cooling process. Enhancing spray cooling performance by forming a chemical coating on the surface is complicated because of the mechanical and thermal stabilities of the formed chemical layer. In spray cooling systems, generated droplets have enough momentum to degrade the chemical coating and eventually remove it from the target surface. Therefore, enhancing the thermal performance of a spray cooling system through geometrical surface modifications is the most stable and durable both thermally and mechanically. Several experimental studies have been performed to improve the thermal performance of spray cooling systems by modifying the target surface with different geometries. For example, Silk et al. [40] experimentally studied the effects of surface modifications on the spray cooling heat transfer performance in a system working with P-5060 as a cooling medium. The surface modification consisted of adding cubic pin fins, pyramids, and straight fins on the top of the target surface, then the surface; then surfaces were cooled by 2×2 nozzle arrays. The results show that in the degassed case, the surface with straight fins had the largest enhancement in heat flux, and its critical heat flux (CHF) increased up to 55% in comparison to the plain surface under the same operating conditions; whereas, the cubic pin finned and pyramid surfaces had heat flux enhancement of 30% - 40% in comparison with the straight fins.

It was observed that in the gassy case, the straight fins provided the largest critical heat flux (CHF) enhancement of 48% followed by the cubic pin fins and pyramids, which had improvements of 31% and 18% respectively. Also, Silk et al. [41] did another study to investigate the impact of the cubic fins on the spray cooling heat transfer performance. The dimensions of the cubic fins height, width, and pitch were varied from 1 to 2 mm and these surfaces were cooled by 2×2 nozzle array working with PF-5060 as a coolant. The results showed that both the fin width and the distance between them are the high impact parameters on the spray cooling performance in the gassy and degassed conditions. The maximum enhancement ratio for the degassed and gassy conditions were 51% and 38% respectively.

In addition these studies, Silk et al. [42] examined different enhanced surfaces; the surface enhancements consisted of embedded structures and compound extended surfaces. The embedded surfaces were modified with dimples, pores, and tunnels, while the compound enhancements were modified with straight fins, cubic pin fins, and dimples. These surfaces have a projected cross-sectional area of 2 cm^2 and were cooled by 2×2 nozzle arrays. PF-5060 was used as a working fluid. The results showed that the surfaces straight fins and porous tunnels had the highest critical heat flux (CHF) among other surfaces in both gassy and degassed conditions with an enhancement of 77% and 62% respectively, compared to a plain surface.

Moreover, Silk et al. [43] conducted experiments to study the effects of the surface modifications and the inclination angle on spray cooling heat transfer in a closed system working with PF-5060 as a working fluid. Three different copper surfaces modified with cubic, pyramid, and straight fins were used and exposed to nozzles array.

The results showed that the surfaces with fins had a larger heat flux than a plain surface, and the surface with straight fins provided the largest heat flux, followed by the surface with cubic fins and the surface with the pyramid. Also, the surface with straight fins had heat flux enhanced up to 75% at 30° inclination angle, compared to a plain surface with 0° inclination angle. Coursey et al. [44] examined five heat sinks modified with straight channels having a width of 360μm and fins having a width of 500 μm and lengths of 0.25 mm, 0.50 mm, 1.0 mm, 3.0 mm, and 5.0 mm. These surfaces were cooled in a spraying system employing PF-5060 as a working fluid, and the nozzle pressure difference ranged between 20-60 psi. The experimental results indicated that the surface with the longer fins in all cases had better heat transfer performance than the surface with the shorter fins in the single-phase regime. Also, in the two-phase regime, fins promoted the onset boiling, which improved the heat transfer coefficient at relatively low surface temperature. Moreover, fins with a length between 1-3 mm had the optimum heat transfer performance.

Sodtke and Stephan [45] studied the effect of the surface properties on the heat transfer characteristics in a spray cooling system experimentally by varying many spray cooling parameters. In this work, three different surfaces, S1, S2, and S3, modified with different micro-scale pyramids with heights and widths of 75×150, 150×300, and 225×450 μm, respectively, were examined under different operating conditions in a spray cooling system utilizing water as a coolant. The experimental results illustrated that surfaces modified with microstructure pyramids did not improve the heat transfer performance in the single-phase regime significantly compared to the plain surface, whereas it has an improvement in the two-phase regime.

This enhancement resulted from the increase in the three-phase contact line (water, vapor, copper) on the microstructured surfaces. The researchers also found S3 had better heat transfer performance compared to other surfaces. Moreover, Souza et al. [44, 45] experimentally tested both a plain and two enhanced surfaces with a diameter of 25 mm in a closed-loop spray cooling system working with R-134a as working fluid. The first surface, modified with a 10-pore-per- inch copper porous foam, had a porosity of 90%. The second surface was modified with six radial grooves with a height of 3 mm and width of 2 mm. The results showed that both modified surfaces improved the heat transfer performance compared to the plain surface. However, the heat transfer coefficient enhancement for the copper-foam surface factor was 1.35 times higher due to the increase in the active nucleation sites, but there was no improvement in the critical heat flux. The heat transfer coefficient of the copper-foam surface, based on the external surface, was significantly lower than that for the plain surface due to a decrease of film velocity and an increase in film thickness.

Zhang et al. [48] examined two groups of modified surfaces in a spray cooling system, working with deionized water as a coolant. In the first group, surfaces were modified with different straight grooves having the same depth of 200 μm with different widths and pitches of 400, 200, and 150 μm, respectively. In the second group, the roughness of the surfaces was changed between 142-2258 nm by using sandpapers with different grits. The experimental results showed that the heat transfer performance of modified surfaces was better than a plain surface, and the first group, surfaces with small features, was better than other modified surfaces. Moreover, in the second group of surfaces, the heat transfer performance was better for rough surfaces.

Yang et al. [49] used three types of microcavity surfaces to improve the spray cooling performance of a system working with ammonia as a coolant. These surfaces were modified with micro-holes that had a depth of 0.5 mm, radii ranged from 0.15 mm to 0.48 mm, and a pitch of 1 mm. The results showed that microcavity holes did not improve the heat transfer performance compared to a flat surface in the single-phase regime and at low surface superheats because convection heat transfer is the dominant contributer in that regime. At high surface superheats, there was a significant heat transfer enhancement at higher surface superheats due to the effect of nucleate boiling, which is the dominant heat transfer mechanism. Also, surface MC1 had uniform temperature distribution, and achieved the maximum heat transfer enhancement because it had the lowest Bond number.

Moreover, Hou et al. [50] investigated the effects of surface modifications on the thermal performance of a spray cooling system. The surfaces were modified geometrically by adding cubic pin fins and straight pin fins that had different dimensions with microscale level; these surfaces were cooled by eight nozzles utilizing water as a cooling medium. The experimental results indicated that straight fins2 and fins3 with dimensions of (200×300×400 and 200×200×200 μm) had the best heat transfer performance in the single-phase regime at a volumetric flow rate less than 3.48×10^{2} $m^3/ s/m^2$. Additionally, in the two-phase regime, cubic pin fins had the best heat transfer performance among surfaces. Bostanci et al. [51] examined surfaces modified with different scaling levels in a spray cooling system working with ammonia as a working fluid. Test surfaces involved microscale indentations and protrusions, macro-scale pyramidal, triangular, rectangular, and square pin fins, and multi-scale structures that combine macro and microscale structures.

The results indicated that the enhancement ratio of micro-structured surfaces, macrostructures surfaces, and hybrid surfaces was up to 81%, 44%, and 161%, respectively. Also, surfaces mi (-f,-m,-c) were the best among microstructures surfaces; the surface with pyramidal fins was the best among macrostructures surfaces, especially those with short height fins, and surface Mpf-0.25mp-c was the best among hybrid surfaces. Moreover, Zhang and Wang [52] experimentally, investigated the influences of the surface modifications and the volumetric flux on the spray cooling heat transfer performance in a spray cooling system working with water as a coolant. Six straight grooved surfaces were tested and compared with a plain surface under the same operating conditions. The results showed that a surface with a groove of 0.5 mm depth and 0.4 mm width has the largest heat flux at a volumetric flux of 1.604 $L/m^2.s$. However, a surface with a groove of 0.5 mm depth and 0.2 mm width has the optimal heat flux at a volumetric flux of 12.73 $L/m^2.s$. Also, the residual velocity of the droplet, which has a significant effect on the removed heat transfer, was much higher at a volumetric flux of 12.73 $L/m^2.s$.

Zhang et al. [2] examined four enhanced surfaces under different inclination angles in a spray cooling system working with HFE7100 as a coolant. The surfaces were enhanced with a straight, triangular, cubic pin, and mixing fins, created on the top of the copper surfaces. The experimental results indicated that surface with straight fins had the best heat transfer characteristics at all inclination angles, followed by surfaces modified with mixing, cubic pin, and triangle fins. Liu et al. [53] studied the effect of inclination angle on the spray cooling thermal performance of modified surfaces. The surfaces were modified with different shapes of fins, such as rectangular, trapezoidal, and triangular, and tested at inclination angles of $0°, 9°, 18°, 27°,$ and $36°$.

The results showed that a surface modified with rectangular fins has the highest thermal performance at an inclination angle of 18° compared to other surfaces. The maximum heat transfer enhancement was 20% compared to vertical spray, and it was obtained at a surface temperature of 53℃. Zhou et al. [54] examined enhanced surfaces in a closed system using R-410A as a working fluid to evaluate their thermal performance. These surfaces were enhanced with square and pyramid fins, and two orders of roughness as well as nano-porous layers with different pores were formed on the enhanced surfaces. The results demonstrated that modified surfaces improve the spray cooling thermal performance meaningfully. A surface-modified with pyramid fins has better thermal performance than a surface modified with square fins. Also surfaces with higher roughness and porosity improve the thermal performance tremendously.

2.4 SUMMARY OF PREVIOUS WORK

In a brief summary of previous work on heat transfer characteristics of spray cooling systems, it was observed that the influence of the parameters of the spray on the thermal performance of a plain surface has been investigated extensively to determine the most influential parameter. The results of most experimental studies illustrated that the coolant volumetric flow rate is the most influential parameter. The thermal performance of a spray cooling system enhances as the coolant volumetric flow rate increases. Also, the results of numerical investigations illustrated that the coolant volumetric flow rate is the most influential parameter among other operating parameters on the thermal performance of spray cooling systems. Nozzle-to-surface distance has a critical value, and at this value the maximum heat transfer performance occurs. The critical value was found to be at a distance less than the distance required to cover the entire surface area of the target surface.

Decreasing nozzle-to-surface distance enhances the spray cooling thermal performance of a plain surface slightly. Furthermore, heat transfer enhancements via geometrical surface modifications in spray cooling systems have gained significant attention and several experimental investigations have been performed at different operating conditions. The thermal performance of different configurations, such as straight, cubic, pin, trapezoidal, and pyramid fins, were evaluated experimentally. Most of the studies showed that straight fins had the best thermal performance among other configurations, and the thermal performance of all modified surfaces enhance as the coolant volumetric flow rate increases.

CHAPTER 3

THEORETICAL BACKGROUND OF SPRAY COOLING AND HEAT TRANSFER MECHANISMS

In this chapter, a theoretical background about the fundamentals of droplets formation and its characteristics in spray cooling systems are explained in detail. Additionally, correlations are used to calculate droplet characteristics, such as Sauter mean diameter, velocity, and flux. Moreover, the forces which act on droplets before impacting the target surface are analyzed, and heat transfer mechanisms involved in spray cooling systems are deliberated in detail.

3.1 SPRAY COOLING MECHANISM

Spray cooling occurs when a highly pressurized liquid flows through a small orifice; the liquid breaks up into fine droplets with high momentum and larger fluid surface area [55]. Spray cooling systems are classified into pressure and atomized sprays based on the method used to break-up a liquid into droplets. In pressure sprays, droplets are generated by pumping liquid at high pressure through a small orifice, scattering into fine droplets; while atomized sprays employ a high-pressure gas stream to assist the liquid breakup and form fine droplets [2-4]. The effectiveness of the spray cooling depends primarily on the droplet breakup process, which consists of three stages: formation of liquid sheets, then dispersion into ligaments and eventually break-up into fine droplets, as graphically explained in Figure 3.1 [18]:

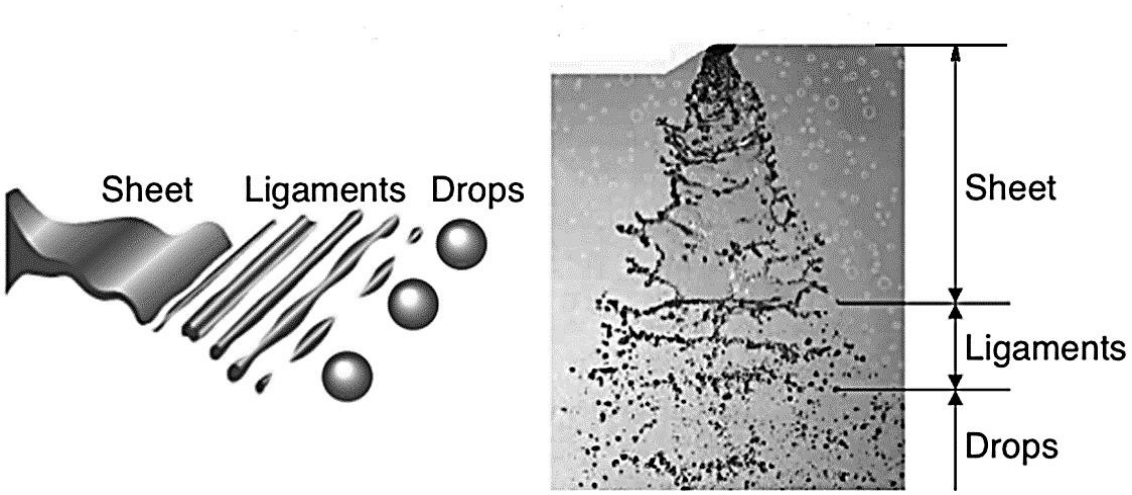

Figure 3.1 Droplets break-up physics [18].

The characteristics of droplets, such as diameter, velocity, and flux, depend mainly on the pressure difference across a nozzle, the thermophysical properties of the working fluid, and the nozzle characteristics, such as orifice diameter and spray angle. The characteristics of droplets are explained as follow:

3.1.1 SAUTER MEAN DIAMETER (SMD OR D_{32})

SMD is defined as the diameter of the droplet that has the same volume to surface area ratio [55], and it is considered one of the most effective parameters on spray cooling heat transfer performance. In spray cooling systems, critical heat flux (CHF) of a surface enhances as SMD decreases [58]. Also, SMD is used as an appropriate and accurate means of characterizing the size of droplets for spry cooling systems because generated droplets have different diameters, and it is difficult to measure the diameter accurately. A correlation for the most working fluid, with a mean absolute error of 12.4%, was proposed by Mudawar et al. [23]. This correlation is used to calculate SMD as shown below:

$$\frac{d_{32}}{d_o} = 3.07 \left(\frac{\rho_a^{0.5}\,\Delta p\, d_o^{1.5}}{\sigma^{0.5}\mu_l}\right)^{-0.259} \tag{3.1}$$

3.1.2 Droplet Velocity.

Droplet velocity plays a vital role in spray cooling heat transfer performance, and it is one of the critical physical parameters that effect such performance. The amount of energy exchange between the target surface and the working fluid depends primarily on droplet momentum and characteristics. Droplet velocity depends highly on nozzle differential pressure, nozzle characteristics, and the thermophysical properties of the coolant. Droplet velocity at nozzle's orifice is calculated by using a correlation based on energy balance, which was proposed by Ghodbane and Holman [22], as follows:

$$v_o = \left[v_{tube}^2 + \frac{2\Delta p}{\rho_l} - \frac{12\sigma}{\rho_l d_{32}}\right]^{1/2} \tag{3.2}$$

The droplets are exposed to many forces such as drag force, buoyancy force, and gravity force before impacting the target surface [52]. These forces have a significant effect on the droplet velocity and ultimately on the spray cooling performance, and the effect of the forces depends on the length of the droplet path, droplet size, velocity, and chamber environment. Figure 3.2 shows a schematic of forces acting on a single droplet before impacting the target surface.

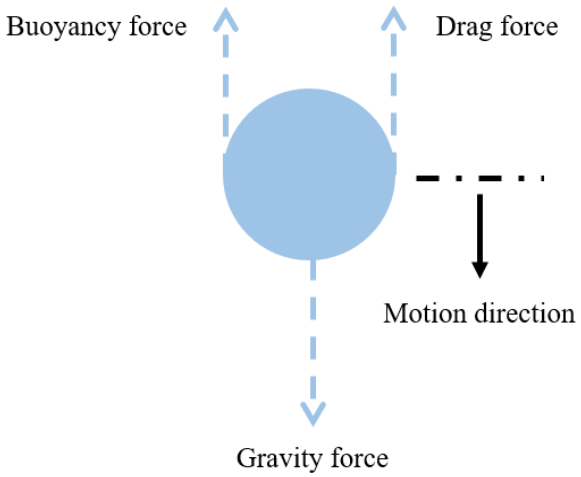

Figure 3.2 Schematic of forces acting on a single droplet.

In order to calculate local droplet velocity before impacting the target surface, forces, such as buoyancy, gravity, and drag, acting on a droplet were analyzed in detail as explained below [52]:

$$F_B = \frac{1}{6}\pi d_{32}^3 \rho_a g \tag{3.3}$$

$$F_G = \frac{1}{6}\pi d_{32}^3 \rho_l \tag{3.4}$$

The drag force on a droplet was calculated by an equation proposed by [59], as shown below:

$$F_D = C_D \frac{\pi d_{32}^2}{4} \rho_a \frac{u^2}{2} \tag{3.5}$$

The drag coefficient C_D was calculated from the following correlation:

$$C_D = \frac{24}{Re_a}(1 + 0.02Re_a) \tag{3.6}$$

$$Re_a = \frac{u\, d_d}{\vartheta_a} \tag{3.7}$$

Based on the balance of forces and the spherical droplets assumption, the acceleration of a single droplet can be calculated by using Newton's second law as follows:

$$\vec{a} = \frac{F_g + F_B - F_D}{m} \tag{3.8}$$

Calculations showed that the gravity effect on droplets can be neglected due to the high velocity of droplets and due to its Froude number ≥ 100 [60]. The droplets were assumed to move in rectilinear motion with a constant acceleration. Therefore, the local droplet velocity can be calculated by using the following equation [61]:

$$v\, dv = \vec{a}\, ds \tag{3.9}$$

By integrating the above equation, the local droplet velocity can be calculated by:

$$u = \sqrt{v_o^2 + 2\vec{a}H} \tag{3.10}$$

3.1.3 DROPLET FLUX

The droplet flux is defined as the number of drops generated per unit second, and it depends on the nozzle differential pressure. It increases with the increase in the nozzle differential pressure and it plays a major role in spray cooling heat transfer performance [62]. Also, it increases the liquid surface area and maintains the surface wettability, which prevents or delays the occurrence of the dry out phenomenon on the target surface. It can be calculated by using the following [22]:

$$\dot{N} = \frac{6\,(v\,.\,A)_{tube}}{\pi d_{32}^3} \tag{3.11}$$

3.2 DROPLET INTERACTION WITH A SOLID SURFACE

The amount of energy exchange between the solid and the working fluid mainly depends on the interaction between them. When a droplet impacts a solid surface, it may adhere, rebound, spread, break-up and rebound, break-up and spread, or splash on the surface, as shown in Figure 3.3. The droplet behavior on a solid surface mainly depends on Weber number, Laplace number, and surface temperature [63], as shown in Figure 3.4. Weber number represents the ratio of droplet kinetic energy to surface tension, defined as:

$$We = \frac{\rho d_d u_d^2}{\sigma} \tag{3.12}$$

Laplace number measures the relative importance of surface tension and the viscous force acting on the drop, defined as:

$$La = \frac{\rho \sigma d_d}{\mu_f^2} \tag{3.13}$$

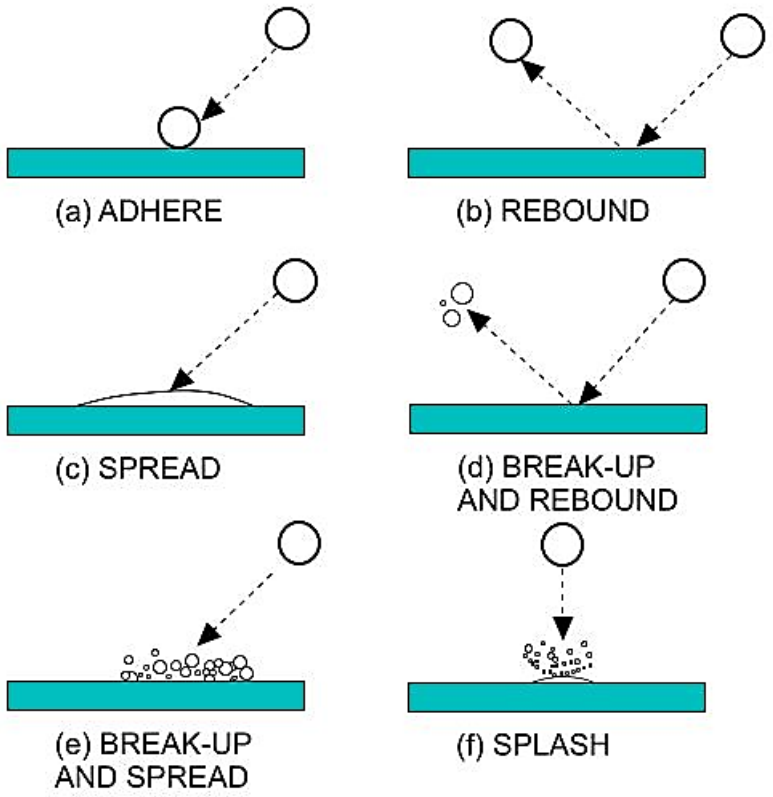

Figure 3.3 Schematic of a droplet behavior on a solid surface [64].

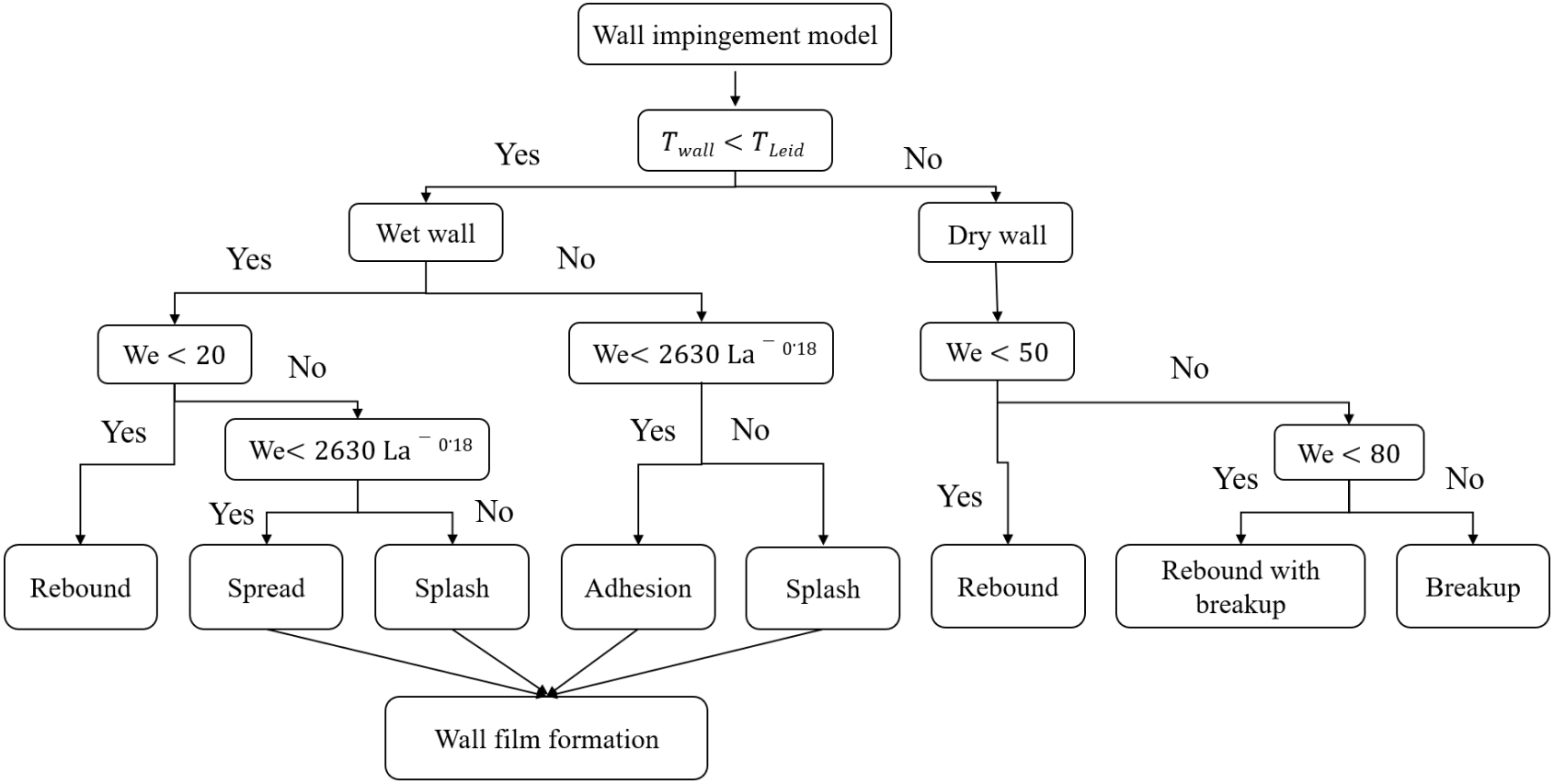

Figure 3.4 Diagram of droplet behavior on a surface [61].

3.3 HEAT TRANSFER MECHANISMS IN SPRAY COOLING

In spray cooling systems, many heat transfer mechanisms are involved before and after the impingement, such as convection, radiation, and phase-change heat transfer. The fraction of radiation heat transfer to the overall spray cooling heat transfer was estimated by Choi and Yao [65], and it was found to be 0.5% of the spray cooling heat transfer. Therefore, it is negligible, and heat transfer mechanisms are mainly classified based on the surface temperature into a single-phase or a two-phase regime:

3.3.1 HEAT TRANSFER MECHANISMS IN THE SINGLE-PHASE REGIME

In the single-phase heat transfer regime, the convection is the primary mechanism of heat transfer, which occurs when there is a substantial temperature difference between the target surface and the working fluid. Convection heat transfer happens during the spraying process, and it occurs between the droplets and the chamber's environment before impinging a solid surface and in the liquid film before reaching the fluid saturation temperature. The convective heat transfer rate is enhanced with increasing volumetric flow rate due to the increase in the flow velocity over the target surface and the reduction in the thermal boundary layer thickness. Also, the droplets' flux increases, which helps to disrupt both thermal and hydraulic boundary layers and eventually reduce the liquid thermal resistance [55]. Moreover, there is a form of convective heat transfer that occurs between the liquid film and the chamber environment at the interface due to the temperature difference between the two fluids. The convective heat transfer resulting from the simultaneous conduction of heat from the heated surface to the fluid can be calculated by using the following equation [66]:

$$Q = \dot{m}\, C_p (T_{out} - T_{in}) \tag{3.14}$$

3.3.2 HEAT TRANSFER MECHANISMS IN THE TWO-PHASE REGIME

In spray cooling, the heat transfer phase change occurs when the surface temperature is higher than the fluid saturation temperature between the solid surface and the coolant. In the beginning, many small bubbles form on the solid surface due to the temperature difference. The growth rate of bubbles depends on the heat flux and surface topography. These bubbles are exerted by external forces to detach the bubbles from the solid surface and stir the thin liquid film. There are two primary heat transfer mechanisms in the two-phase regime of spray cooling:

3.3.2.1 Nucleate boiling

Phase change in heat transfer starts with nucleation boiling, which is defined as a process of forming vapor nucleus in a liquid film, and it is initiated when there is a sufficient temperature difference between solid surface temperature and the saturation temperature of a fluid. It starts with the generation of very small bubbles of vapor on the solid surface at specific places, which are known as nucleation sites. The bubbles grow on these sites until they reach a critical size then depart from the solid surface due to the forces exerted upon them, and this process is known as heterogeneous nucleation. The heterogeneous nucleation begins on the solid surfaces when the free energy of formation that occurs either on the surface or in a cavity on that surface film is enough to generate a vapor bubble [67], [68]. The bubbles growth rate and departing rates depend on the heat flux, surface topography, and fluid thermophysical properties. Figure 3.5 illustrates a schematic description of the nucleation boiling process on a solid surface.

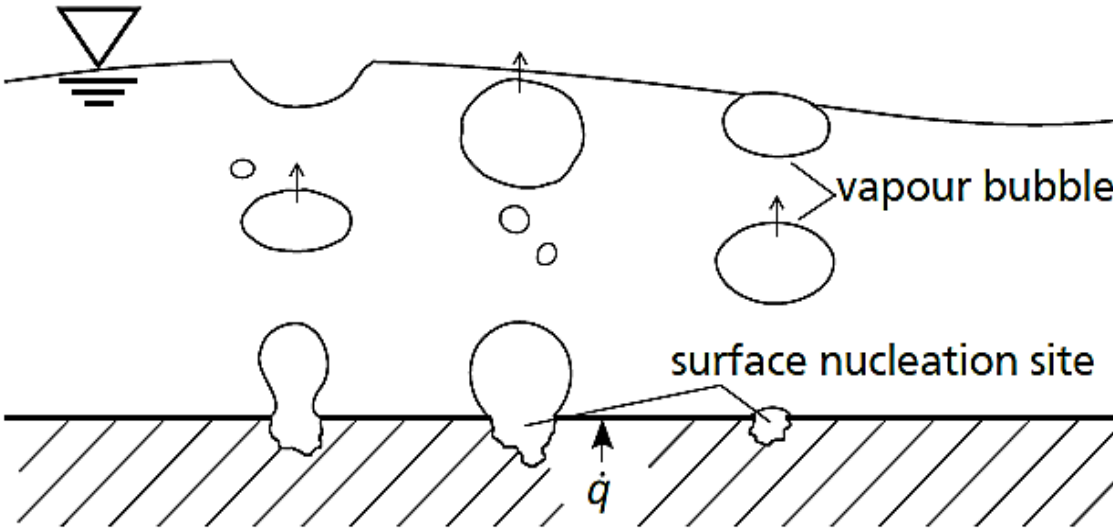

Figure 3.5 Schematic of nucleate boiling process on a solid surface[69].

In addition to the heterogeneous nucleation boiling, secondary nucleation boiling may exist in the liquid film, the process is initiated when some bubbles break-up or shrink into small vapor bubbles within the liquid film resulting from the impingement of the liquid droplets, or from other external exerted forces. Secondary nucleation generates more nucleation sites in addition to those formed on the solid surface. Therefore, spray cooling heat transfer is enhanced rapidly because secondary nucleation boiling is more dominant among the other spray cooling heat transfer mechanisms. Furthermore, it can be increased by increasing the number of droplets entering the liquid film, or in other words, by increasing the coolant volumetric flow rate, and the heat flux. Homogeneous nucleation boiling may occur if the free energy of formation within the liquid film is enough to generate a vapor bubble, and it usually occurs at high superheated temperatures. This process can improve the heat transfer characteristics significantly since it produces extra nucleation sites [67], [69], [70]. Figure 3.6 illustrates a schematic description of the secondary nucleation boiling.

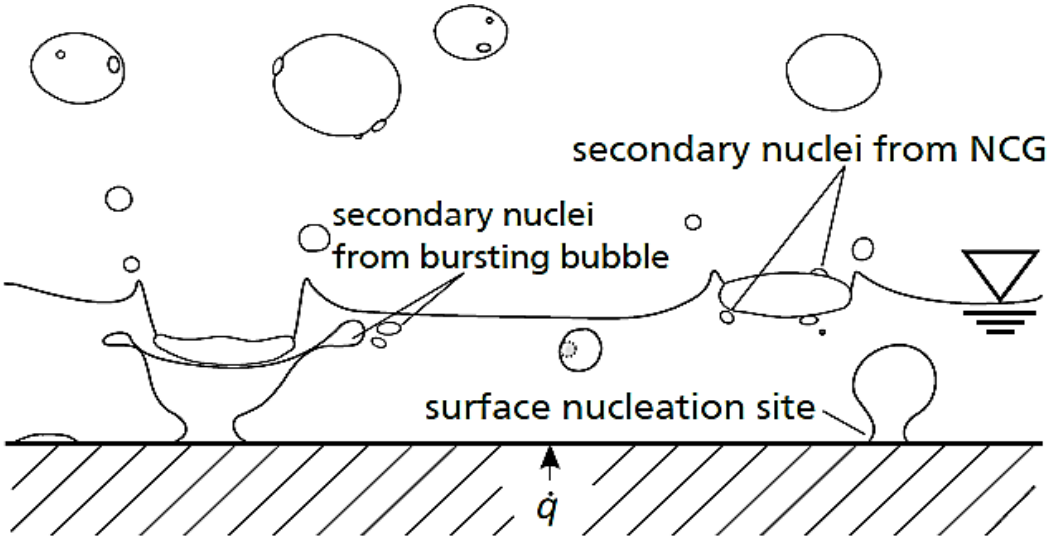

Figure 3.6 Schematic of secondary nucleate boiling [69].

3.3.2.2 Evaporation

Evaporation happens after nucleation boiling. It is a typical heat and mass transfer phenomenon that occurs at the liquid film interface and plays a secondary role in the spray cooling heat transfer process [4]. The intensity of the evaporation depends on the liquid film temperature, the ambient temperature, the vapor pressure at the interface, and the thickness of the liquid film [66]. Evaporation provides sustainable and rapid spray cooling heat transfer enhancement [71]. Due to the temperature gradient within the liquid film, thin liquid film is better than thick film at the same surface temperature for enhancing heat transfer because it has lower thermal conductive resistance. The relative contribution of the evaporation depends on the liquid film thickness, heat flux, and spray mass flux, where the thin film evaporation increases as the spray mass flux decreases. Therefore, forming a thinner liquid film on the whole heat transfer surface is very desirable in an evaporative spray cooling system [72].

CHAPTER 4

EXPERIMENTAL FACILITY AND METHODOLOGY

Numerous experiments were designed and conducted to investigate the spray cooling performance of different surfaces at different operating conditions. The components of the experimental facility, test procedures, and methodologies used in these studies are described in detail below.

4.1 EXPERIMENTAL FACILITY

Designing a spray cooling system requires a comprehensive systematic methodology with a high degree of accuracy due to a number of the influential parameters on the performance of the system [18]. Therefore, in the present study, an integrated closed-loop spray cooling system was designed and built with a high degree of flexibility to perform experiments on different surfaces at different operating conditions. The experimental setup provides the opportunity to vary heat flux, volumetric flow rate, and nozzle-to-surface distance. Figure 4.1 and Figure 4.2 show a schematic diagram and an actual picture of the experimental setup. The system consists of five main components: a spraying system, a spray chamber, a heating system, a data acquisition system, and a cooling system. Below is a brief description of the main parts of the experimental system.

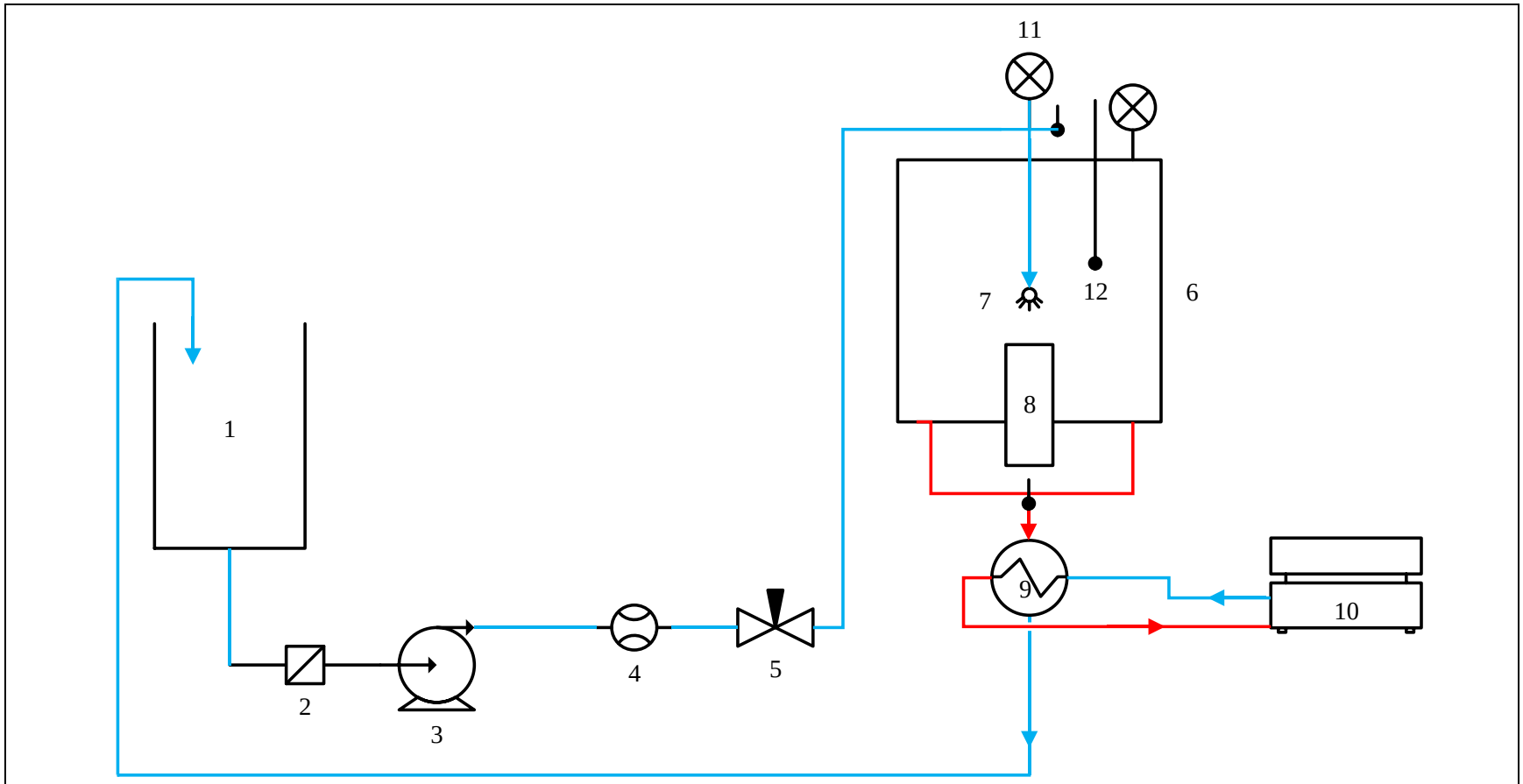

1: Water tank	2: Strainer	3: Pump	4: Flow meter	5: Valve	6: Spray chamber
7: Nozzle	8: Heater assembly	9: Heat exchanger	10: Chiller	11: Pressure indicator	12: Temperature indicator

Figure 4.1 Schematic diagram of the experimental setup.

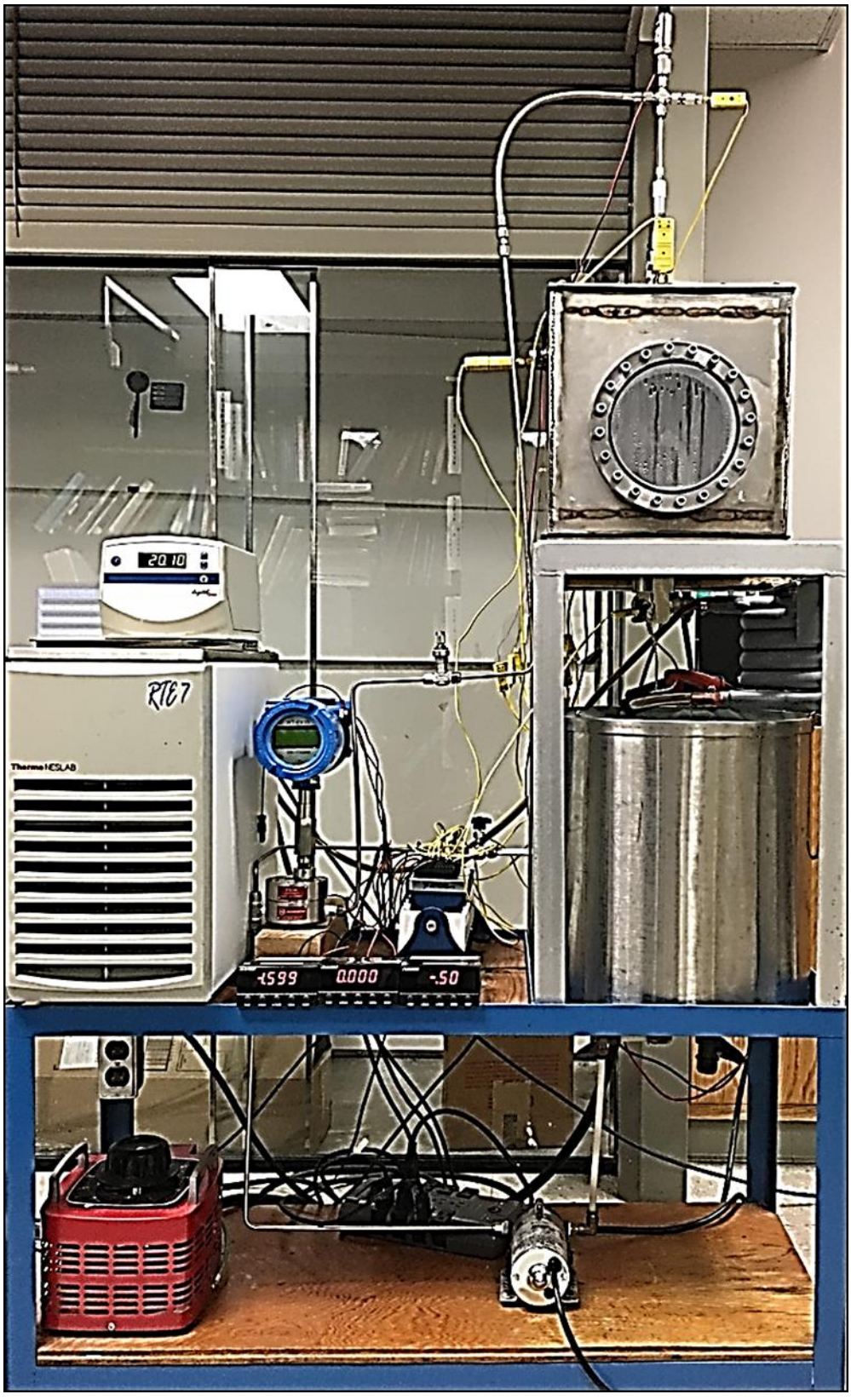

Figure 4.2 Actual picture of the experimental facility.

4.1.1 SPRAYING SYSTEM

In the spraying system, the deionized water is driven from the reservoir by a positive displacement bypass diaphragm pump, (model 8020-503-250, SHURFLO). This pump can supply fluids at a maximum flow rate of 5.3 L/min and a maximum pressure of 413.6 kPa. A miniature strainer with a screen mesh of 100 grit is placed on the suction line of the pump to remove all impurities. The flow rate is controlled by a needle valve and measured by a positive displacement flow meter (JVM-20KG-25-NPT, AW-LAKE Company) provided with a RT-Ex15 flow monitor. A full cone nozzle (TG 0.3, Spraying Systems Company) is utilized to generate the droplets. The nozzle-to-surface distance was adjusted by an accurate micrometer with a positioning accuracy of $\pm 1\%$.

4.1.2 SPRAY CHAMBER

Figure 4.3 shows a schematic of the spray chamber, which is the central part of the experimental setup; it is a cube with dimensions of ($30 \times 30 \times 30$ cm), assembled mostly from stainless steel. The chamber is provided with front and back sight glasses for flow visualization. The heater assembly is integrated into the bottom of the chamber, and the spray nozzle is positioned in a downward orientation, and the nozzle-to-surface distance is adjusted accurately with the aid of a micrometer. The liquid is drained through two outlet ports at the bottom of the chamber; the outlet liquid is cooled by a coaxial coil before returning to the reservoir. A pressure transducer (PX319-030GI, Omega Engineering) is used to measure the spray chamber's pressure, and temperature indicators are used to measure the temperature at the inlet, outlet, and chamber.

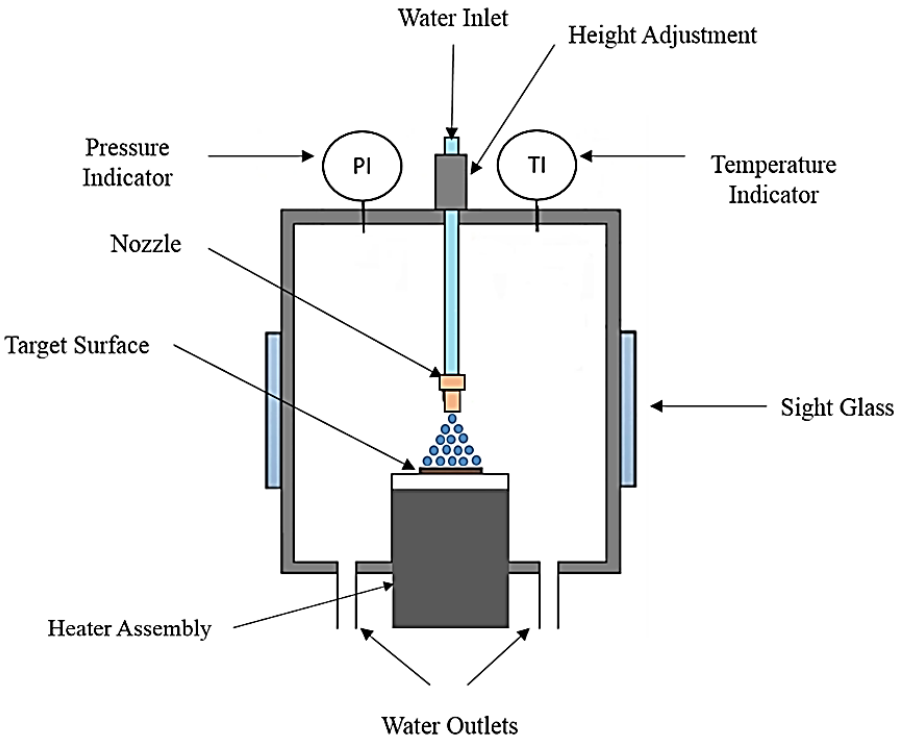

Figure 4.3 Schematic of the spray chamber

4.1.3 HEATING SYSTEM

The target surface is heated by a 1000W cartridge heater (HDC00516, TEMPCO), which is inserted in a super-conductive 101 copper block, as shown in Figure 4.4. A variable transformer (Variac) model TDGC-3K (M) is connected to the cartridge heater to supply variable heat fluxes. The copper block is surrounded by a stainless-steel pipe having inner and outer diameters of 4.8 and 6 cm respectively. The gap between the copper block and the pipe is filled with fiberglass insulation to reduce heat loss to the environment; all sides of the copper block are insulated except for the top side, which is exposed to spray. Eight different thermocouples (5TC-TT-K-30-36, Omega Engineering) are embedded below the target surface as illustrated in Figure 4.5; the temperature readings from these thermocouples are used to calculate the effective heat flux, surface temperature, and effective heat transfer coefficient. The gaps between the thermocouples and the holes were

filled with Arctic Silver 5 thermal grease to increase the conductivity between thermocouples and the copper block which increases the accuracy of readings. All thermocouples were connected to the data acquisition system in order to acquire and record their readings and measurements.

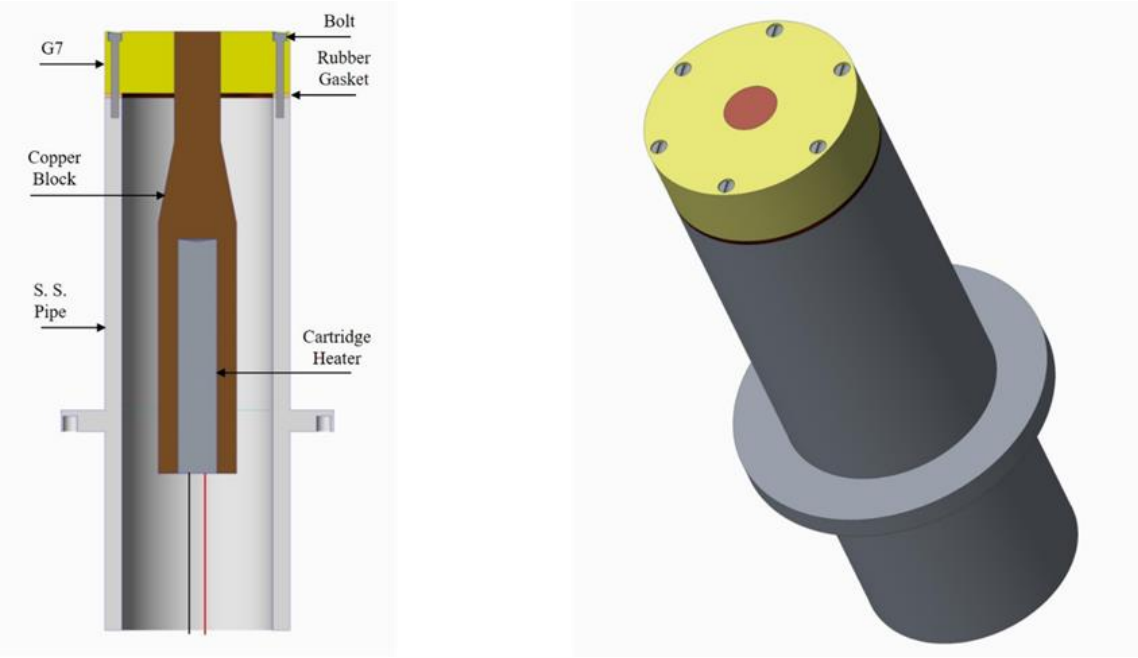

Figure 4.4 CAD view of the heater assembly.

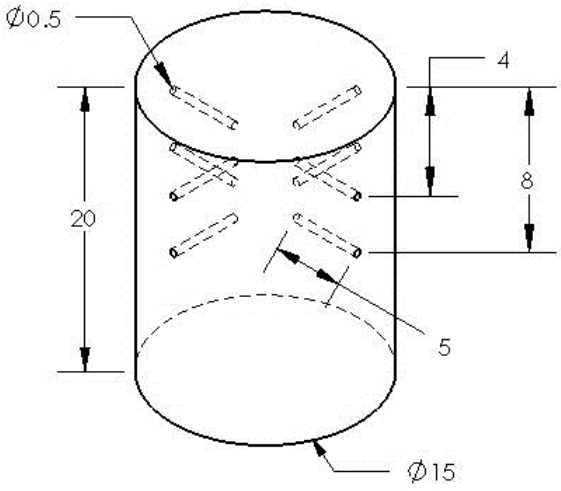

Figure 4.5 CAD view of the thermocouple positions (all dimensions in mm).

4.1.4 DATA ACQUISITION SYSTEM

All measurements, such as temperatures, pressures, and flow rates were connected to a data acquisition system model (NI cDAQ-9172) manufactured by Nationals Instruments Company in order to acquire and record all data. The thermocouples were placed at different points, such as below the test surface, at the inlet of the chamber, at the outlet of the chamber, and inside the chamber, as well as connected to NI 9211 DAQ module. The pressures of the water at the inlet of the nozzle and the pressure inside the chamber were measured by using pressure transducers. The pressure transducers and the flow meter were connected to the NI 9203 DAQ module. The data acquisition system was connected to a computer to record the experimental data by using LabVIEW Signal Express 2012, as shown in Figure 4.6:

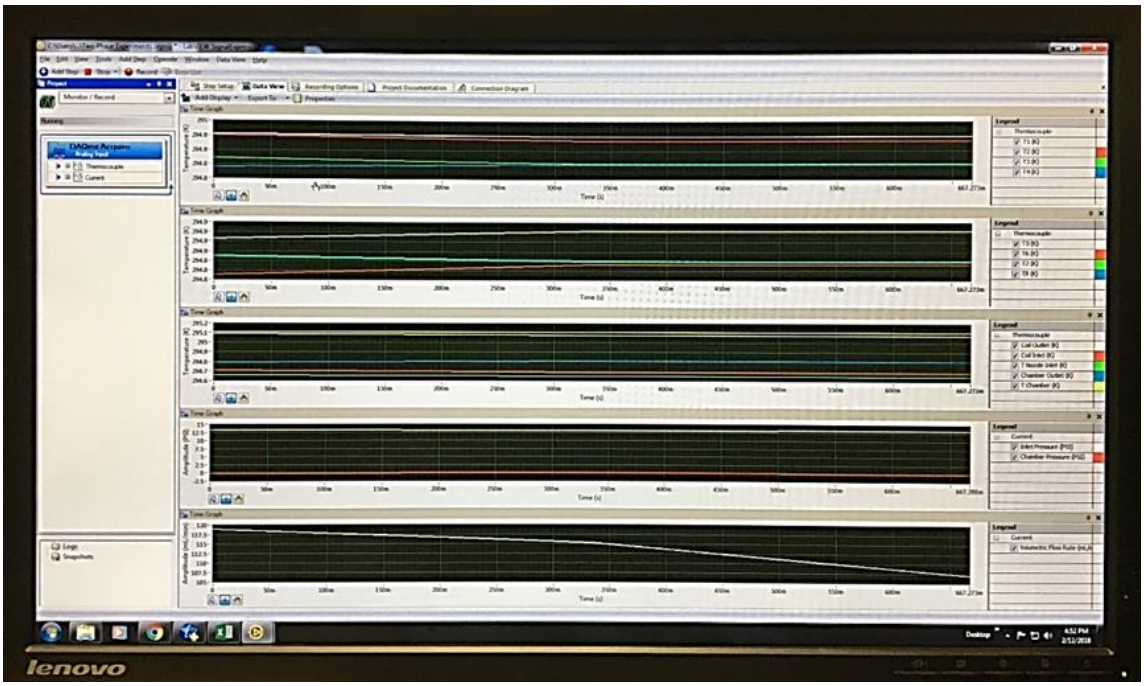

Figure 4.6 Screenshot of the LabVIEW for monitoring and recording data.

4.1.5 Cooling System

The primary objective of this system is to control the operating conditions, such as chamber water inlet and outlet temperatures, which help the experimental setup reach the steady-state condition efficiently. The cooling system consists of a 1.76 kW chiller model (RTE7, Thermo NESLAB) and a coaxial coil model (CX-H 075, Doucette Industries) used to cool outlet water of the spraying chamber before returning to the water reservoir. These components were connected to form a controllable closed cooling system.

4.1.6 Calibration of Instruments

After assembling the experimental rig, different instrumentations, such as thermocouples, pressure transducers, and flow meter, were used to acquire and record the data. All instruments were tested and calibrated before integration into the experimental setup. The positive displacement flow meter model (JVM-20KG-25-NPT, AW-Lake Company), provided with an RT-Ex15 flow monitor, was calibrated using a stopwatch and a graduated beaker. The results showed that the maximum accuracy of the flow meter was less than ±5%, and Figure 4.7 shows the comparison between the displayed and the measured readings. Thermocouples model (5TC-TT-K-30-36, Omega Engineering) were used to measure the temperatures below the target surface, and to calculate the heat flux, the target surface temperature, and the heat transfer coefficient. All thermocouples were connected to the data acquisition system and calibrated with a certified ThermoNESLAB model RTE7 and used as a reference temperature. The results of calibration showed that the average deviation between the thermocouples and water bath varied from ±0. 2% to ±0.6%, as shown in Figure 4.8.

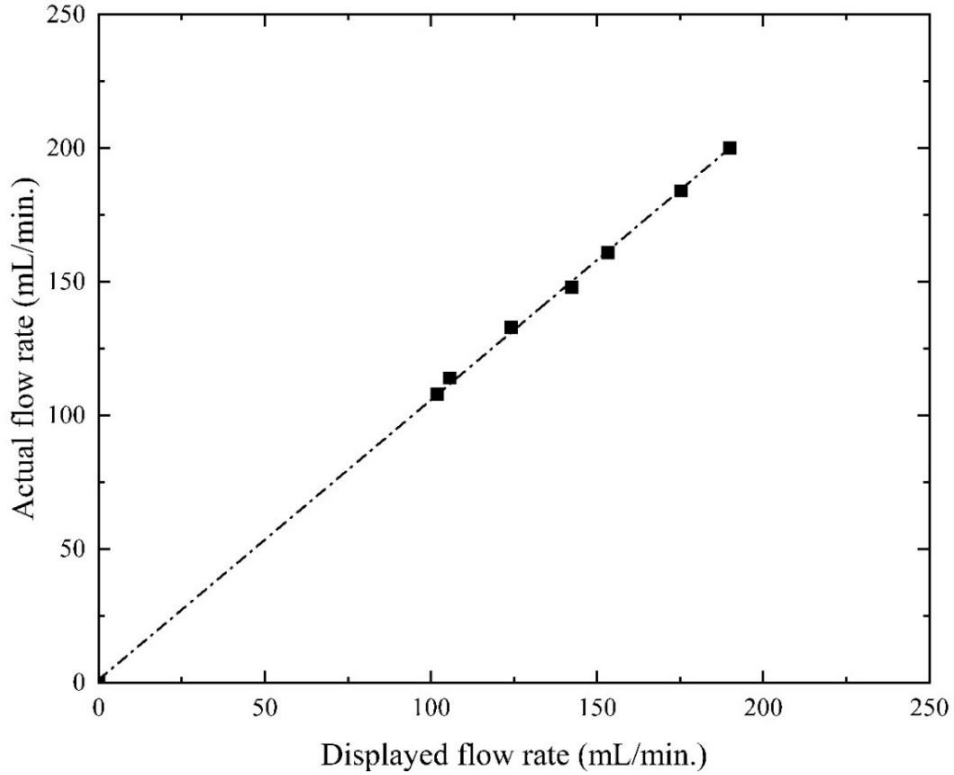

Figure 4.7 Flow meter calibration.

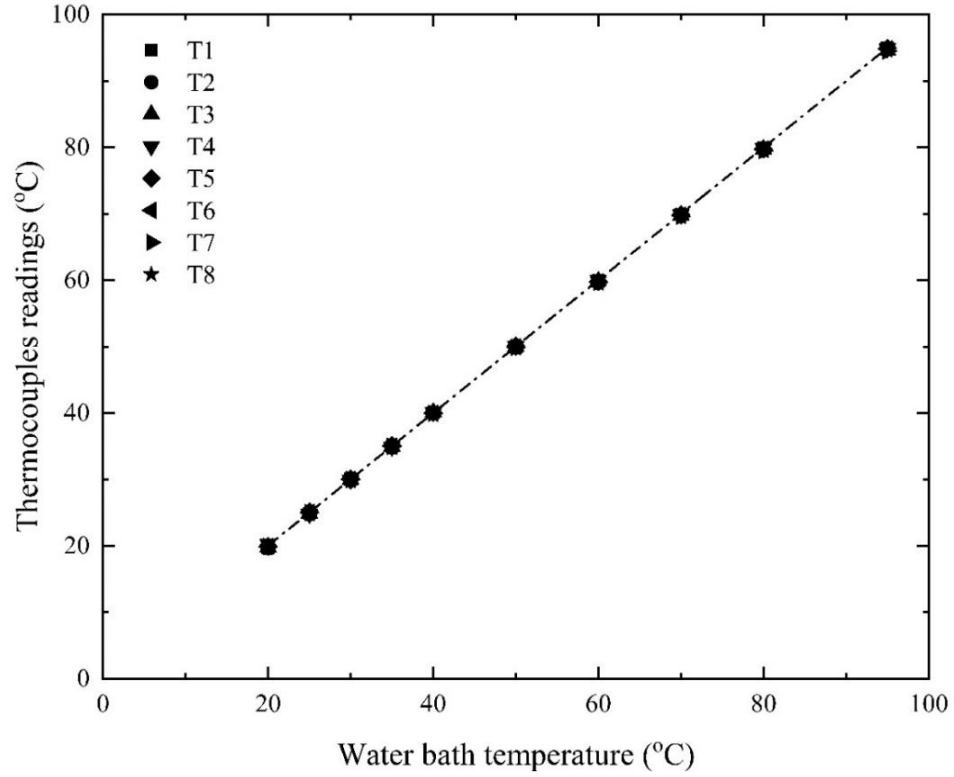

Figure 4.8 Thermocouples calibration.

The pressure transducers models (PX319-050GI & PX319-030GI) were calibrated and certified by the manufacturing company Omega Engineering and have an accuracy of ±0.25%.

4.2 TEST PARAMETERS AND PROCEDURE

The deionized water was driven from the water tank by a positive displacement pump, and water was passed through a strainer to remove all impurities from the working fluid. Before each experiment, the target surface was cleaned by Nitric acid solution with a concentration of 32.5%, which was purchased from Sigma Aldrich. It was then rinsed with deionized water to remove the copper oxide layer. Then both the pump and the cooling system were turned on for 25 minutes to let the flow rate, the pressures, and the temperatures of the system reach the steady-state condition. After that, the heat was supplied to the target surface, and the power was increased gradually in small increments by using a variable transformer (Variac) to maintain the surface temperature uniformity and avoid the problem of burning out. The time step between two increments was set to 30 minutes to make sure that the system reached the steady state condition before recording the data. These steps were repeated at each experiment to study the effects of different influential parameters, such as volumetric flow rate and nozzle-to-surface distance, on heat transfer characteristics of plain and modified surfaces. Figure 4.9 - Figure 4.11 show the steady state level of surface temperature, nozzle differential pressure, and volumetric flow rate, which have an absolute average deviation of ± 0.055, ± 0.42, ± 1.9 %, respectively.

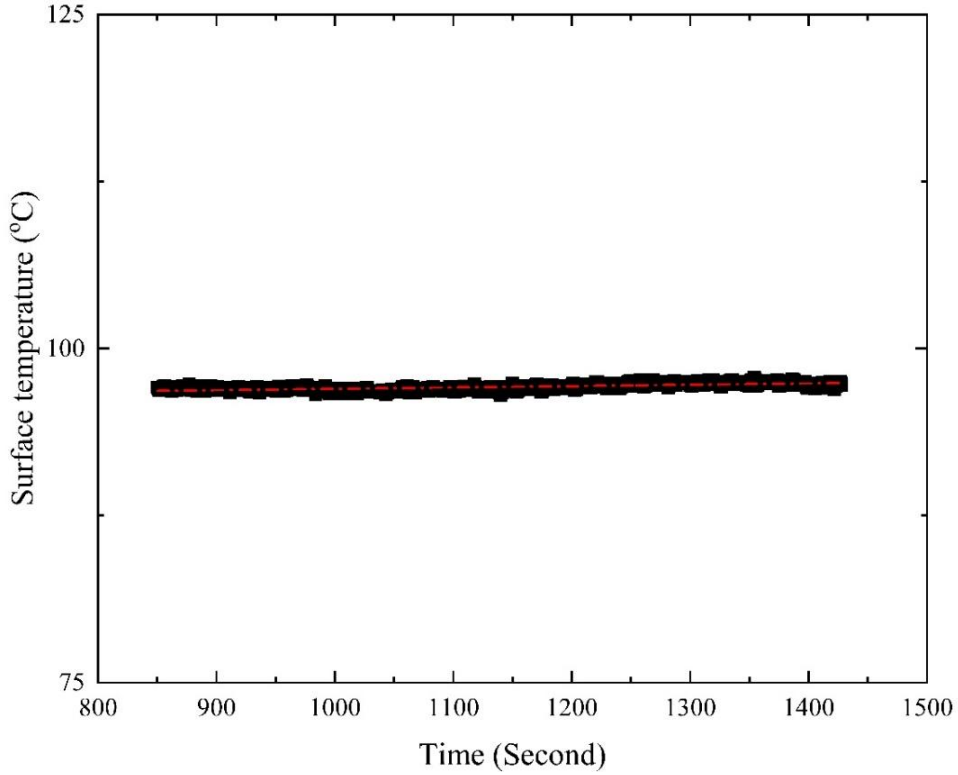

Figure 4.9 Steady state level of surface temperature.

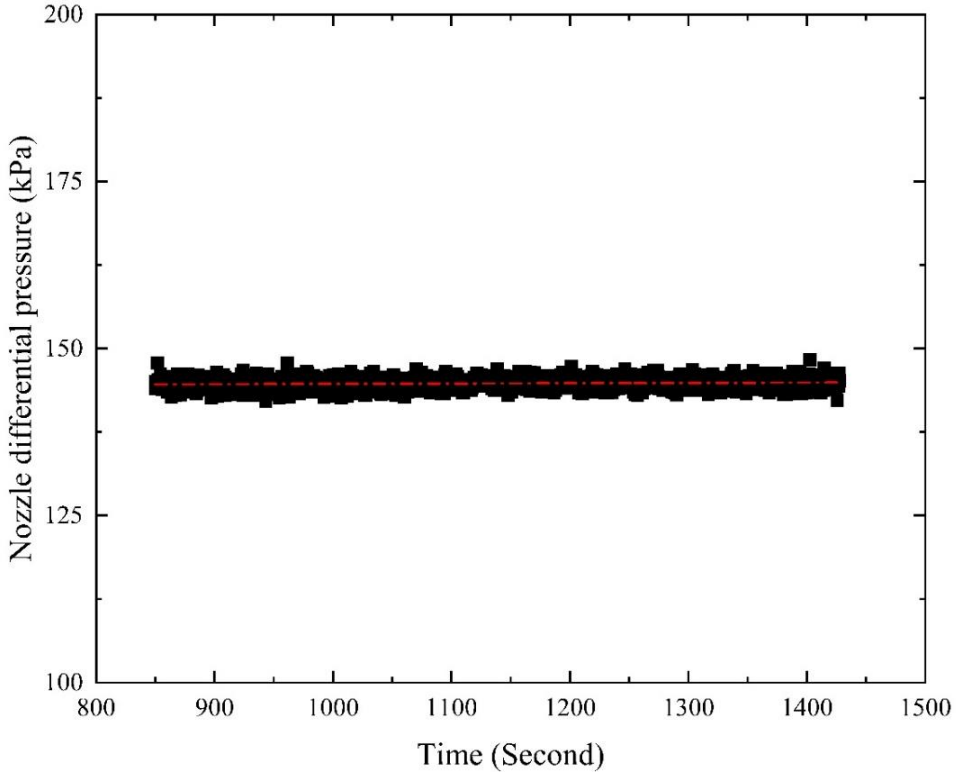

Figure 4.10 Steady state level of nozzle differential pressure.

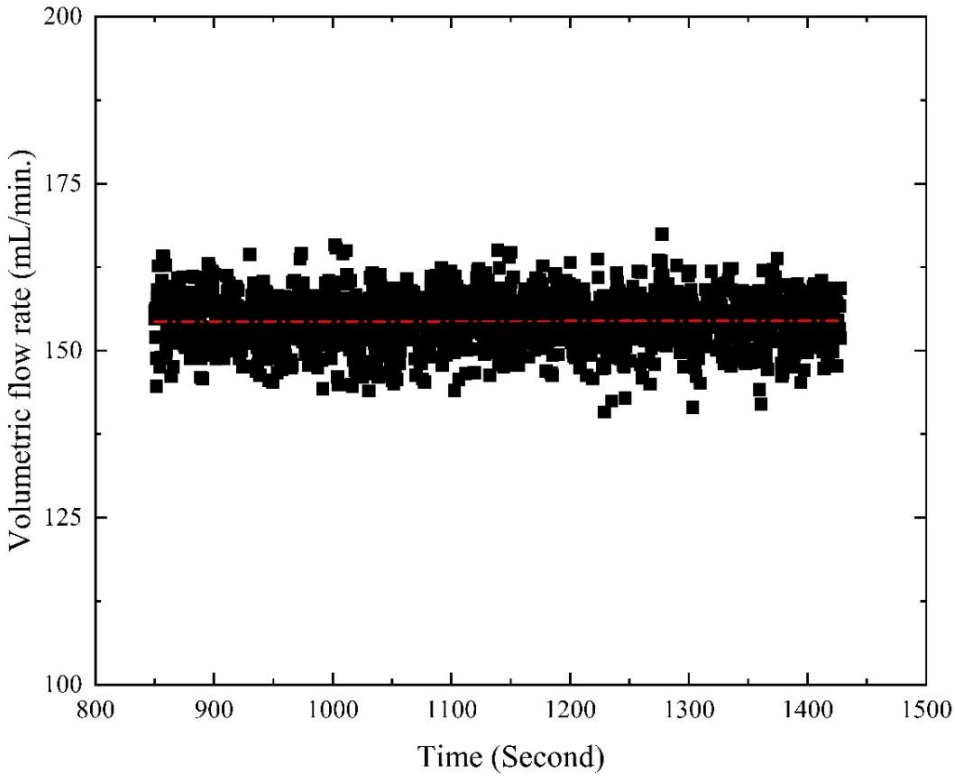

Figure 4.11 Steady state level of volumetric flow rate.

4.3 DATA REDUCTION

Eight thermocouples were embedded below the target surface to measure the temperature gradients. The thermocouples (T_1, T_2, T_3, and T_4) and (T_5, T_6, T_7, and T_8) were positioned below the target surface at 4 and 8mm, respectively, as shown in Figure 4.5. Since the copper has a high thermal conductivity and is well insulated, one-dimensional heat conduction was assumed to calculate the heat flux by using Fourier's law, as shown in the following equation [73]:

$$q^{"} = -k\frac{dT}{dx} \tag{4.1}$$

The experimental readings were substituted in the following equation, to calculate the effective heat flux.

$$q^{"} = -k\frac{\frac{T_1+T_2+T_3+T_4}{4} - \frac{T_5+T_6+T_7+T_8}{4}}{L} \tag{4.2}$$

The surface temperature T_S is then calculated with the heat flux determined before and the distance of the upper thermocouples to the reference level. As shown in Figure 4.5, T_A is the average of four thermocouples (T_1, T_2, T_3, and T_4), and T_B is the average of four thermocouples (T_5, T_6, T_7, and T_8). The surface temperature for plain and modified surfaces was calculated based on Fourier's law by using the following equation:

$$T_S = T_B - \frac{kq^{"}}{L} \tag{4.3}$$

After calculating the heat flux and the surface temperature from the above equations, the heat transfer coefficient for the plain surface was calculated according to Newton's cooling law, as shown below [73]:

$$h = \frac{q^{"}}{T_S - T_{in}} \tag{4.4}$$

The percentage of heat loss to the environment due to the effectiveness of the thermal insulation was calculated by using the following equation:

$$HL = \left(\frac{Q_{in} - Q_E}{Q_{in}}\right) \times 100 \tag{4.5}$$

The input power was calculated by using the following equation:

$$Q_{in} = I.V \tag{4.6}$$

The calculations showed that the average percentage of heat loss was 8%. Moreover, the enhancement ratio was calculated by using the following expression:

$$ER = \left(\frac{q_M^{"} - q_P^{"}}{q_P^{"}}\right) \times 100 \tag{4.7}$$

4.4 UNCERTAINTY ANALYSIS

The measured quantities in these experiments are temperatures, pressures, and volumetric flow rates. The average heat flux, surface temperature, and average heat transfer coefficient were calculated by using Fourier's equation with one-dimensional and steady-

state assumptions. Thus, some errors were introduced to the calculated quantities resulting from the uncertainties of the thermocouples and the normal distance between thermocouples. The following equation is used to calculate the propagated in the calculated quantities [74] :

$$q = f(x_1, x_2, x_3, \dots . x_n) \rightarrow U(q) = \sqrt{\sum_{i=1}^{n} \left(\frac{\partial q}{\partial x_i} U(x_i)\right)^2} \quad (4.8)$$

The calculations showed that the average uncertainties of average heat flux, surface temperature, and average heat transfer coefficient were $\pm$ 3, $\pm$ 5, and $\pm$ 5.4 %, respectively.

4.5 EXPERIMENTAL SETUP VALIDATION

In order to ensure the validity and reliability of the results of the experimental setup, several experiments were conducted at different volumetric flow rates, nozzle-to-surface distances, and heat fluxes. The experimental results were compared with a correlation that has an average error of 12%, proposed by Oliphant et. al [75], as shown below:

$$\overline{Nu_L} = 32.5\left(Re^{*0.51}\right) \quad (4.9)$$

The comparison between the present study and the proposed correlation showed that the average absolute deviation is found to be between $\pm$ 0.2 - 4 %, as shown in Figure 4.12. Additionally, the experimental results were compared with a correlation proposed by Rybiki and Mudawar [24]. The proposed correlation is derived based on the Sauter mean diameter and has an overall mean absolute error of $\pm$13.1%. The correlation used for comparison is expressed by the equation below:

$$Nu_{d32} = 4.7 Re_{d32}^{0.61} Pr_f^{0.32} \quad (4.10)$$

The comparison between the experimental results and the proposed correlation showed that the deviation ranged between 3.2-7.3% as shown in Figure 4.13.

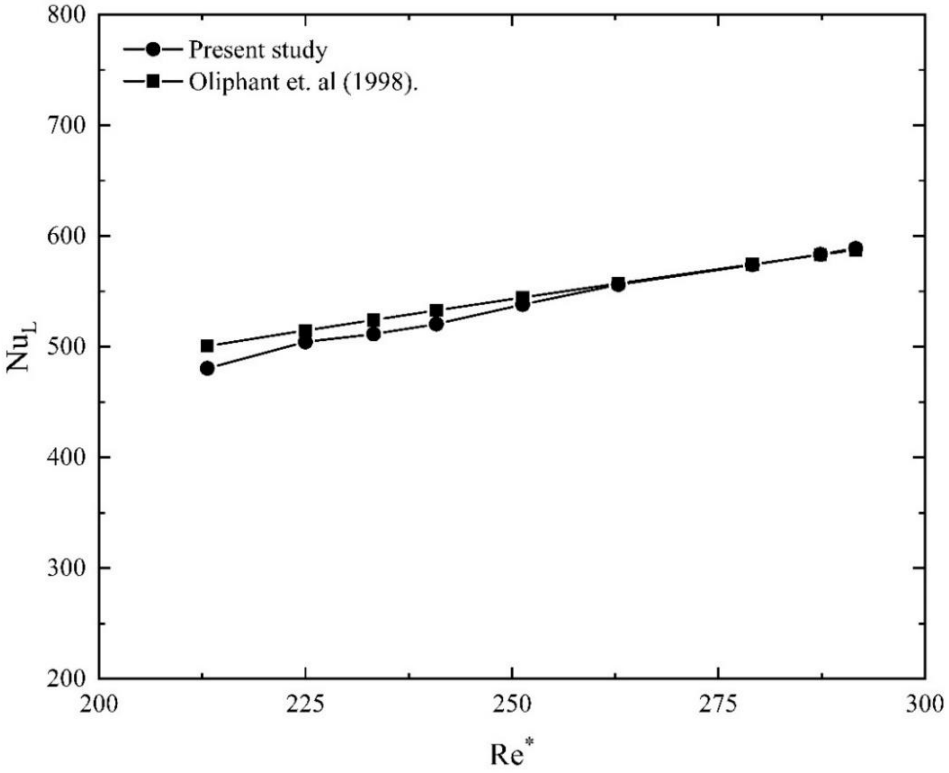

Figure 4.12 Comparison of the experimental results with Oliphant et. al [75].

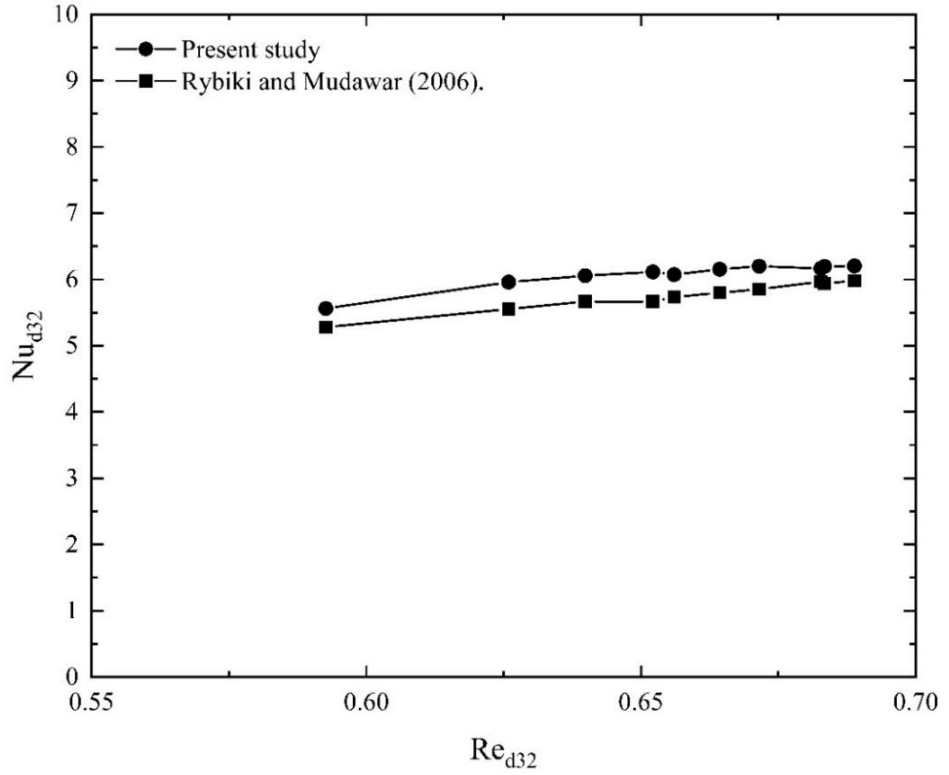

Figure 4.13 Comparison of the experimental results with Rybiki and Mudawar [24].

CHAPTER 5

EVALUATION OF SPRAY COOLING PERFORMANCE

In this chapter, the effect of operating conditions, such as volumetric flow rate, nozzle-to-surface distance, and temperature difference between the target surface and the working fluid, on the spray cooling performance was analyzed. A flat surface having a diameter of 15 mm was tested at volumetric flow rates of 115, 153, and 180 mL/min, and nozzle-to-surface distances of 8, 10, and 12 mm. The coolant inlet temperature, surface temperature, and chamber pressure were maintained at ~22 ℃,< 100 ℃, and atmospheric pressure, respectively. A full cone nozzle (TG 0.3, Spraying System Co.) was used as droplets generators to cool the target surface. The main objective of this study is to find the optimal economic thermal performance of a spray cooling system based on a new criterion, which considers the effect of heat transfer characteristics and consumed pumping power. All these parameters are discussed in the following sections:

5.1 THE INFLUENCE OF VOLUMETRIC FLOW RATE

Volumetric flow rate is one of the most influential parameters on the thermal performance of a spray cooling system. Figure 5.1 and Figure 5.2 show the influence of the volumetric flow rate on heat transfer characteristics, such as average heat flux and average heat transfer coefficient at a nozzle-to-surface distance of 10 mm, similar findings were reported by Abdulrazzaq et al [76] . It is clear from these figures that both heat flux and heat transfer coefficient increase proportionally as the volumetric flow rate of the coolant increases.

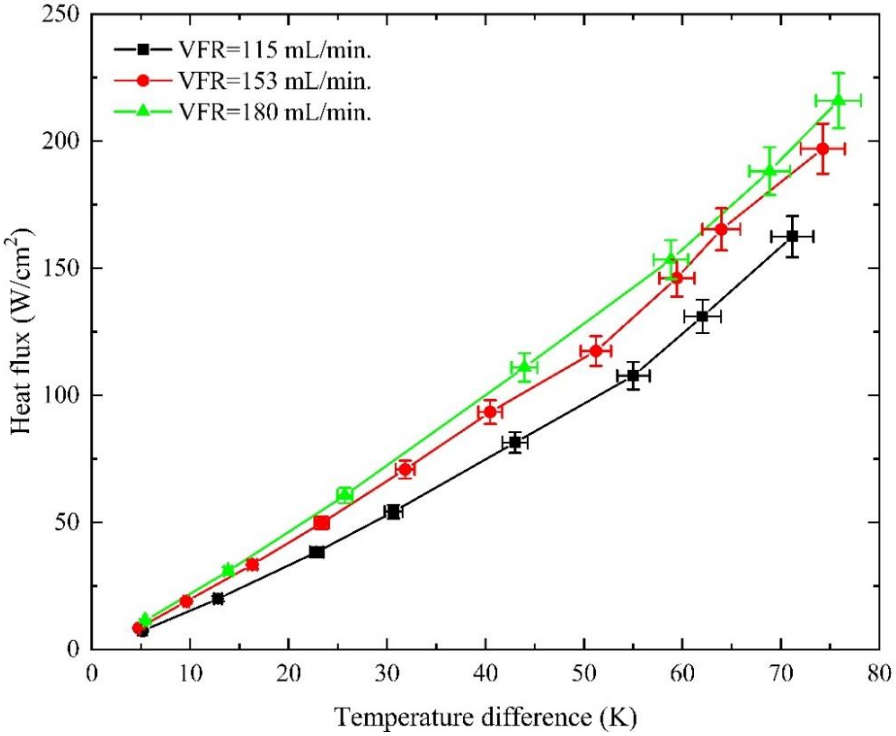

Figure 5.1 Effect of volumetric flow rate on heat flux at nozzle-to-surface distance of 10 mm.

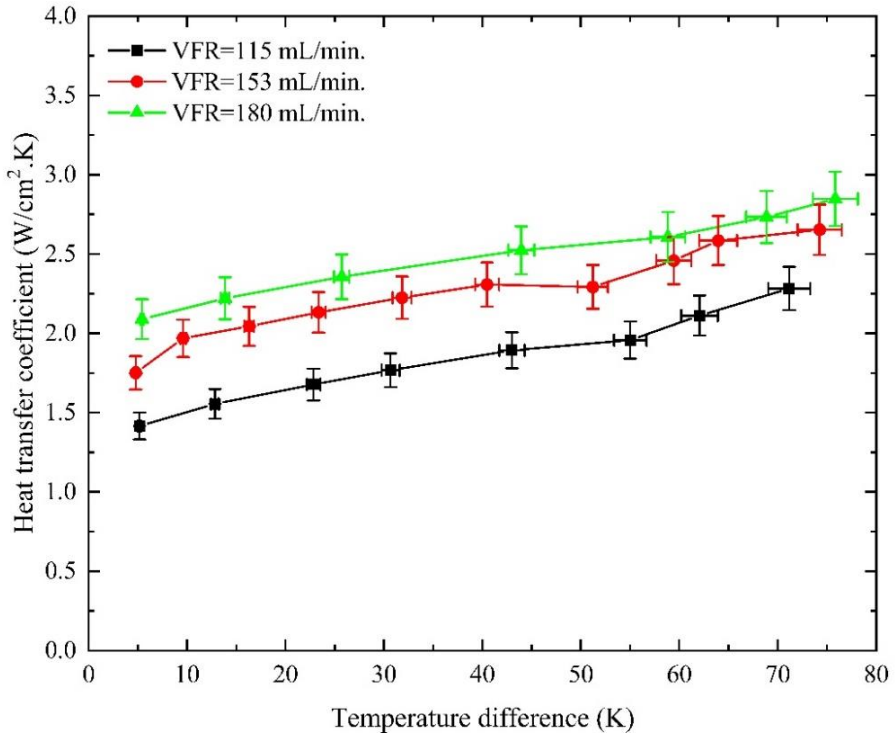

Figure 5.2 Effect of volumetric flow rate on average heat transfer coefficient at nozzle-to-surface distance of 10 mm.

Moreover, it was observed that at all volumetric flow rates, the heat transfer characteristics are enhanced as the temperature difference between the target surface and deionized water inlet temperatures increase. The increment of heat transfer characteristics with the increase of coolant volumetric flow rate mainly results from the increase in the pressure difference across the nozzle, as shown in Figure 5.3. Increasing nozzle differential pressure leads to an increase in the break-up forces. As a result, droplet flux increases and droplet size decreases, which increases the fluid surface area, also it speeds up droplets formation, and expands the spray angle, as shown in Figure 5.4 and eventually increases the spray impingement area. Moreover, it increases the droplet break-up velocity, which represents the droplet velocity at the nozzle's orifice; in other words, it increases the momentum of droplets. In addition, it increases droplet flux and decreases the Sauter mean diameter (SMD) of droplets. Figure 5.5 shows the relationship between the volumetric flow rates and droplet velocity, flux, and size.

In addition, spraying smaller droplets with high momentum forms a thinner liquid film on the target surface, especially in the impingement zone. Droplets with higher momentum increase the fluid velocity and the turbulence intensity over the target surface. Moreover, increasing the rate of droplet production agitates the boundary layer and ultimately increases the temperature gradient within the liquid film and reduces the thermal boundary layer thickness [55]. For the above reasons, spray cooling heat transfer performance is enhanced as the volumetric flow rate increases. Also, Figure 5.1 and Figure 5.2 show that the heat transfer characteristics increase as the temperature difference increase because of the change in the thermophysical properties of the working fluid. The thermophysical properties have a significant effect on thermal performance.

Increasing the temperature difference decreases the surface tension and the density of the working fluid decrease, and it increases the specific heat of the working fluid first.

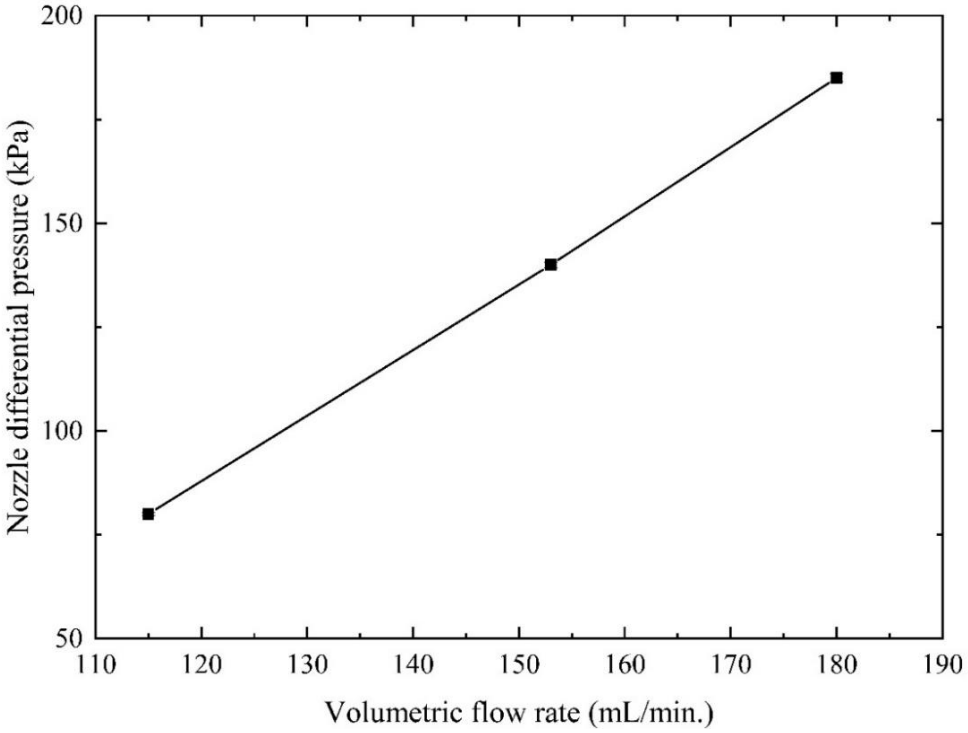

Figure 5.3 Nozzle differential pressure versus volumetric flow rate.

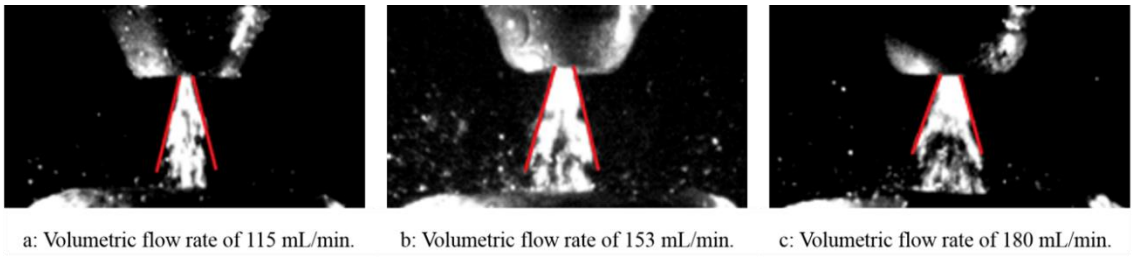

Figure 5.4 Flow visualization at volumetric flow rates.

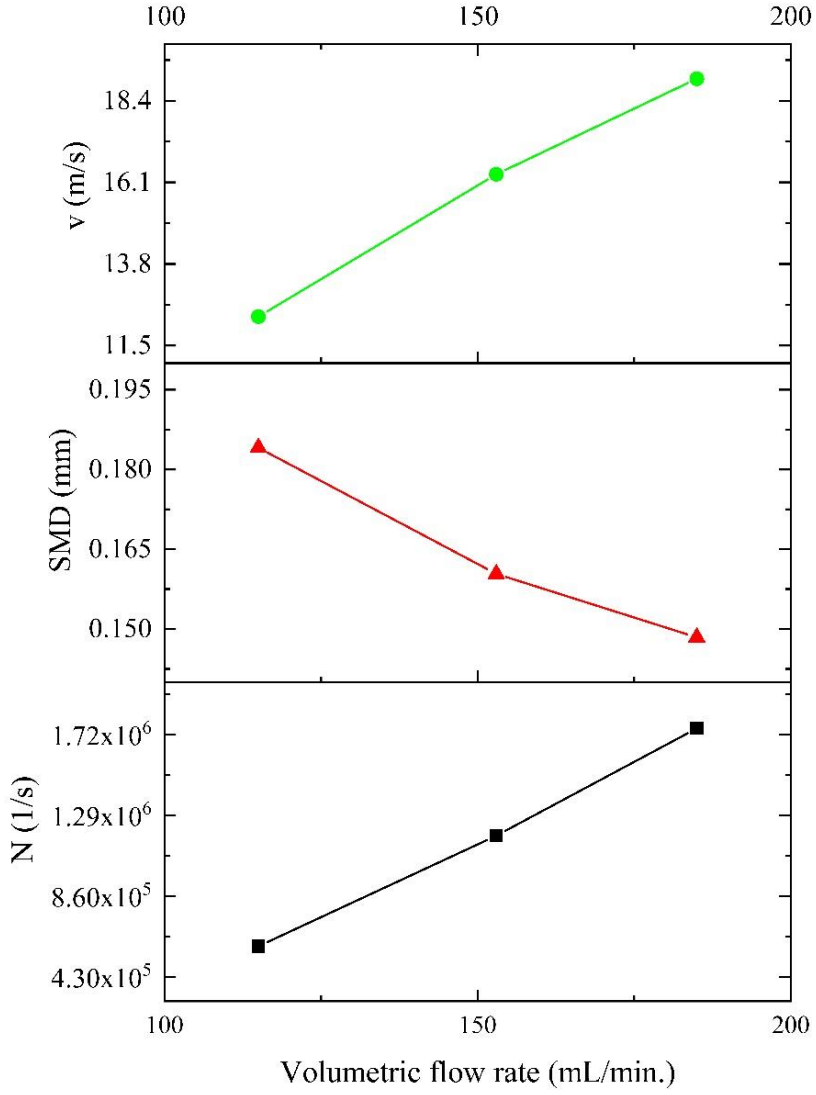

Figure 5.5 Effect of volumetric flow rate on droplet flux (N), Sauter mean diameter (SMD), and break-up velocity (v).

Additionally, to understand the effect of volumetric flow rate upon forces acting on a droplet before hitting the target surface, the forces were analyzed at different operating conditions, such as nozzle pressures and chamber temperatures. The analyses showed that increasing the nozzle differential pressure increases the drag force on a droplet proportionally due to an increase in the droplet velocity. It also decreases the buoyancy force acting on a droplet due to the decrease in the droplet size, as shown in Figure 5.6.

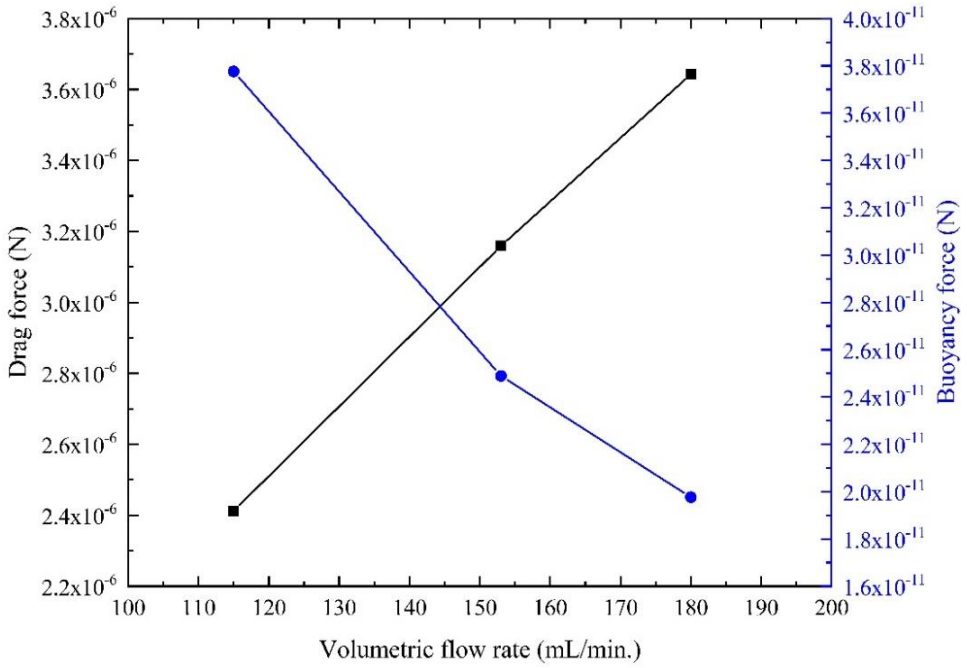

Figure 5.6 Relation between forces acting on a droplet before impacting the target surface at different volumetric flow rates.

Furthermore, the influence of chamber temperature, which depends on the surface temperature, on droplet diameter and velocity was studied at different operating conditions. The results showed that droplet size and velocity depend primarily on nozzle characteristics, such as inlet pressure and orifice diameter. Moreover, the effect of chamber temperature on both droplet size and velocity is negligible, as shown in Figure 5.7 and Figure 5.8; similar conclusions were reported by Salman and Khan [33]. The average deviations of droplet diameter and droplet break-up velocity at different chamber and surface temperatures ranged between $\pm$0.2 - 0.42%, and $\pm$0.17 - 0.75%, respectively.

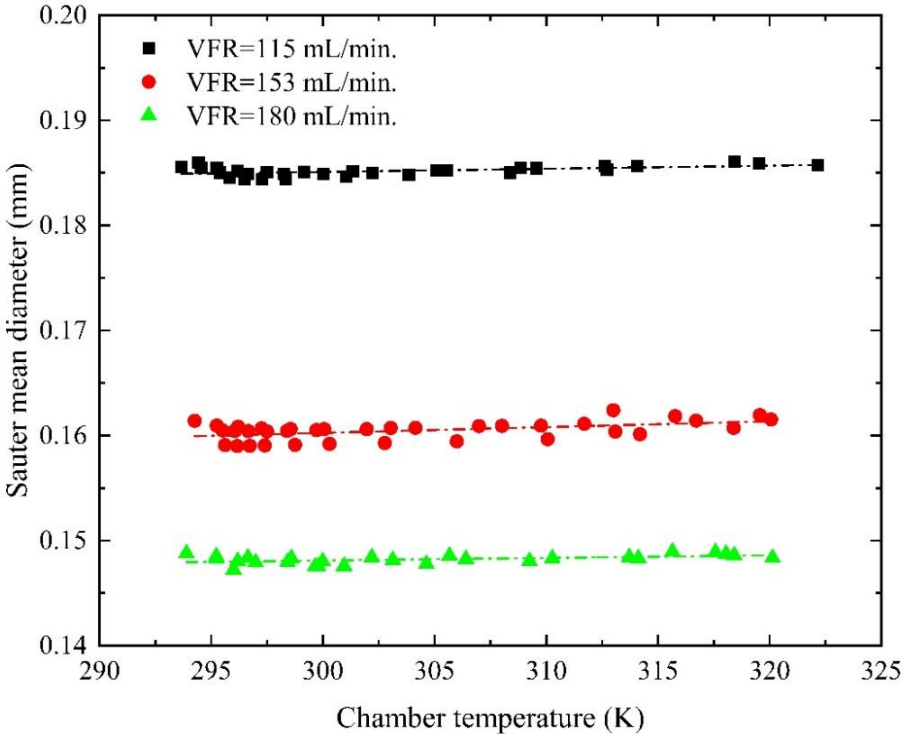

Figure 5.7 Effect of chamber temperature on droplet diameter.

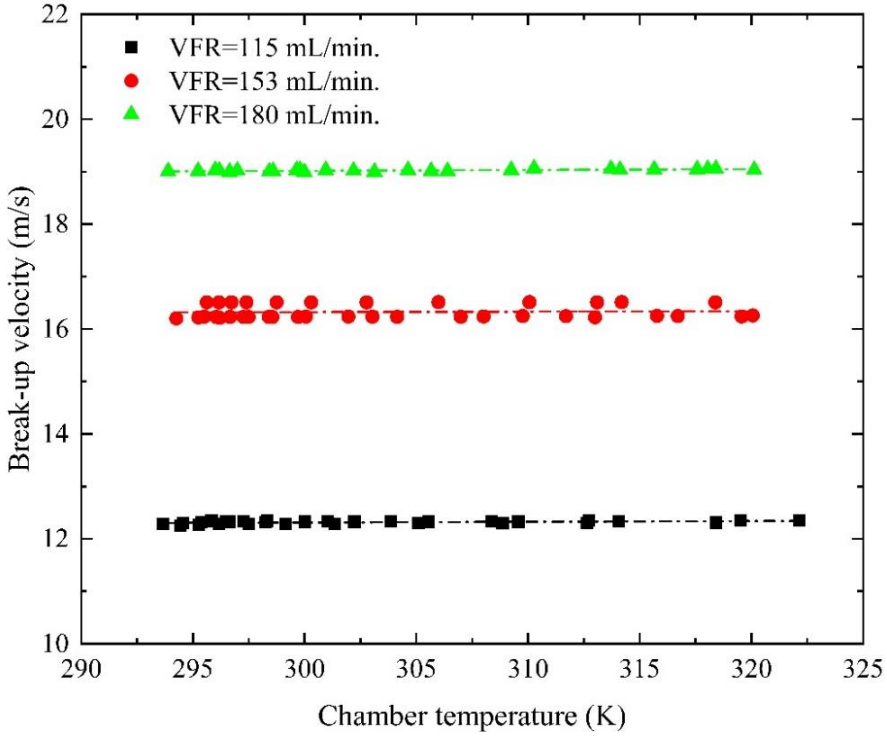

Figure 5.8 Effect of chamber temperature on droplet break-up velocity.

5.2 THE INFLUENCE OF NOZZLE-TO-SURFACE DISTANCE

Nozzle-to-surface distance is one of the passive heat transfer enhancement parameters in spray cooling systems. In this study, the effect of nozzle-to-surface distance was investigated to determine its influence on the heat transfer characteristics of spray cooling. Changing the nozzle-to-surface distance alters the spraying impingement area (thin-film area), thick film area, droplet formation, and droplet impact momentum. For instance, increasing the nozzle-to-surface distance increases the sprayed area decreases the thick film area, also, it increases the fluid surface area, and droplet momentum at the same time, as shown in Figure 5.9.

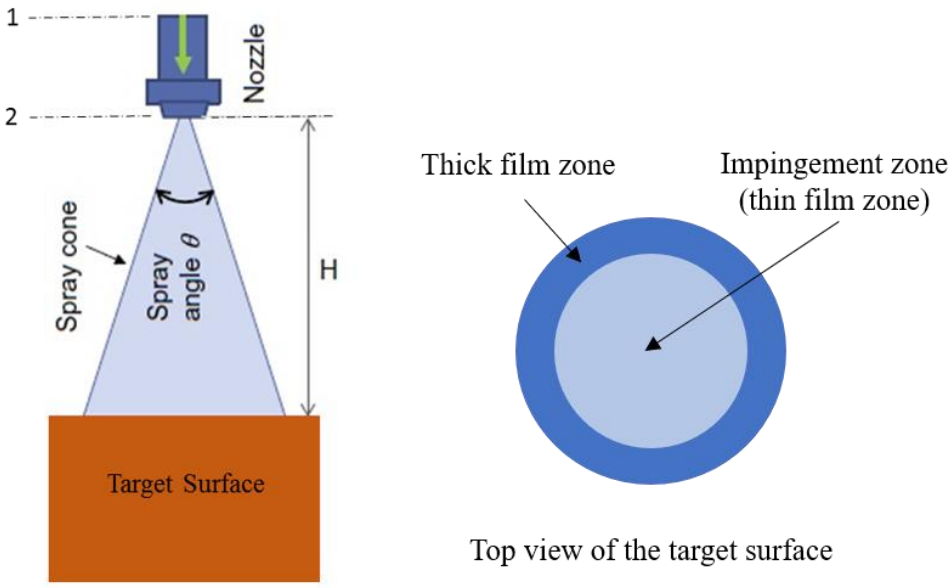

Figure 5.9 Schematic of spraying over a surface.

In this study, the nozzle-to-surface distance ranged between 8-12 mm at different operating conditions, such as volumetric flow rate and heat flux. The experimental results indicate that the nozzle-to-surface distance does not have a significant effect on spray cooling heat flux, but it does have an effect on the heat transfer coefficient at a volumetric flow rate of 115 mL/min, as illustrated in Figure 5.10 and Figure 5.11.

This effect is a result of the insignificant change in the spray impingement area, liquid film area, and droplet momentum. Also, it was observed that at temperature differences lower than 45 K, the highest heat transfer coefficient was achieved at the nozzle-to-surface distance of 12 mm, followed by 10 and 8 mm, respectively, due to the increase in the spray impingement area. Conversly at temperature differences higher than 45 K, the deviation between heat transfer coefficients can be neglected. It seems that at temperature differences higher than 45 K, the thermophysical properties of the coolant start playing a major role in the heat transfer process and minimize the effects of spray impingement and liquid film areas.

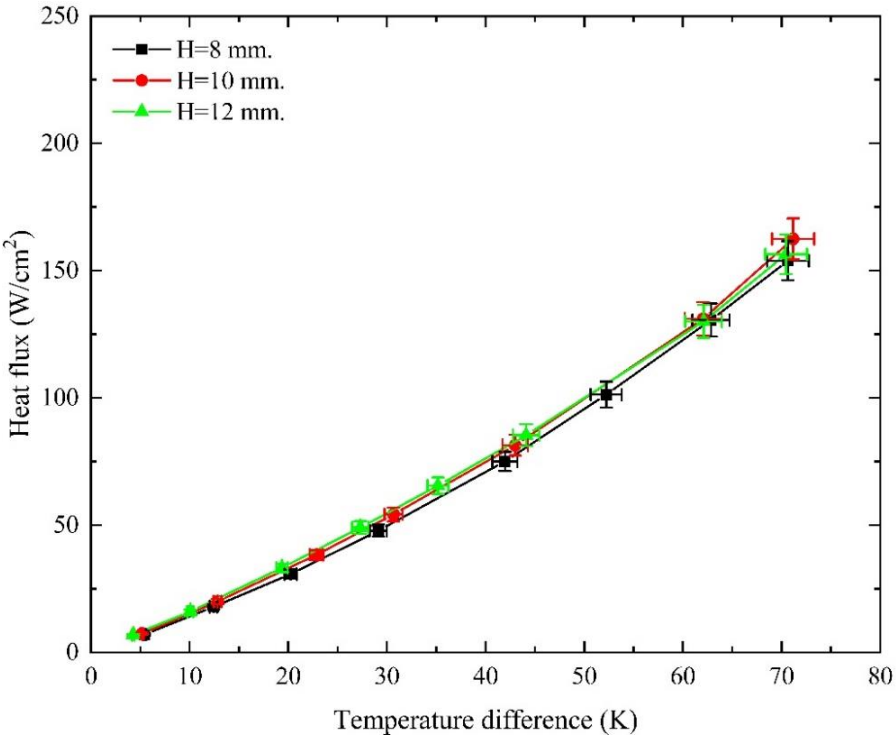

Figure 5.10 Effect of nozzle-to-surface distance on heat flux at a volumetric flow rate of 115 mL/min.

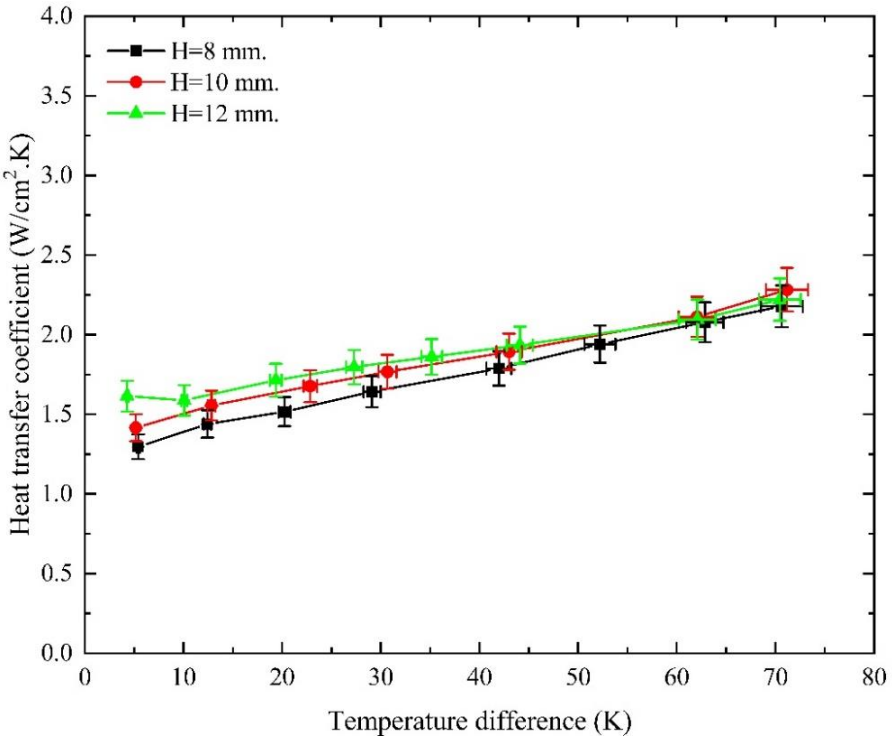

Figure 5.11 Effect of nozzle-to-surface distance on average heat transfer coefficient at a volumetric flow rate of 115 mL/min.

Whereas, at volumetric flow rates of 153 and 180 mL/min, nozzle-to-surface distance has a slight effect on the spray cooling heat flux and heat transfer coefficient, as shown in Figure 5.12 - Figure 5.15. However, the results showed that decreasing the nozzle-to-surface distance enhances the heat transfer characteristics; similar findings were reported by Salman et al., and Smakulski et al. [12, 25]. The effect of the nozzle-to-surface distance becomes greater at temperature differences higher than 45 K, as a result of the effect of the thermophysical properties of the deionized water.

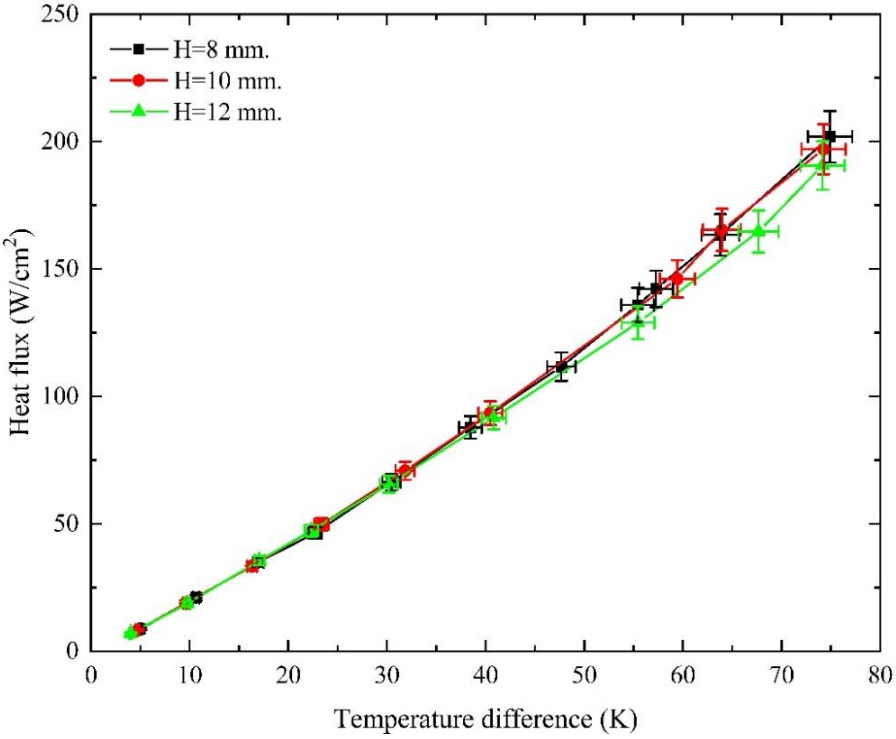

Figure 5.12 Effect of nozzle-to-surface distance on heat flux at a volumetric flow rate of 153 mL/min.

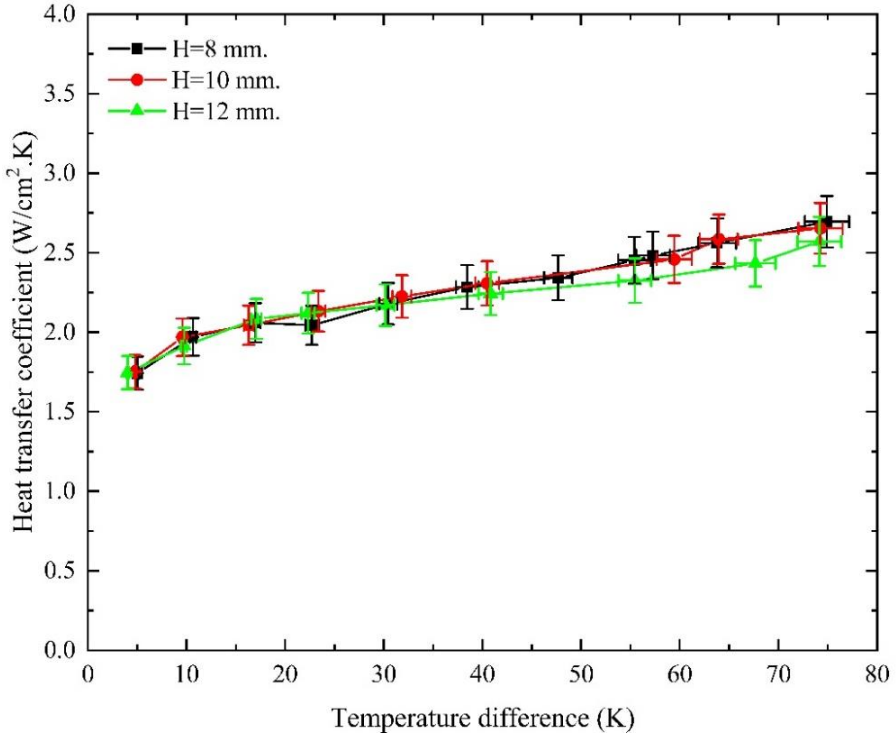

Figure 5.13 Effect of nozzle-to-surface distance on average heat transfer coefficient at a volumetric flow rate of 153 mL/min.

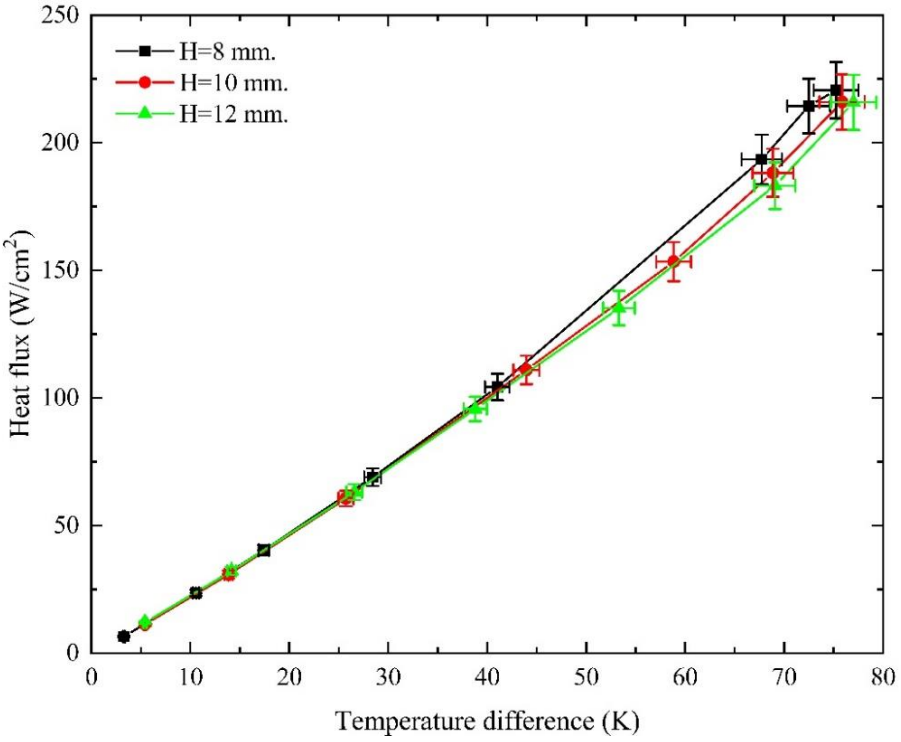

Figure 5.14 Effect of nozzle-to-surface distance on heat flux at a volumetric flow rate of 180 mL/min.

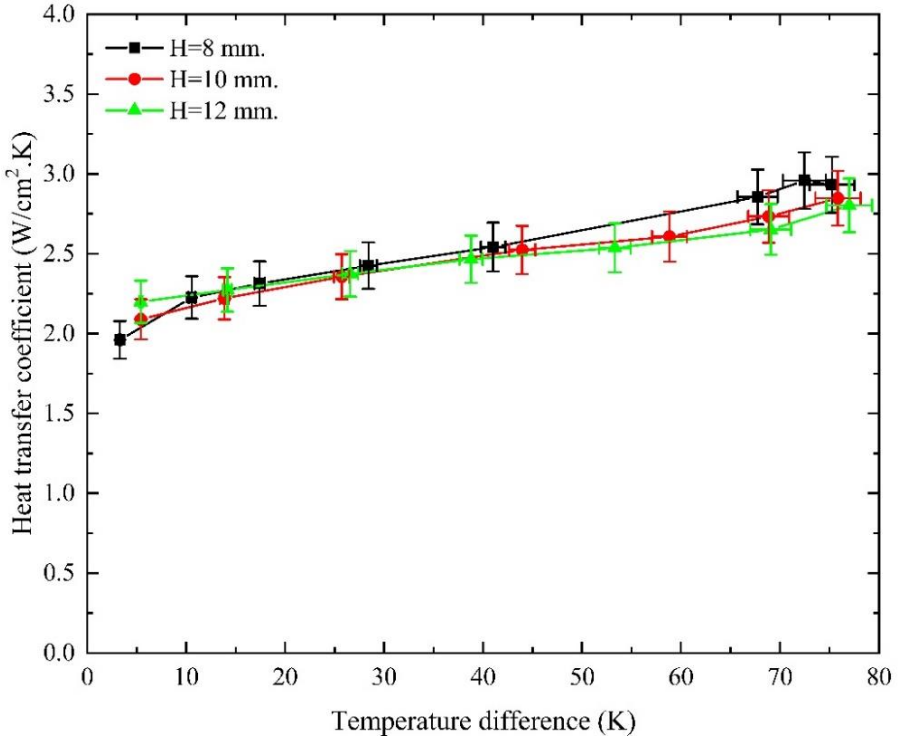

Figure 5.15 Effect of nozzle-to-surface distance on average heat transfer coefficient at a volumetric flow rate of 180 mL/min.

Furthermore, increasing the nozzle-to-surface distance reduces the droplet velocity and liquid film velocity over the surface due to the effects of forces acting on a droplet. Figure 5.16 shows the local droplet velocity at different volumetric flow rates; where the velocity decreases with increasing the nozzle-to-surface distance due to the impact of forces acting on a droplet, which increase linearly as the droplet path increases.

Also, it was observed that the percentage of reduction in droplet velocity, for the same nozzle-to-surface distance, increases with the increase of volumetric flow rate. This reduction is a result of an increase in the magnitude of the drag force on the droplet, which increases as the nozzle differential pressure increases. Also, it was found that drag force is the dominant force among other forces acting on a droplet, as explained in Figure 5.6.

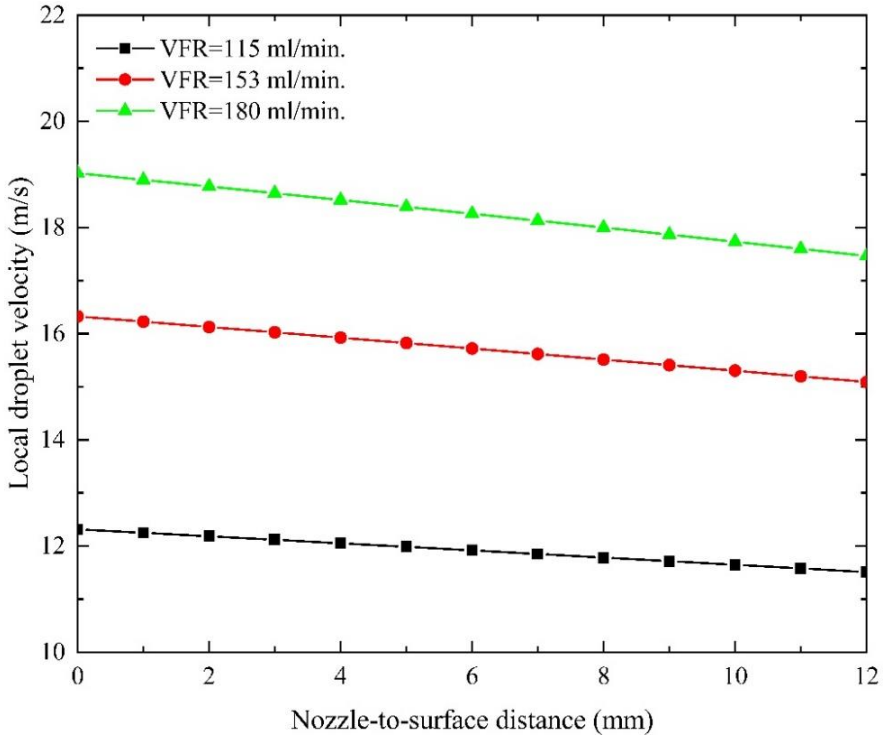

Figure 5.16 Local droplet velocity at volumetric flow rates.

5.3 PERFORMANCE EVALUATION CRITERION OF SPRAY COOLING

The results of the present study and previous works show that the thermal performance of spray cooling systems is enhanced as the coolant volumetric flow rate increases. In order to evaluate the spray cooling performance precisely, a new criterion was introduced to assess the spray cooling performance by taking the combined effect of heat transfer characteristics and consumed pumping power into account. This criterion is used to quantify the amount of heat removed per watt of pumping power, and it can be calculated by using the following expression:

$$\mathrm{PEC_{SC}} = \frac{Q_E}{\dot{V} \cdot \Delta p} \tag{5.1}$$

Figure 5.17 - Figure 5.19 indicate that improving the spray cooling thermal performance by increasing the volumetric flow rate is not an economical approach based on the new evaluation criterion $\mathrm{PEC_{SC}}$. The highest performance evaluation criterion of spray cooling was achieved at a volumetric flow rate of 115, followed by 153 and 180 mL/min, at all nozzle-to-surface distances. These findings mean that the amount of heat removed per watt of pumping power is inversely proportional to the coolant volumetric flow rate. This relationship is a result of the increase in the pumping power and the liquid thermal resistance over the surface. Therefore, enhancing the thermal performance of a spray cooling system by increasing the volumetric flow rate is not a good economic approach.

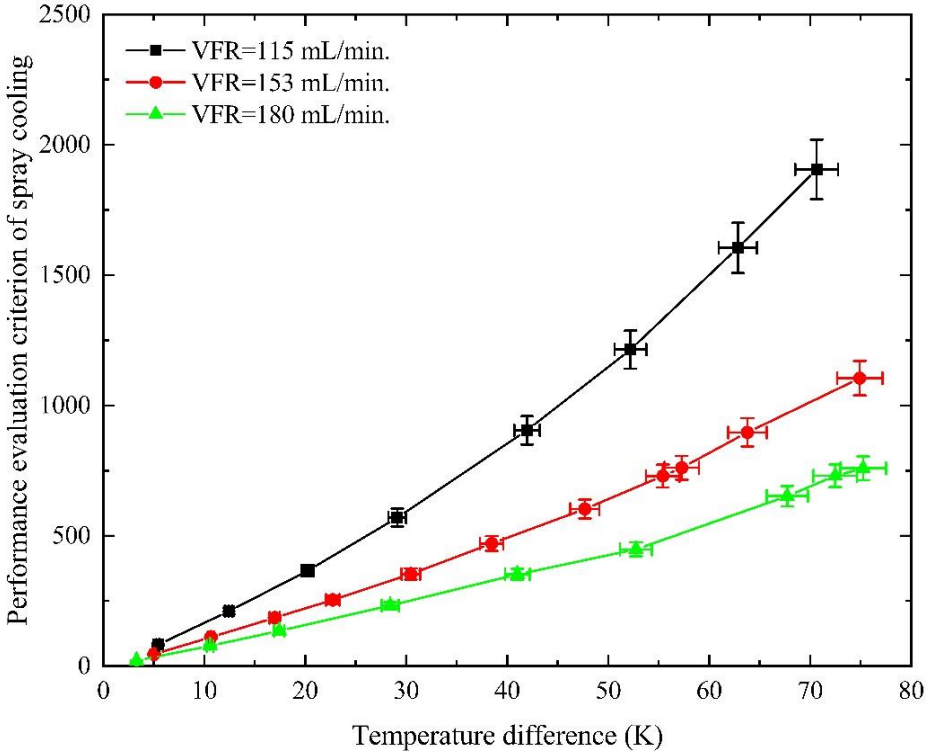

Figure 5.17 Performance evaluation criterion of spray cooling at different volumetric flow rates and a nozzle-to-surface distance of 8 mm.

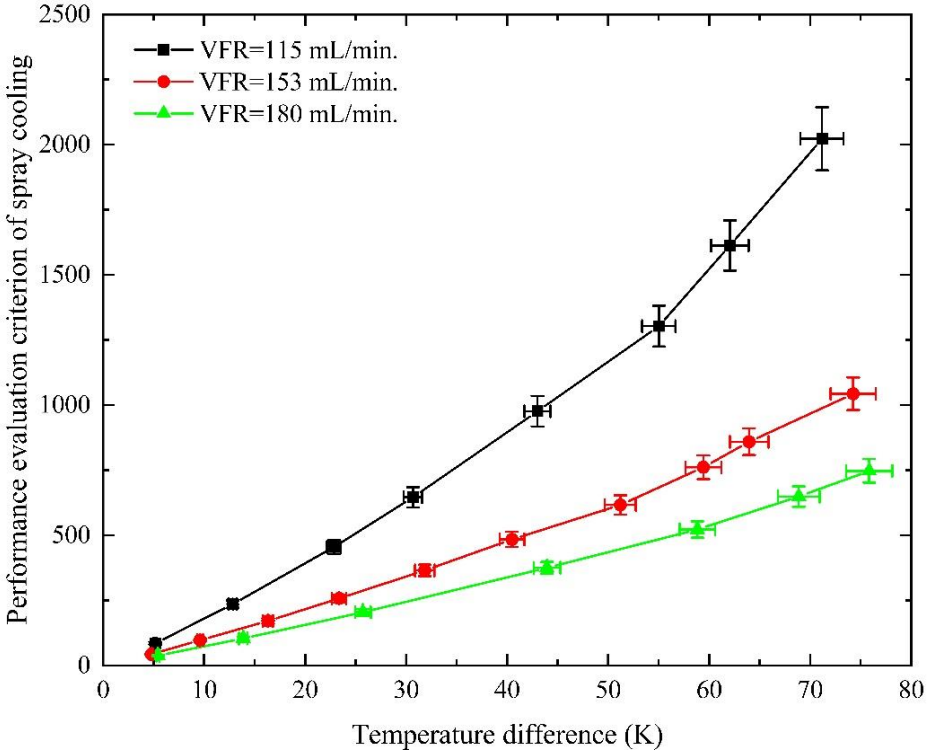

Figure 5.18 Performance evaluation criterion of spray cooling at different volumetric flow rates and a nozzle-to-surface distance of 10 mm.

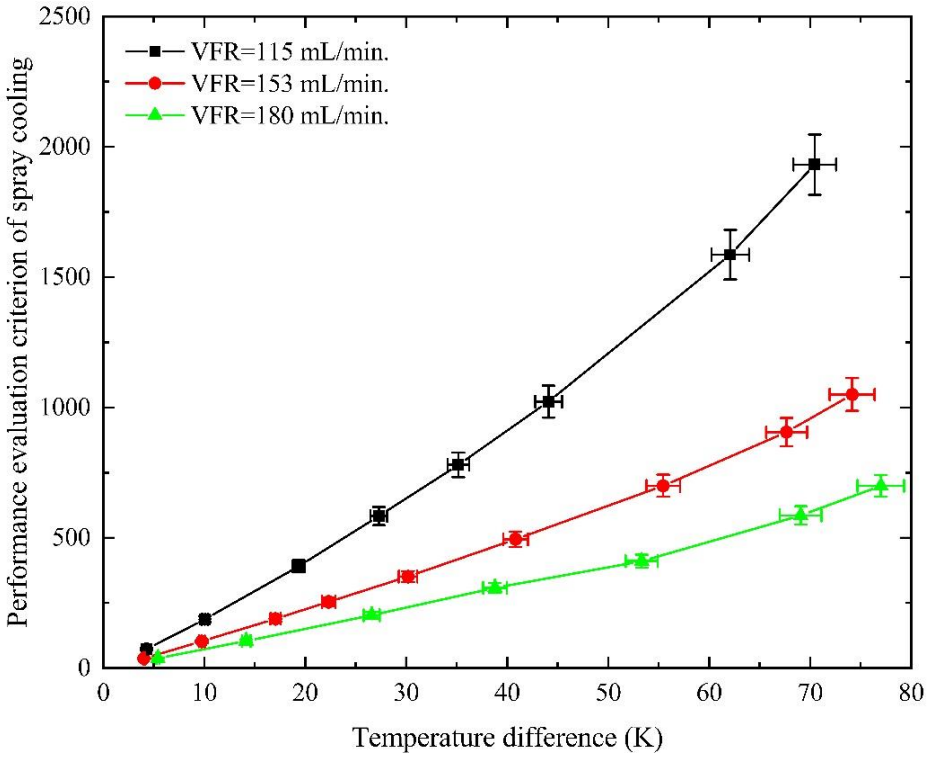

Figure 5.19 Performance evaluation criterion of spray cooling at different volumetric flow rates and a nozzle-to-surface distance of 12 mm.

5.4 SUMMARY

The influence of spray parameters, such as volumetric flow rate and nozzle-to-surface distance on the thermal performance of a plain surface were investigated experimentally. A plain surface was tested at volumetric flow rates ranging between 115-180 mL/min and nozzle-to-surface distances ranging between 8-12 mm. Chamber pressure and deionized water inlet temperature were kept constant approximately at atmospheric pressure and 22℃, respectively. The following conclusions can be drawn:

1. The heat transfer characteristics, such as heat flux and heat transfer coefficient, are enhanced as the volumetric flow rate increases due to the increase in droplet flux and velocity, as well as the decrease in droplet size.
2. The chamber temperature has a negligible effect on droplet characteristics, such as size and break-up velocity.

3. The influence of nozzle-to-surface distance on spray cooling performance depends on the volumetric flow rate and temperature difference. Decreasing the distance between the nozzle and the target surface enhances the thermal performance as both the volumetric flow rate and temperature difference increase.
4. Enhancing the thermal performance of a spray cooling system is not a good economical option based on the performance evaluation criterion of spray cooling (PEC_{SC}).

CHAPTER 6

NUMERICAL MODELING OF SPRAY COOLING

In this chapter, details of the numerical model and computational fluid dynamics solver will be provided and discussed elaborately. A three-dimensional multi-phase model is created in STAR-CCM+, 12.04.010-R8 and used to simulate the heat transfer process in the spray cooling system and to provide some more insights into the heat flow mechanism that is involved in spray cooling systems. The modeling and solving steps are explained in detail as below.

6.1 NUMERICAL METHODS AND COMPUTATIONAL DOMAIN

Simulating the entire actual spray chamber is difficult due to the size of the chamber and the complexity of the numerical model. Therefore, the central part of the actual chamber was selected as a computational domain based on flow visualization in order to consider the effects of sprayed droplets and splash rate on the flow field. The computational domain consisted of solid and fluid regions, and it was created using the 3-D CAD module within STAR-CCM+. A solid full cone nozzle with a spray cone angle of 50° was set up within the fluid region with an adjustable nozzle-to-surface distance. Figure 6.1 and Table 6.1 show a 3D CAD view of the computational domain and the dimensions.

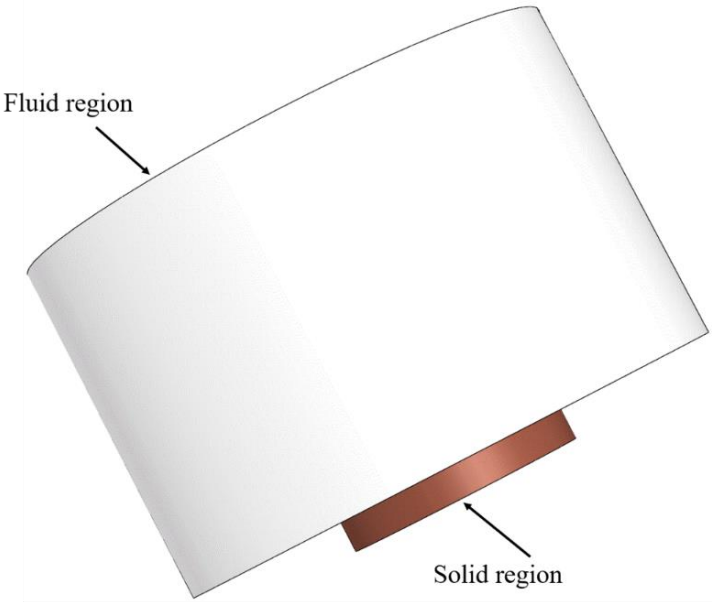

Figure 6.1 3D CAD view of the computational domain.

Table 6.1 Dimensions of the computational domain.

Region	**Height (mm).**	**Diameter (mm).**
Solid	4	15
Fluid	22	35

The following assumptions were established to simplify the governing equations:

1. Constant thermo-physical properties.
2. No slip boundary condition on the walls.
3. No phase change.
4. Laminar flow within the fluid film.

6.2 GOVERNING EQUATIONS

6.2.1 CONTINUOUS PHASE (AIR)

The continuous phase was treated as unsteady, incompressible, and turbulent flow. 3D time-averaged Naiver-Stokes equations based on the standard $k-\varepsilon$ turbulence model

was used to study the effect of droplets on air flow. The conservation equations of mass, momentum, and energy of the continuous flow (air) are expressed as follows [38]:

Continuity equation:

$$\frac{\partial \rho}{\partial t} + \frac{\partial (\rho u_j)}{\partial x_j} = S_m \tag{6.1}$$

Momentum equation:

$$\frac{\partial (\rho u_j)}{\partial t} + \frac{\partial}{\partial x_i}\left(\rho u_i u_j\right) = \rho \overrightarrow{g_j} - \frac{\partial P}{\partial x_j} + \frac{\partial \tau_{ij}}{\partial x_i} + F_j \tag{6.2}$$

Where τ_{ij} is the stress tensor defined as:

$$\tau_{ij} = \mu\left(\frac{\partial u_i}{\partial x_j} + \frac{\partial u_j}{\partial x_i} - \frac{2}{3}\delta_{ij}\frac{\partial u_k}{\partial x_k}\right) \tag{6.3}$$

Energy equation:

$$\frac{\partial (\rho C_P T)}{\partial t} + \frac{\partial}{\partial x_i}(\rho C_P u_i T) = \frac{\partial}{\partial x_i}\left(\lambda_{eff}\frac{\partial T}{\partial x_i}\right) + \mu\Phi + S_h \tag{6.4}$$

Where S_m,F_j , and S_h are the source terms to include the effect of the Lagrangian-phase on air. The terms $\mu\Phi$ and λ_{eff} in the energy equation refer to heat dissipation and effective heat conductivity, respectively.

6.2.2 DISCRETE PHASE (water droplets)

In spray cooling, droplets are generated when a liquid is pumped through a small orifice, the liquid is scattered into fine droplets with high momentum [55]. These droplets move in a trajectory through the air, and the interaction between droplets and air depends on mass, momentum, and energy transfers between the droplets and their environment. Newton's second law governs the droplet motion through the air, and can be written as [77] :

$$m_d \frac{d(V_d)}{dt} = F_D + F_G \tag{6.5}$$

Where m_d is the droplet mass, V_d is the droplet velocity vector, F_D is the drag from the gas flow on the droplet, and F_G is the gravity force. The drag force acted on a spherical droplet can be calculated from the following expression [64]:

$$F_D = \frac{1}{2} C_D \rho A_d V_r^2 \tag{6.6}$$

Liu dynamic drag coefficient was used to calculate the drag of water droplets on their distortion under the action of aerodynamic forces, as shown in the following expression:

$$C_{D,sphere} = \begin{cases} \frac{24}{Re_p}\left(1 + \frac{1}{6} Re_d^{2/3}\right) & Re_d \leq 1000 \\ 0.424 & Re_d > 1000 \end{cases} \tag{6.7}$$

6.2.3 FLUID FILM

When droplets with potential momentum impact a solid surface, they burst on the surface and form a liquid film; this film plays a major role in heat and mass transfer processes. The conservation equations of mass, momentum, energy, and species, all of which govern the behavior of fluid film, are expressed as follows [64]:

Continuity equation:

$$\frac{d}{dt}\int_V^{\cdot} \rho_f dV + \int_A \rho_f \left(v_f - v_g\right).da = \int_V \frac{S_m}{h_f} dV \tag{6.8}$$

Where, ρ_f is the film density, v_f is the film velocity, v_g is the grid velocity, h_f is the film thickness, S_m is the mass source/sink per unit area, and the f denotes the fluid film values.

Momentum equation:

$$\frac{d}{dt}\int_V \rho_f v_f dV + \int_A \rho_f v_f \left(v_f - v_g\right).da = \int_V T_f.da - \int_A p_f.da + \int_V \left(\rho_f f_b + \frac{S_m}{h_f}\right) dV \tag{6.9}$$

Where, p_f is the pressure, f_b is the body force (for example, gravity or the pseudo-force in a moving reference frame), and T_f is the viscous stress tensor within the film.

Energy equation:

$$\frac{d}{dt}\int_V \rho_f E_f dV + \int_A \left[\rho_f H_f \left(V_f - V_g\right) + V_g p_f\right].da = \int_A q"_f.da - \int_A T_f.V_f da +$$

$$\int_V f_b.V_f dV + \int_V \frac{S_e}{h_f} dV \qquad (6.10)$$

where E_f is the film total energy, H_f is the total film enthalpy, $q"_f$ is the film heat, and S_e is the energy source/sink term per unit film area.

The species mass conservation equation of species i is:

$$\frac{d}{dt}\int_V \rho_f Y_{i,f} dV + \int_A \rho_f \left(v_f - v_g\right) Y_{i,f}.da = \int_A \left(\frac{\mu}{\sigma}\right) \nabla Y_{i,f} da + \int_V \frac{S_{m,i}}{h_f} dV \qquad (6.11)$$

Where $Y_{i,f}$ is the mass fraction of species i , and σ is the molecular Schmidt number. The quantity $S_{m,i}$ is the mass source or sink for species i.

6.3 BOUNDARY AND INITIAL CONDITIONS

The initial conditions for liquid film thickness, surface temperature, chamber temperature, and chamber pressure are 0 mm, 334 K, 300 K, and 101.325 kPa, respectively. The boundary conditions of the computational domain and the operating conditions are shown in Figure 6.2 and Table 6.2.

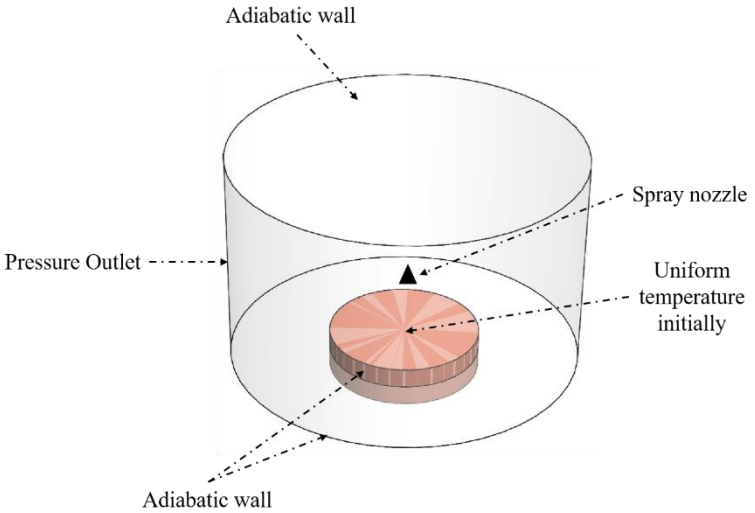

Figure 6.2 Computational boundary conditions.

Experimental data of a previous work conducted by Salman and Khan [33] was used to evaluate and validate the simulation results. The experiment was conducted to study the thermal performance of spray cooling at different operating conditions. A horizontal plain copper surface with a diameter of 15 mm was examined within the non-boiling regime. The droplet characteristics, such as droplet velocity and diameter were calculated based on the experimental conditions, such as nozzle differential pressure, orifice diameter, volumetric flow rate, fluid inlet temperature, and the corresponding thermophysical properties, using equations (3.1 and 3.2).

Table 6.2 Experimental operating conditions used to validate the numerical model.

Case No	Droplet velocity (m/s)	Volumetric flow rate (mL/min)	Droplet diameter (m)	Nozzle to surface distance (mm)
1	12.4	115	$1.8585*10^{-4}$	8
2				10
3				12
4	16.43	153	$1.6111*10^{-4}$	8
5				10
6				12
7	19.9	180	$1.4958*10^{-4}$	8
8				10
9				12

6.4 NUMERICAL SOLVING PROCEDURE AND CONVERGENCE CRITERIA

To simulate the spray cooling heat transfer process with appropriate boundary and initial conditions, STAR-CCM+, 12.04.010-R8 was utilized as a computational fluid dynamics solver. Eulerian-Lagrangian approach was utilized to describe the continuous phase (air) and the discrete phase (water), respectively. The Lagrangian phase is solved by tracking the droplet exchange of mass, momentum, and energy with the Eulerian phase. The realized $k-\varepsilon$ model is applied to describe the turbulence characteristics of the spray flow field because this model provides reasonable solutions in terms of accuracy and computational time [37]. Additionally, Bai-Gosman wall impingement model was activated to study the interaction between droplets and a solid surface.

The liquid-film is formed on the solid surface, resulting from impingement of droplets, was solved in the laminar Eulerian framework. The following models are used to define the fluid type, flow modeling, energy modeling, turbulence modeling, thermophysical properties, discretization schemes, and simulation conditions [63]:

- Reynolds-Averaged Navier-Stokes.
- Turbulence model ($k-\varepsilon$).
- Unsteady implicit simulation.
- Flow loop: Second-order upwind convection scheme.
- Energy loop: Second-order scheme.
- Gravity.
- Coupled energy model.
- Coupled flow model.
- Single-phase fluid (H_2O) with no phase change.

- Two-way coupling between continuous phase (gas phase) and discrete phase (droplet).
- Bai-Gosman wall impingement model.
- Taylor Analogy Breakup (TAB) model.
- Multi-phase interaction model.
- Water injector defined, with solid cone spray.
- Mass flow rate from the spray distributed uniformly throughout the impingement.
- Spray droplet size distribution function: Rosin-Rammler.

The governing equations of a model have been solved simultaneously until convergence is reached. In this study, the convergence criterion was set to be reached when the residual of continuity and energy become $< 10^{-4}$ and $< 10^{-6}$, respectively.

6.5 GRID GENERATION AND GRID INDEPENDENCE TEST.

Meshing is an important step of computational fluid dynamics analysis; inappropriate mesh effects on the accuracy of the results and on the computational time [63]. A trimmed cell mesh with automatic surface repair was selected to discretize the computational domain as it is suitable for electronics cooling simulation and provides a high-quality grid for simple and complex geometries [64]. Also, prism layers were included in the film region at the interface between the solid and liquid film. A grid independence test was performed using a different number of cells within the computational domain, such as 90 k, 180 k, and 360 k, as shown in Figure 6.3. The comparison showed that there is no significant difference in the predicted heat transfer coefficient between 180 k and 360 k, as illustrated in Figure 6.4. Therefore, a mesh of 180 k was selected for use in all simulation cases.

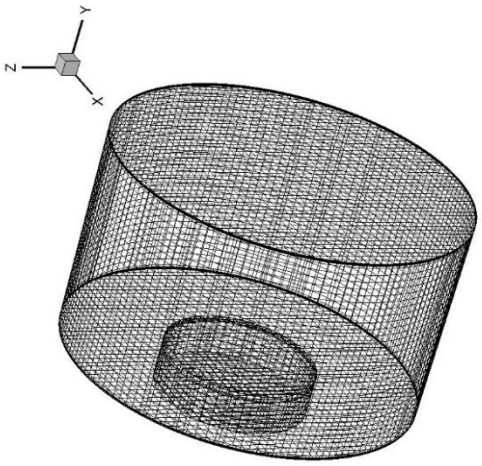

Number of cells is 90k.

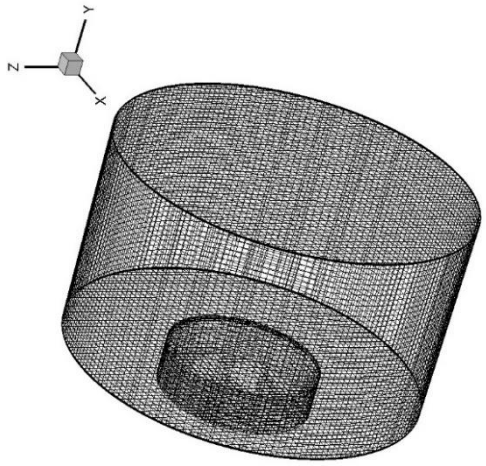

Number of cells is 180k.

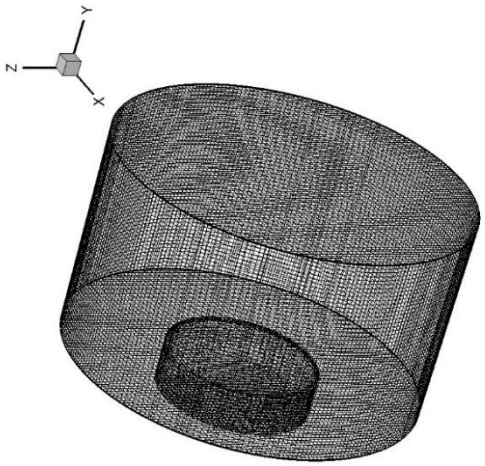

Number of cells is 360k.

Figure 6.3 Views of meshes of the computational domain.

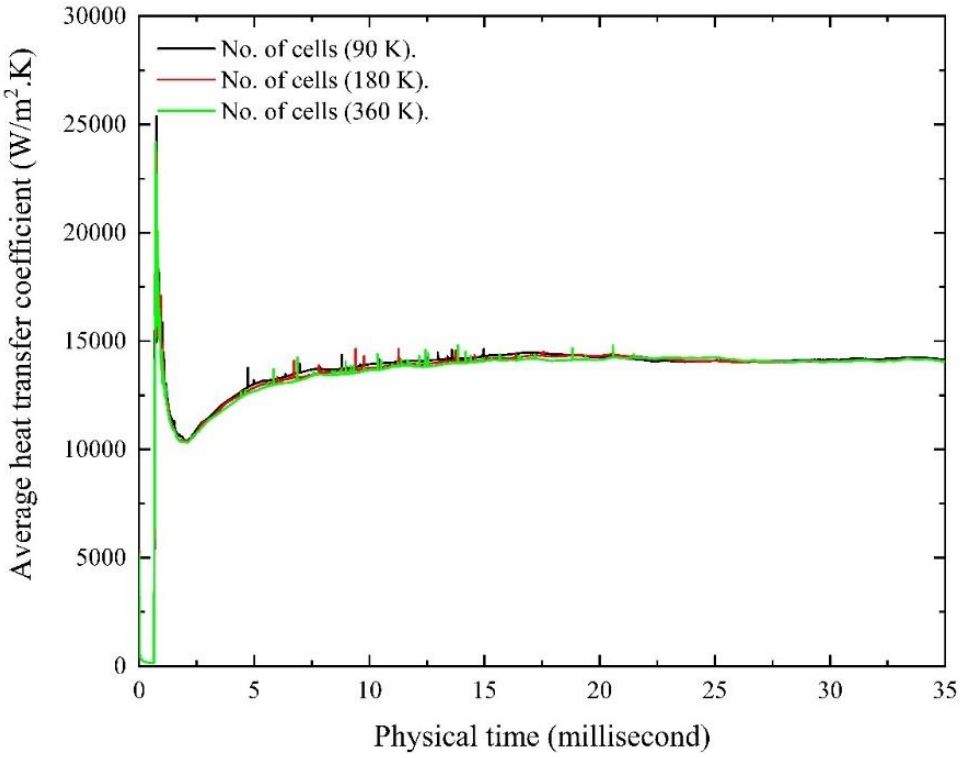

Figure 6.4 Average heat transfer coefficient for three different mesh sizes; 90k, 180k, and 360k.

6.6 NUMERICAL MODEL VALIDATION

After ensuring the grid independence and applying assumptions, experimental operating conditions were used as boundary conditions. Figure 6.5 shows a three-dimensional simulation of liquid film formation on a flat surface. The results of this simulation showed that when the liquid film is formed completely on the surface, the average heat transfer coefficient becomes constant as shown in Figure 6.6, where the average deviation is$\pm$ 0.3%. Therefore, the time solution for each case was set to be 30 milliseconds to investigate the effect of spraying parameters on liquid film characteristics.

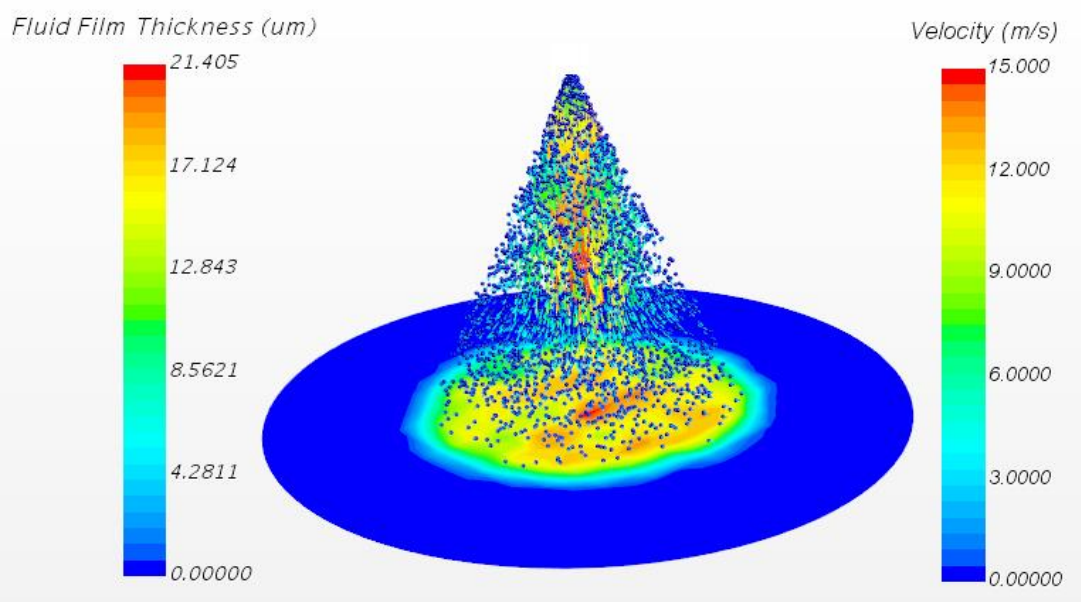

Figure 6.5 Three-dimensional simulation of spray-liquid film formation.

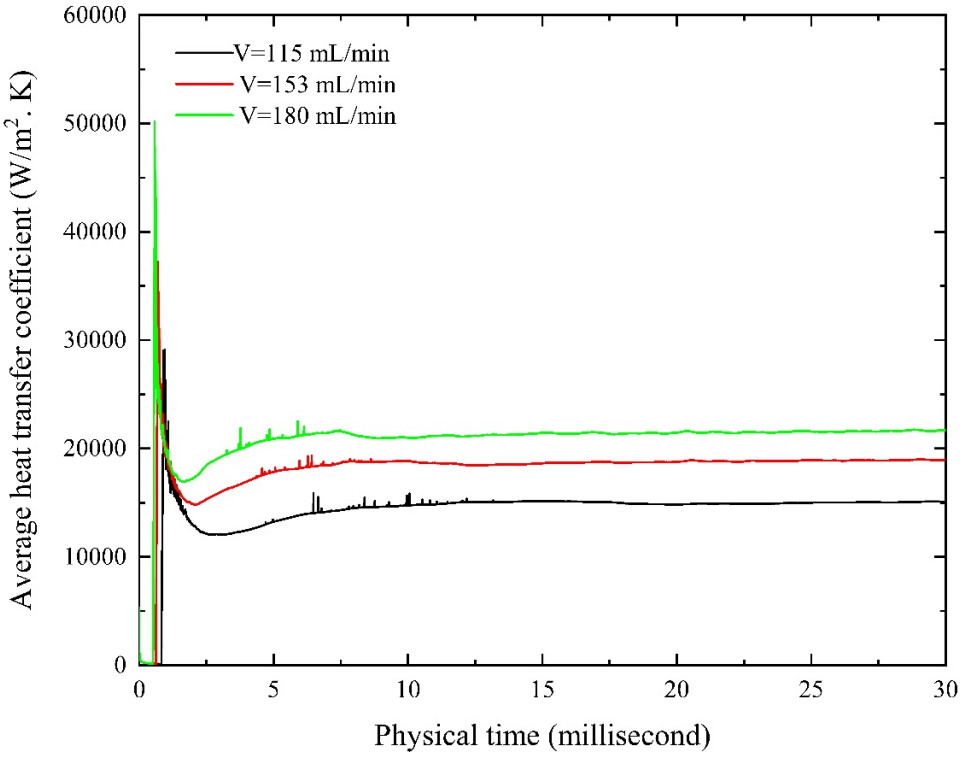

Figure 6.6 Average transient heat transfer coefficient.

In order to evaluate the accuracy and reliability of the numerical model, the predicted results were compared with experimental data at the same operating conditions. The comparison was conducted at different volumetric flow rates and nozzle-to-surface

distances. The comparison showed a satisfactory agreement between the predicted and experimental average heat transfer coefficients, as shown in

Table 6.3, where the absolute average deviation is ±12.7%.

Table 6.3 Comparison between experimental and numerical average heat transfer coefficients.

Case No.	Experimental average heat transfer coefficient (W/m^2. K)	Numerical average heat transfer coefficient (W/m^2. K)	Absolute deviation(±%)
1	16786	14184.1	15.5006
2	17678.5	15000.6	15.148
3	18228	15601.4	14.40997
4	21827	17574.9	19.48087
5	21852.5	18883.3	13.5876
6	21455	19691.9	8.217665
7	24227	20065.9	17.17559
8	23903.5	21529	9.933859
9	24087.5	24126.3	0.160955

6.7 INFLUENCE OF VOLUMETRIC FLOW RATE

The volumetric flow rate is the most influential parameter on spray cooling thermal performance [31]. Therefore, its influences on the spatial distribution of heat transfer coefficient, liquid film thickness, surface temperature, and liquid film velocity were investigated at volumetric flow rates of 115, 153, and 180 mL/min, as well as a nozzle-to-surface distance, surface temperature, and chamber pressure of 10 mm, 334 K, and atmospheric pressure, respectively. Figure 6.7 shows that the spatial heat transfer coefficient increases with increasing coolant volumetric flow rate, especially in the

impingement zone. Also, it shows that the spray impingement zone is more sensitive than the liquid film to the volumetric flow rate. At the same operating conditions, an experimental study was conducted by Salman et al. [57], which showed that the average heat transfer coefficient increases as the volumetric flow rate increases.

The increment of heat transfer coefficient results from the increase in droplet velocity and flux combined with decrease in the droplet size, which leads to an increase in the coolant surface area. Also, increasing the mass flux increases the turbulence intensity on the surface, which enhances the heat exchange between the solid surface and the cooling medium. Moreover, increasing the volumetric flow rate provides a thinner liquid film on the target surface, as shown in Figure 6.8 due to the fact that, at higher volumetric flow rate higher inertia of the fluid flow results thin boundary layers [78], and eventually, reduces the thermal resistance and enhances the overall thermal performance.

Also, it is shown that velocity within the liquid film increases as the volumetric flow rate increases, especially in the impingement zone and the interface between the thin and thick fluid film regions as shown in Figure 6.9. Moreover, the maximum velocity occurs at the spray impingement boundaries. Moreover, the numerical simulation showed that droplets velocity in the main flow stream is greater than in the other flow fields, as shown in Figure 6.10.

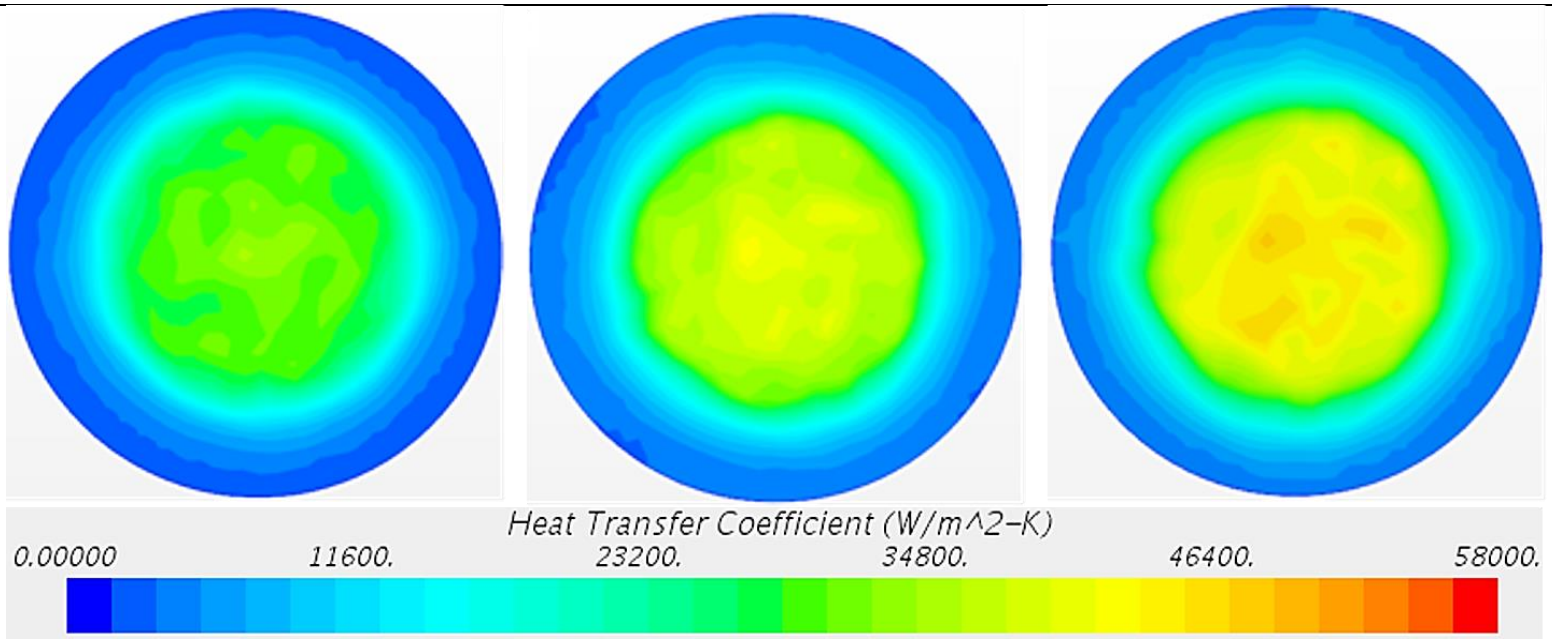

Volumetric flow rate of 115 mL/min.	Volumetric flow rate of 153 mL/min.	Volumetric flow rate of 180 mL/min.

Figure 6.7 Spatial heat transfer coefficient at different volumetric flow rates and a nozzle-to-surface distance of 10 mm.

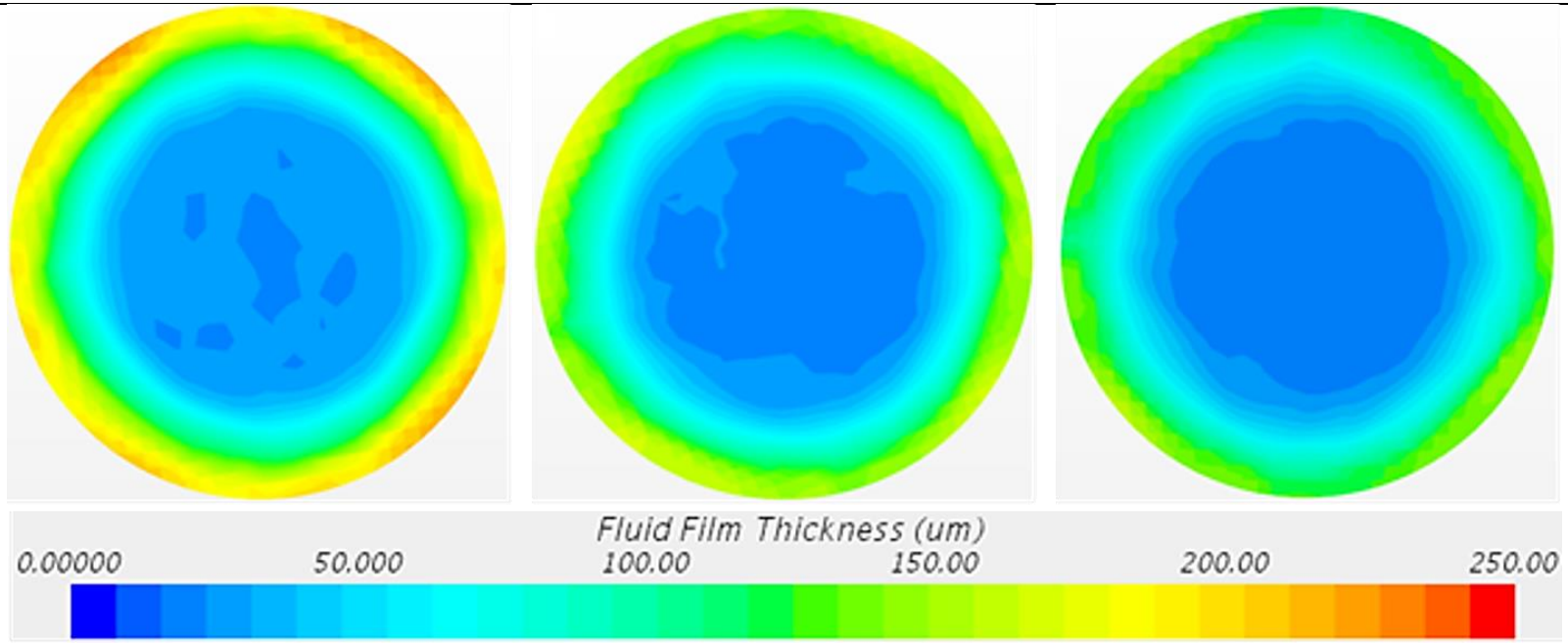

Volumetric flow rate of 115 mL/min.	Volumetric flow rate of 153 mL/min.	Volumetric flow rate of 180 mL/min.

Figure 6.8 Spatial liquid film thickness at different volumetric flow rates and a nozzle-to-surface distance of 10 mm.

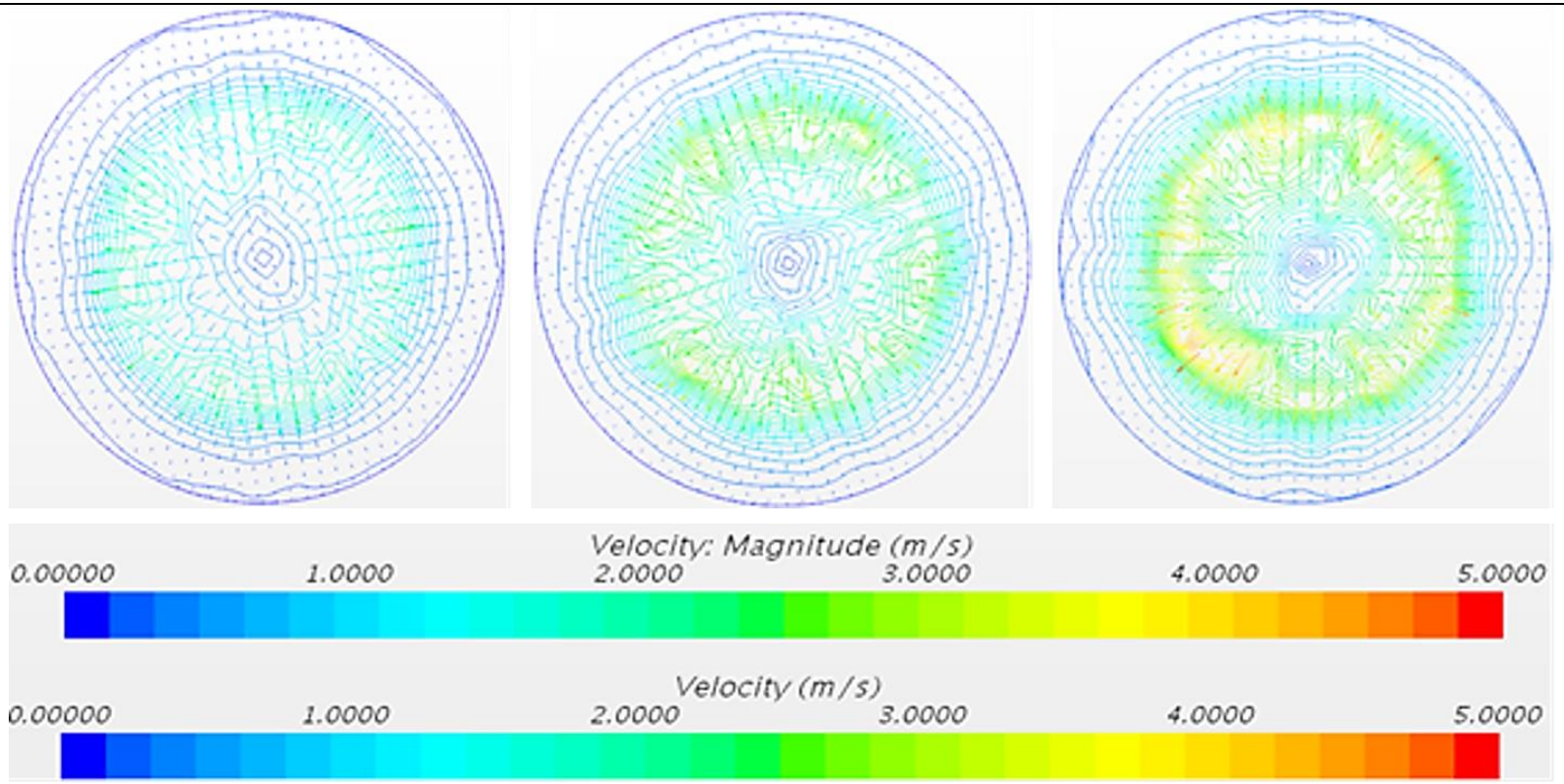

Volumetric flow rate of 115 mL/min.	Volumetric flow rate of 153 mL/min.	Volumetric flow rate of 180 mL/min.

Figure 6.9 Velocity vector and magnitude at different volumetric flow rates and a nozzle-to-surface distance of 10 mm.

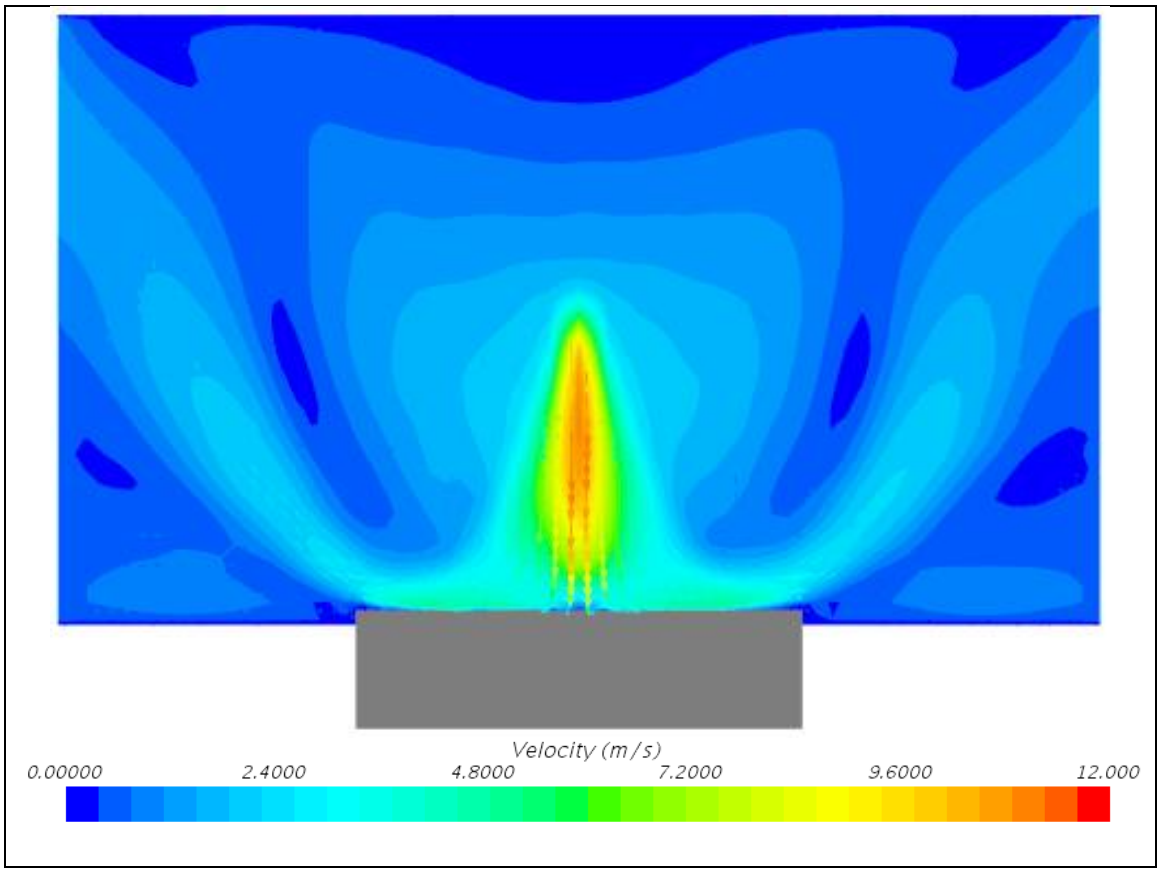

Figure 6.10 Velocity flow field of spray at a volumetric flow rate and nozzle-to-surface distance of 115 mL/min and 10 mm.

6.8 INFLUENCE OF NOZZLE-TO-SURFACE DISTANCE

Nozzle-to-surface distance is an important design parameter in spray cooling systems and impacts on the surface thermal performance. Altering nozzle-to-surface distance changes at the same time, the impingement zone, liquid film area, and droplet momentum, as shown in Figure 5.9. These changes have a significant impact on the spray cooling performance, where these changes affect the spatial distributions of heat transfer coefficient, surface temperature, film thickness, and film velocity, which ultimately affect the overall heat transfer process.

Figure 6.11 - Figure 6.13 show the effect of nozzle-to-surface distance on the spatial heat transfer coefficient at volumetric flow rates of 115, 153, and 180 mL/min. It was shown that heat transfer coefficient in the impingement zone is highly affected by nozzle-to-surface distance at all volumetric flow rates, where decreasing nozzle-to-surface distance increases the heat transfer coefficient in the impingement zone but decreases it in the thick film zone. In addition, the average heat transfer coefficient increases with increases in the nozzle-to-surface distance at all volumetric flow rates. Also, increasing nozzle-to-surface distance provides a more uniform heat transfer coefficient across the surface.

Moreover, the effect of nozzle-to-surface distance on spatial liquid film thickness was investigated at various volumetric flow rates, as shown in Figure 6.14 - Figure 6.16. The results indicated that increasing nozzle-to-surface distance provides more uniform liquid film thickness which leads to a minimized gradient in both surface temperature and heat transfer coefficient across the surface. Increasing both nozzle-to surface distance and volumetric flow rate forms thinner and more uniform liquid film thickness. A thinner and uniform liquid film thickness is noticed at a nozzle-to-surface distance and volumetric flow rate of 12 mm and 180 mL/min, respectively, as shown in Figure 6.16. Also, changing the nozzle-to-surface distance for all volumetric flow rate affects average surface temperature. Increasing nozzle-to-surface distance reduces the average surface temperature, and the reduction in surface temperature increases as the coolant volumetric flow rate increases, as shown in Figure 6.17 - Figure 6.19. The reduction in average surface temperature is highly affected by the fluid film thickness, where the lowest average surface temperature occurs at the thinner liquid film.

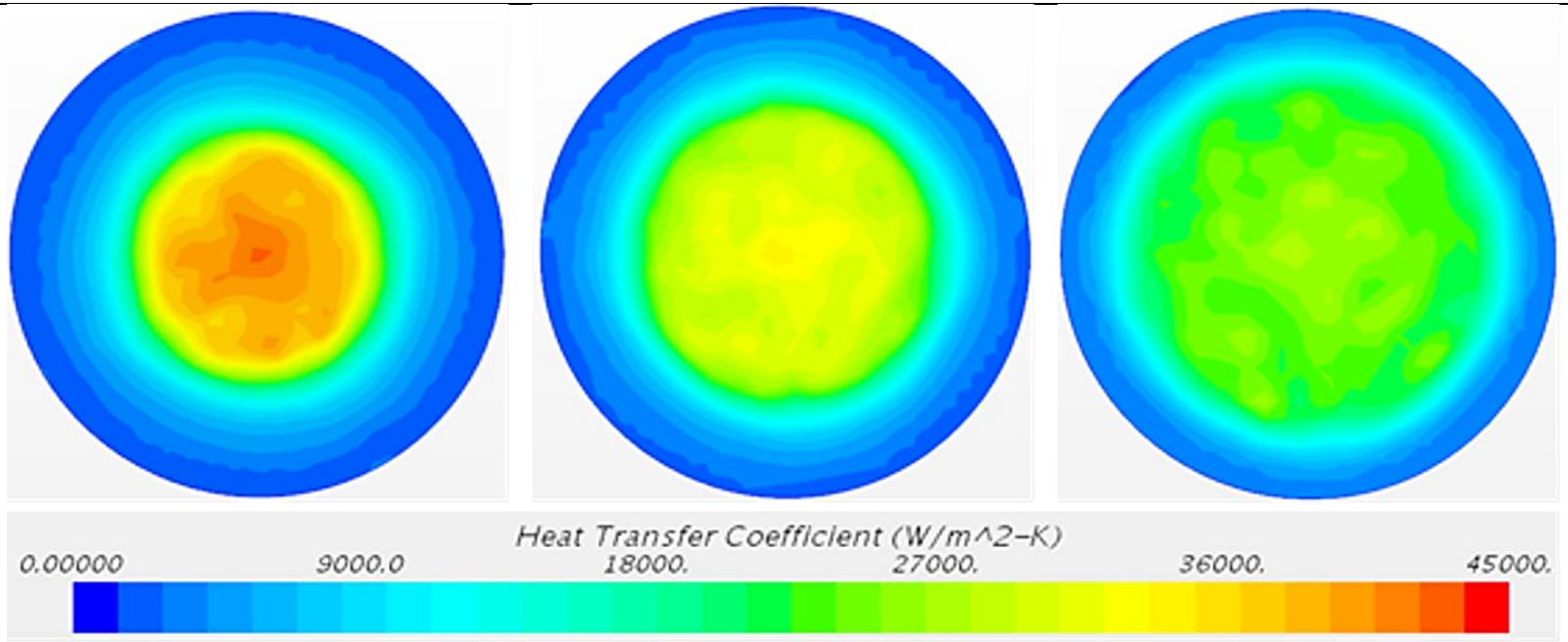

Nozzle-to-surface distance of 8 mm.	Nozzle-to-surface distance of 10 mm.	Nozzle-to-surface distance of 12 mm.

Figure 6.11 Spatial heat transfer coefficient at different nozzle-to-surface distances and a volumetric flow rate of 115 mL/min.

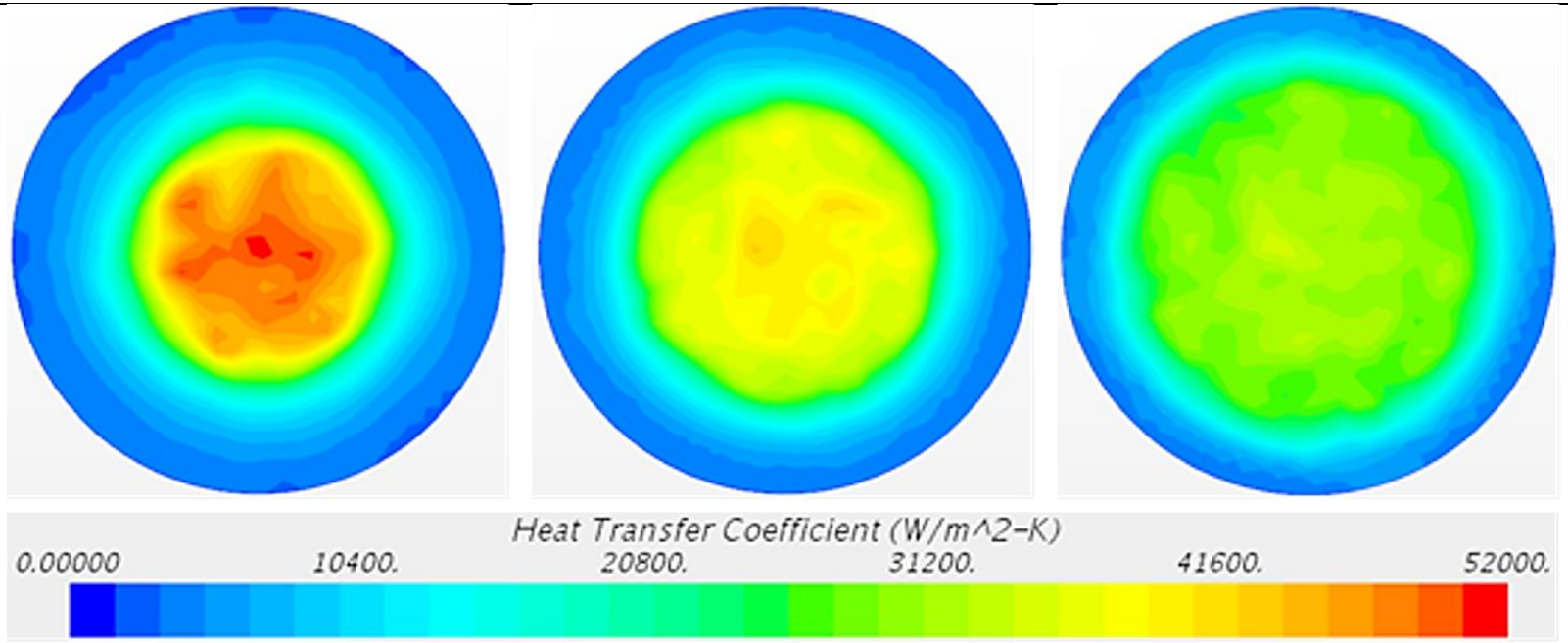

Nozzle-to-surface distance of 8 mm.	Nozzle-to-surface distance of 10 mm.	Nozzle-to-surface distance of 12 mm.

Figure 6.12 Spatial heat transfer coefficient at different nozzle-to-surface distances and a volumetric flow rate of 153 mL/min.

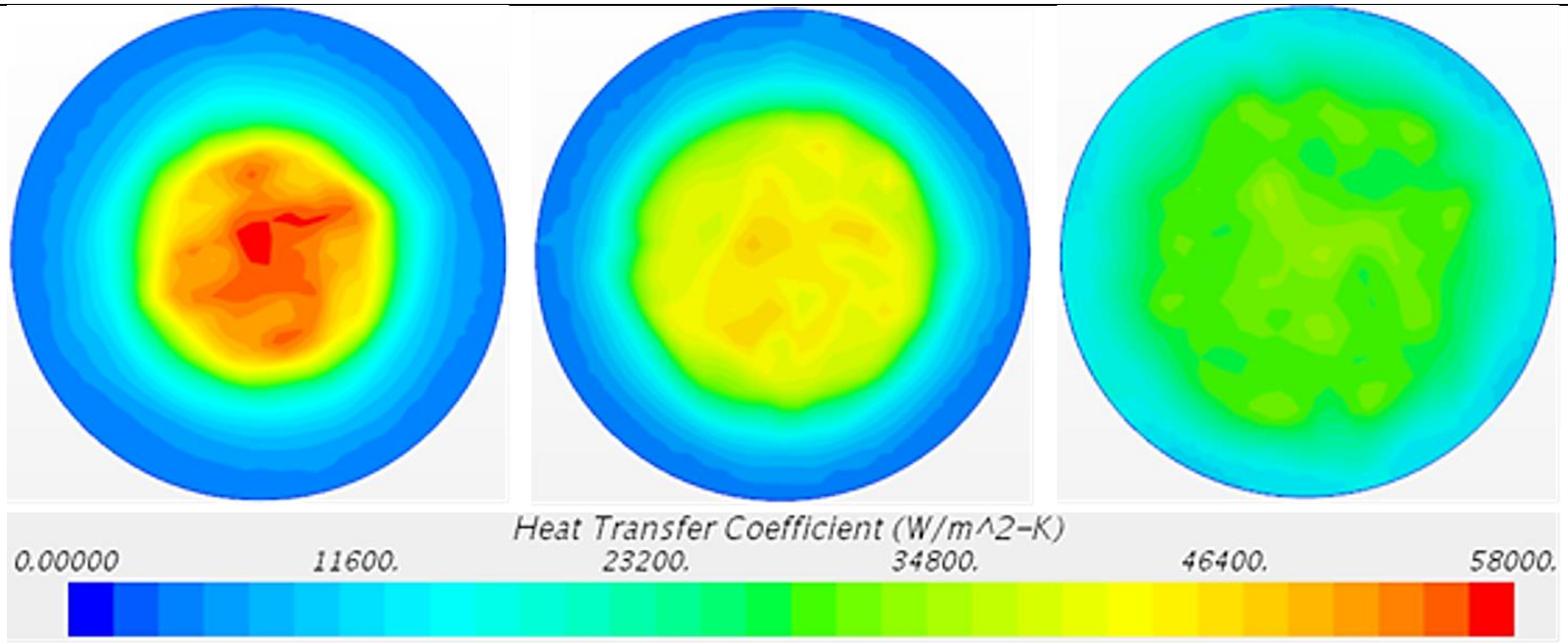

Nozzle-to-surface distance of 8 mm.	Nozzle-to-surface distance of 10 mm.	Nozzle-to-surface distance of 12 mm.

Figure 6.13 Spatial heat transfer coefficient at different nozzle-to-surface distances and a volumetric flow rate of 180 mL/min.

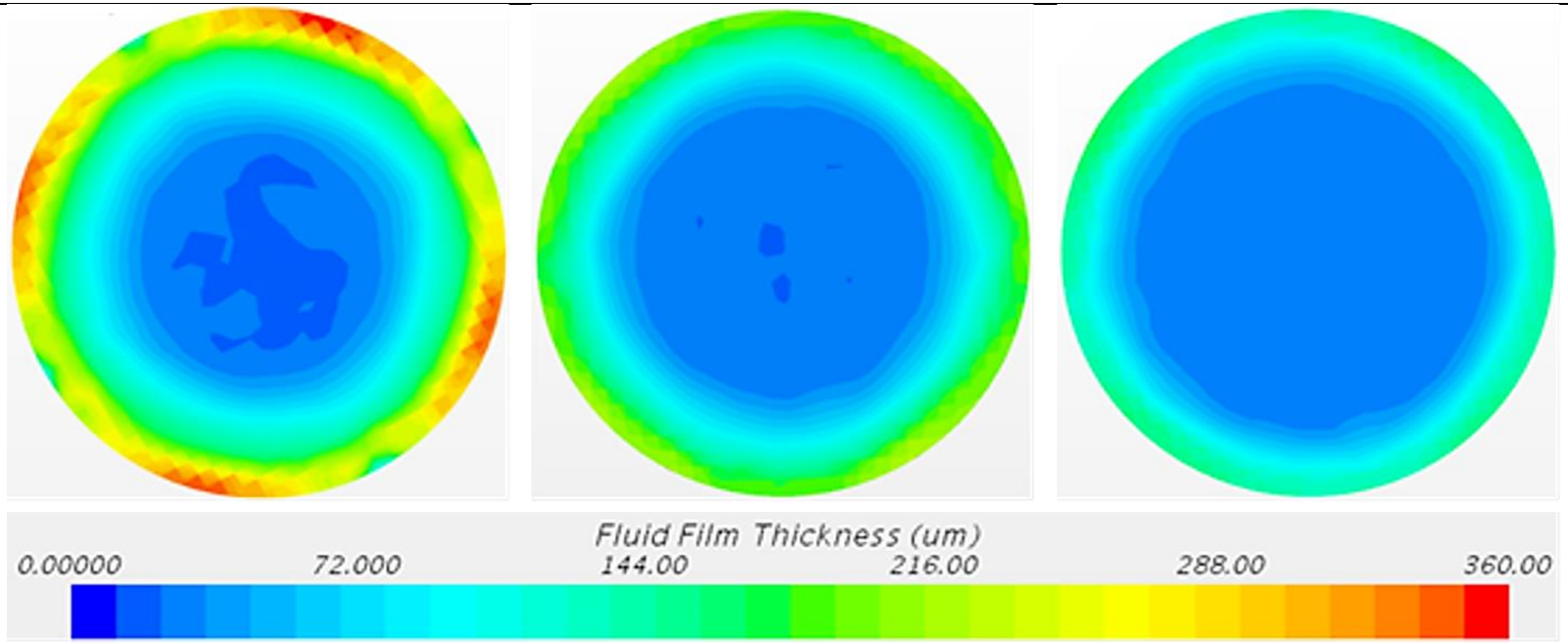

Nozzle-to-surface distance of 8 mm.	Nozzle-to-surface distance of 10 mm.	Nozzle-to-surface distance of 12 mm.

Figure 6.14 Spatial distribution of liquid film at different nozzle-to-surface distances and a volumetric flow rate of 115 mL/min.

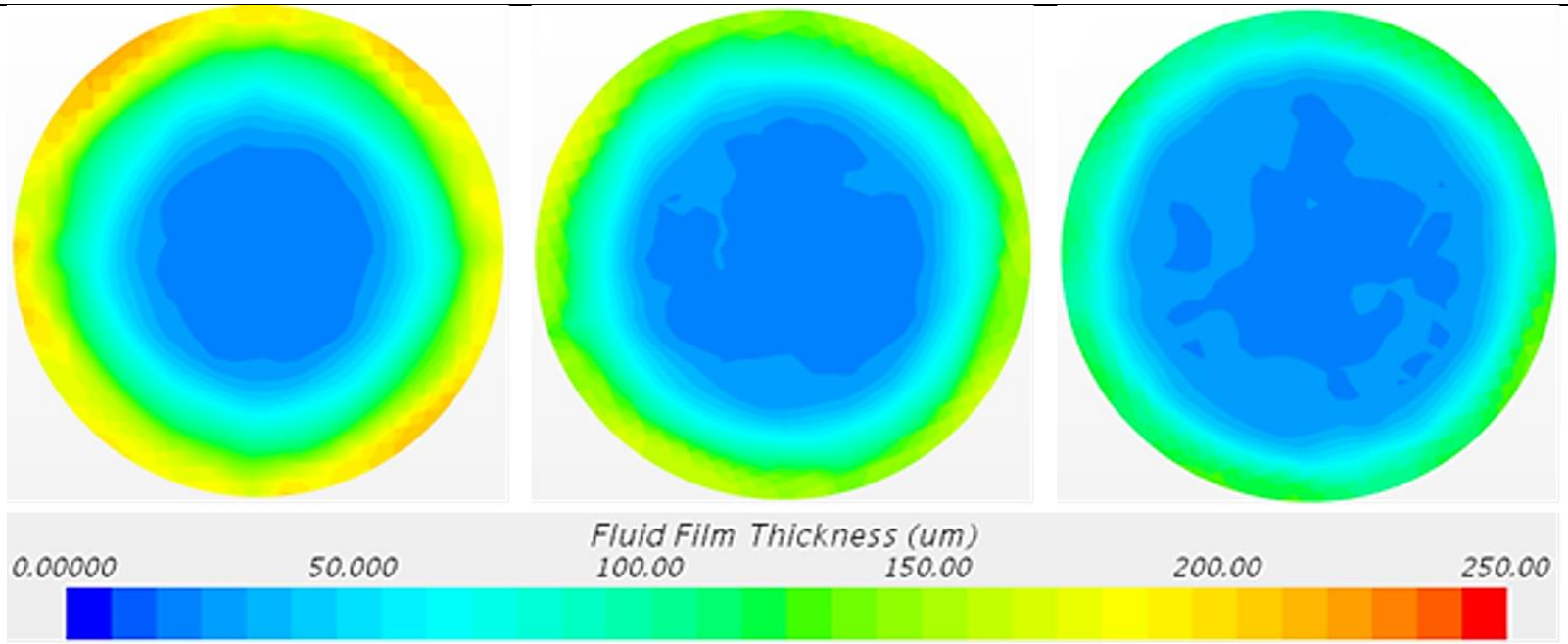

Nozzle-to-surface distance of 8 mm.	Nozzle-to-surface distance of 10 mm.	Nozzle-to-surface distance of 12 mm.

Figure 6.15 Spatial distribution of liquid film at different nozzle-to-surface distances and a volumetric flow rate of 153 mL/min.

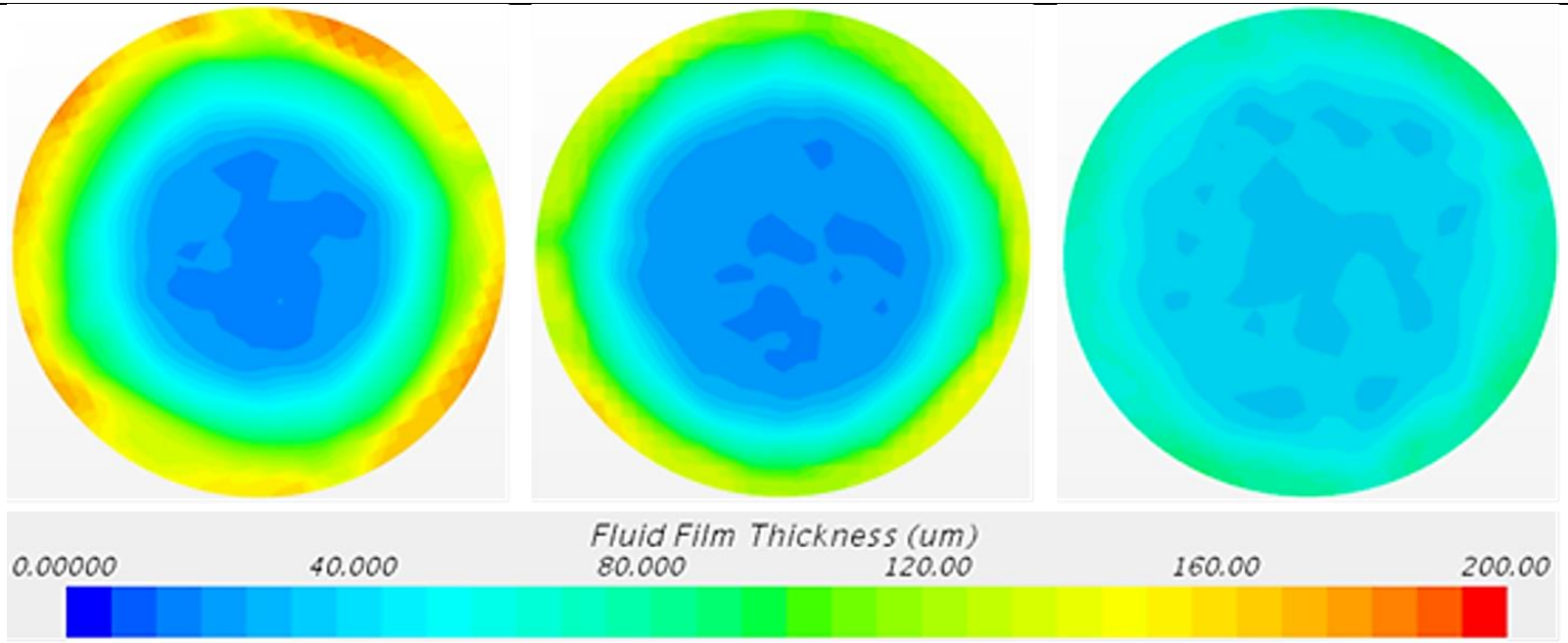

Nozzle-to-surface distance of 8 mm.	Nozzle-to-surface distance of 10 mm.	Nozzle-to-surface distance of 12 mm.

Figure 6.16 Spatial distribution of liquid film at different nozzle-to-surface distances and a volumetric flow rate of 180 mL/min.

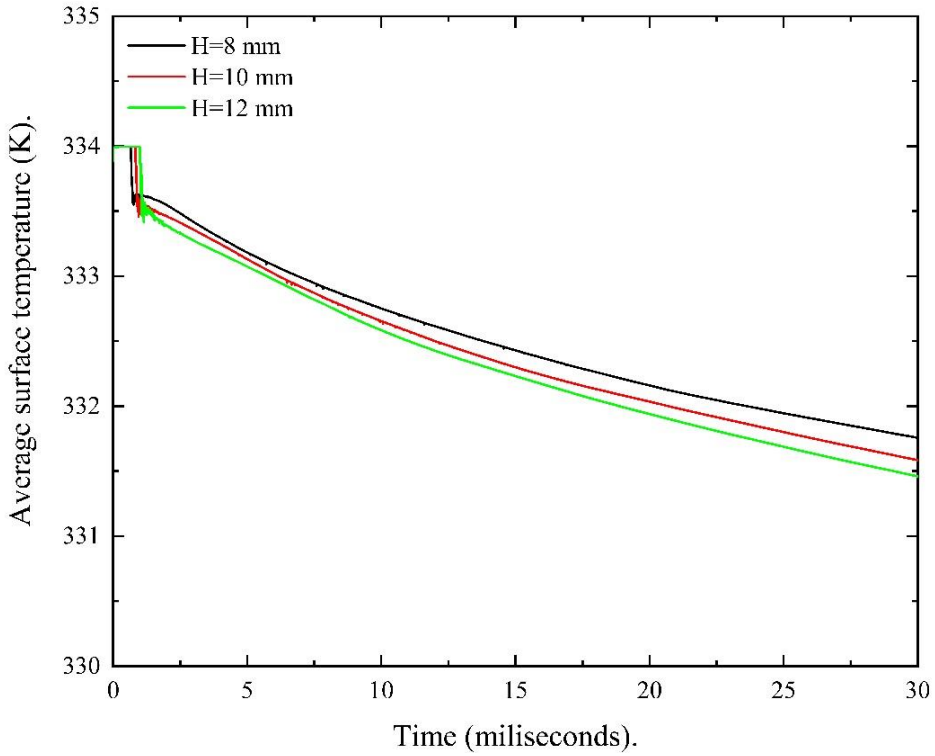

Figure 6.17 Average surface temperature at different nozzle-to-surface distances and a volumetric flow rate 115 mL/min.

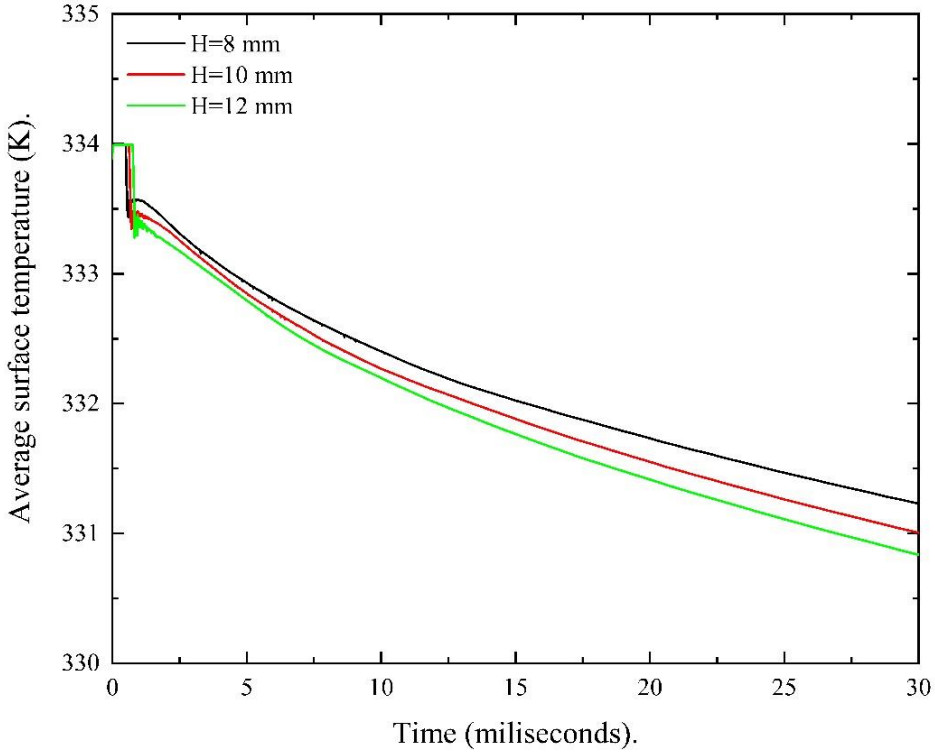

Figure 6.18 Average surface temperature at different nozzle-to-surface distances and a volumetric flow rate 153 mL/min.

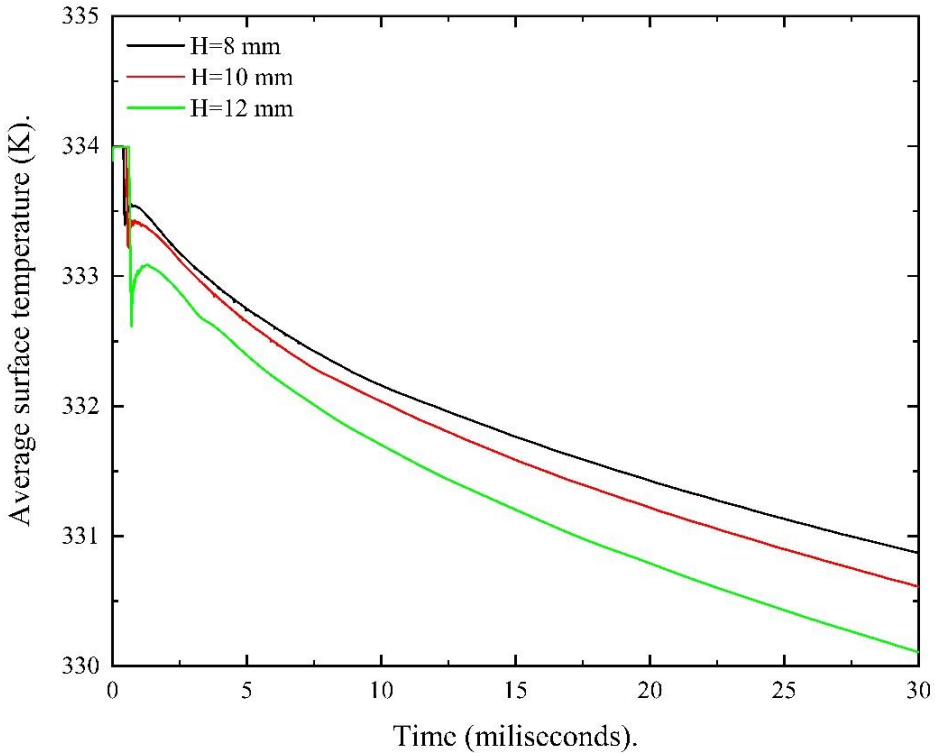

Figure 6.19 Average surface temperature at different nozzle-to-surface distances and a volumetric flow rate 180 mL/min.

6.9 INFLUENCE OF SURFACE TEMPERATURE

Surface temperature has a significant impact on the overall thermal performance of spray cooling systems. Therefore, the influence of surface temperature on heat transfer and fluid film characteristics was investigated in the non-boiling regime. A set of numerical simulations were performed at surface temperatures of 305, 334, and 365 K, a volumetric flow rate of 153 mL/min, a nozzle-to-surface distance of 10 mm, to study the influence of surface temperature on heat transfer characteristics. Figure 6.20 shows that the average heat transfer from the target surface increases as the surface temperature increases at a constant coolant inlet temperature. In contrast, increasing surface temperature decreases the average heat transfer coefficient, as shown in Figure 6.21 due to the increase in the convective heat transfer resistance. Moreover, Figure 6.22 shows that surface temperature have a primary influence on spatial heat transfer coefficient, especially in the impingement

zone, while surface temperature does not have a significant influence on special liquid film, as shown in Figure 6.23. Based on this analysis the heat capacity of the fluid has a dominant influence on heat transfer coefficient among thermophysical properties, where the heat capacity of water deceases as temperature increases. Heat capacity began to increase when water temperature exceeded 45℃.

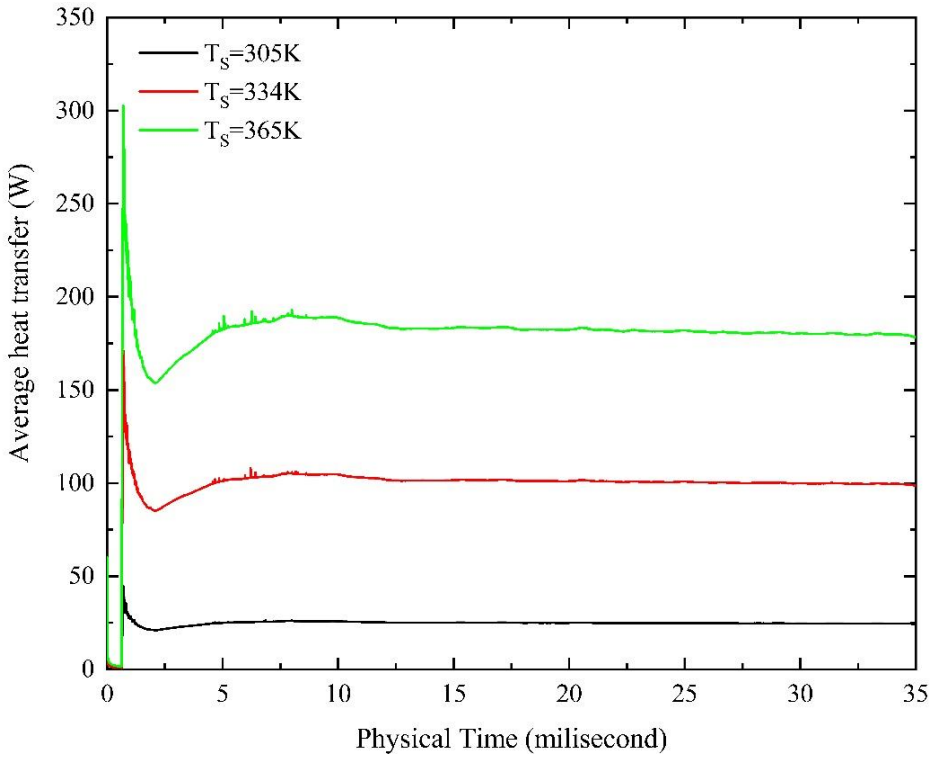

Figure 6.20 Influence of surface temperature on average heat transfer at a volumetric flow rate of 153 mL/min, and nozzle-to-surface distance of 10 mm.

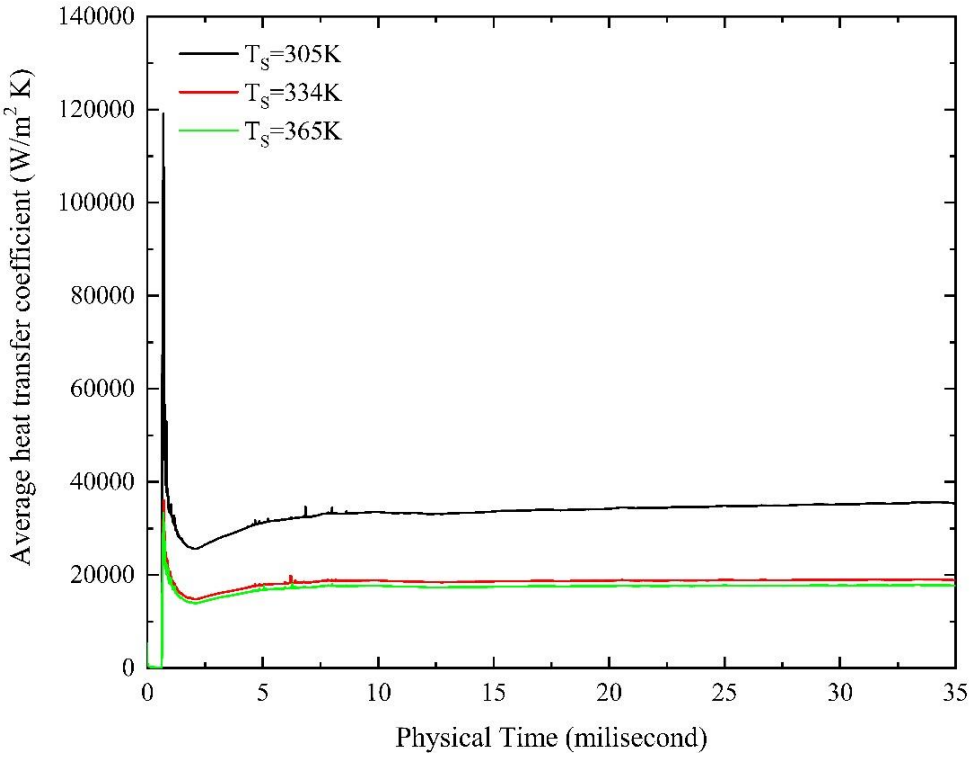

Figure 6.21 Influence of surface temperature on average heat transfer coefficient at a volumetric flow rate of 153 mL/min, and nozzle-to-surface distance of 10 mm.

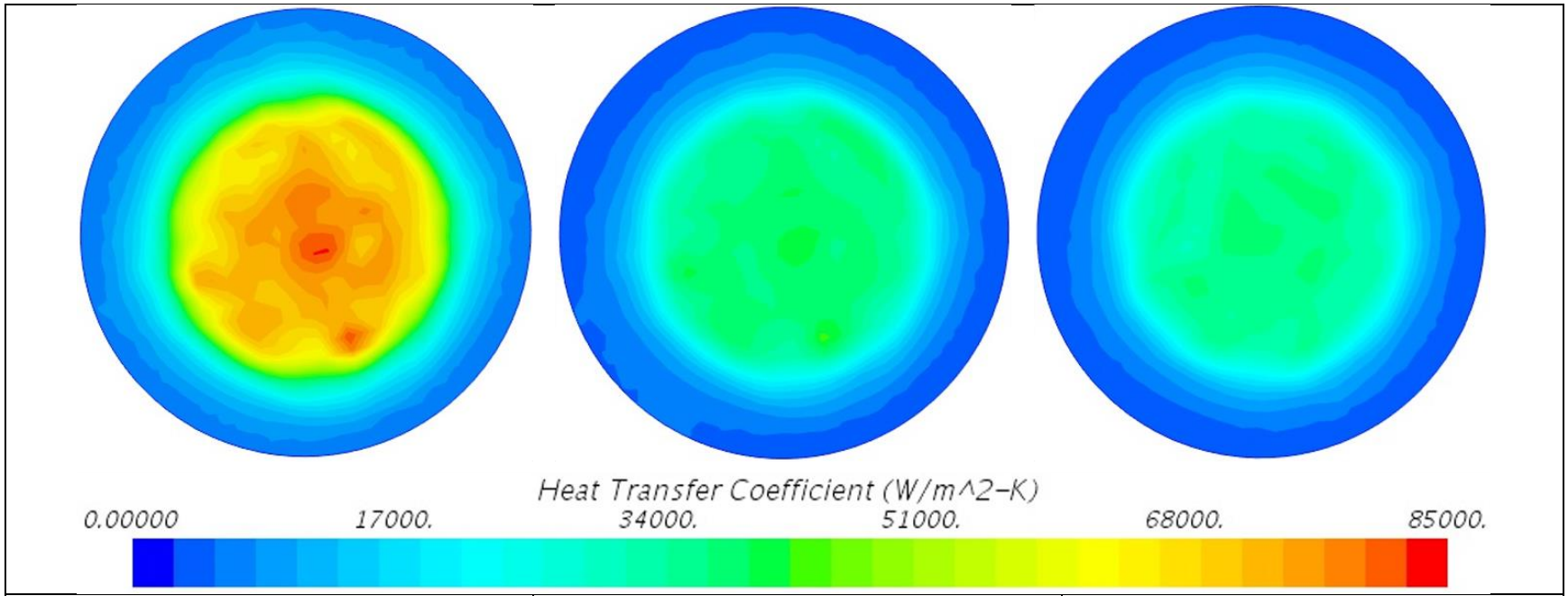

Surface temperature of 305 K.	Surface temperature of 334 K.	Surface temperature of 365 K.

Figure 6.22 Spatial heat transfer coefficient at different surface temperatures, a nozzle-to-surface distance of 10 mm, and a volumetric flow rate of 153 mL/min.

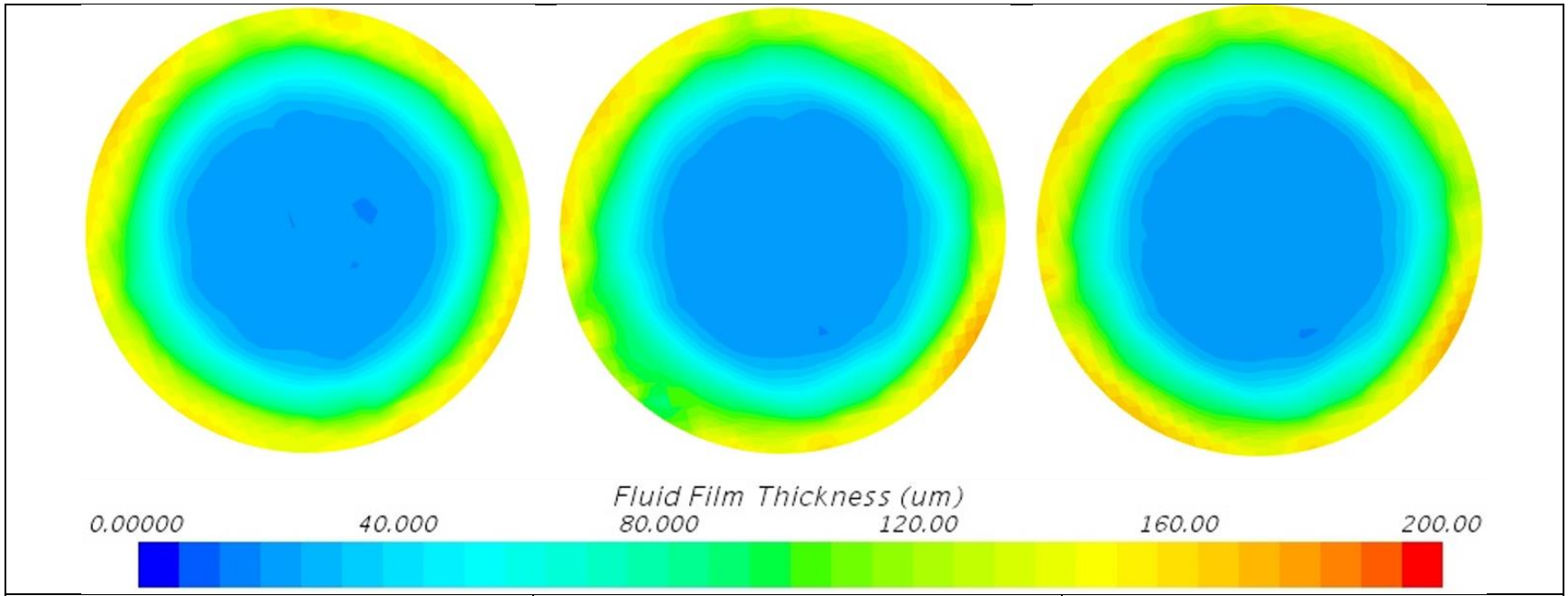

Surface temperature of 305 K.	Surface temperature of 334 K.	Surface temperature of 365 K.

Figure 6.23 Spatial liquid film thickness at different surface temperatures, a nozzle-to-surface distance of 10 mm, and a volumetric flow rate of 153 mL/min.

6.10 SUMMARY

Based on the numerical results, the following can be concluded:

1. As the volumetric flow rate increases, a thinner and more uniform liquid film forms on the target surface, especially in the impingement zone.
2. The spatial heat transfer coefficient in the impingement zone is affected more by the volumetric flow rate than the spatial heat transfer coefficient in the thick-film zone.
3. Increasing the volumetric flow rate increases the fluid velocity over the target surface; the maximum fluid velocity occurs at the interface between the impingement and the thick-film zones.
4. At all volumetric flow rates, decreasing the distance between the nozzle and the target surface increases the spatial heat transfer coefficient in the impingement zone but decreases the average heat transfer coefficient over the target surface.
5. Increasing the nozzle-to-surface distance at all volumetric flow rates provides a thinner and more uniform fluid film over the surface and leads to reduction in the surface temperature, which ultimately enhances the spray cooling thermal performance.

CHAPTER 7

IMPACT OF GEOMETRICAL SURFACE MODIFICATION ON HEAT TRANSFER ENHANCMENT

In this chapter, the influence of surfaces modified with combined circular and radial grooves on the thermal performance of the spray cooling system is discussed. Enhanced surfaces are tested at the same experimental operating conditions that were used to examine the plain surface, which was explained in chapter 5.

7.1 GEOMETRICAL SURFACE MODIFICATIONS

Since the results of the chapter 5 showed that enhancing the spray cooling performance is not an economical option for heat transfer enhancement, this chapter will investigate the option of passive heat transfer enhancement method. Geometrical surface modification is the most reliable and durable heat transfer enhancement method in spray cooling systems. However, a survey of literature showed that no study had been carried out to study the influence of circular grooves on thermal performance of spray cooling systems. Therefore, the present chapter focuses on the thermal performance of milli-structured surfaces, which were modified with circular and radial grooves in the spray cooling system. The first surface (M1) was modified with four circular grooves, each having 0.5 mm width, 0.5 mm depth with 1.5 mm pitch, to increase the surface contact area and the turbulence on the surface. The data analysis of M1 showed it had a good thermal performance at a high volumetric flow rate, but it had a low thermal performance at a low volumetric flow rate.

At low volumetric flow rate, the water replacement rate is also low, and as a result, some of the water stagnates in the channels. This stagnation consequently increases the thermal resistance and negatively affects the heat transfer process. In other words, the performance of this surface depends on the pumping power because the water replacement rate increases with increasing volumetric flow rate. Therefore, the second surface (M2) was modified with four radial grooves with a width and a height of 0.5 mm, in addition to the circular grooves to increase the water replacement rate and the surface contact area. The results showed that M2 had better heat transfer performance than M1 due to the reduction in the water thermal resistance and the activation of the radial momentum. These results indicate that radial flow has a significant effect on spray cooling heat transfer performance. For further passive heat transfer enhancement, a third surface (M3) was modified with eight radial grooves beside the four circular grooves in order to take additional advantage of the flow in the radial direction, increase the wet surface area, and speed up the drainage rate. The results indicated that M3 had the highest heat transfer performance compared to other surfaces and enhanced the heat transfer performance at both low and high nozzle differential pressures. Figure 7.1 shows a CAD view of enhanced surfaces and Table 7.1 summarizes the geometrical parameters of enhanced surfaces.

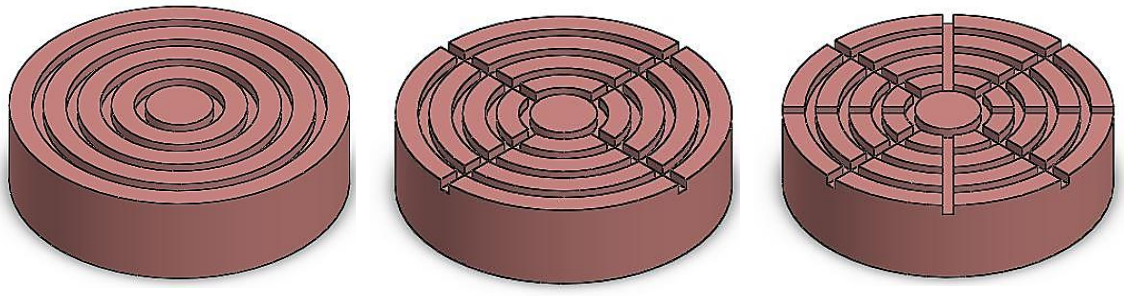

Figure 7.1 CAD view of the enhanced surfaces.

Table 7.1 Summary of the geometrical parameters of enhanced surfaces.

Surface	Surface Area (mm^2)	No. of circular grooves	No. of radial grooves	Area Enhancement Ratio (%).
M1	277.25	4	0	156.9
M2	286.28	4	4	162
M3	295.3	4	8	167.1

In the present work, the spray cooling heat transfer was enhanced passively by modifying the target surface geometrically with circular and radial grooves. The effects of the volumetric flow rate and nozzle-to-surface distance on the thermal performance of the enhanced surfaces were investigated in a closed-loop spray cooling system. The impact of enhanced surfaces under different operating conditions on the spray cooling heat transfer characteristics is explained in the following sections:

7.2 EFFECT OF VOLUMETRIC FLOW RATE

7.2.1 HEAT TRANSFER PERFORMANCE

Figure 7.2 - Figure 7.4 show a comparison of the thermal performance of enhanced surfaces at volumetric flow rates of 115, 153, and 180 mL/min. the results show that M3 had the highest effective heat transfer performance at all operating conditions, followed by M2 and M1. This positive performance can be attributed to the effect of the radial grooves, which increased the drainage rate of the working fluid, thereby decreasing the fluid thermal resistance. Other factors that would have contributed to the improvement in performance would include a change of the flow distribution over the surface, which has a significant effect on the surface temperature distribution [79], the increase of the droplet break-ups, and the splash rate on the surface resulting from the sharp edges on the modified surfaces.

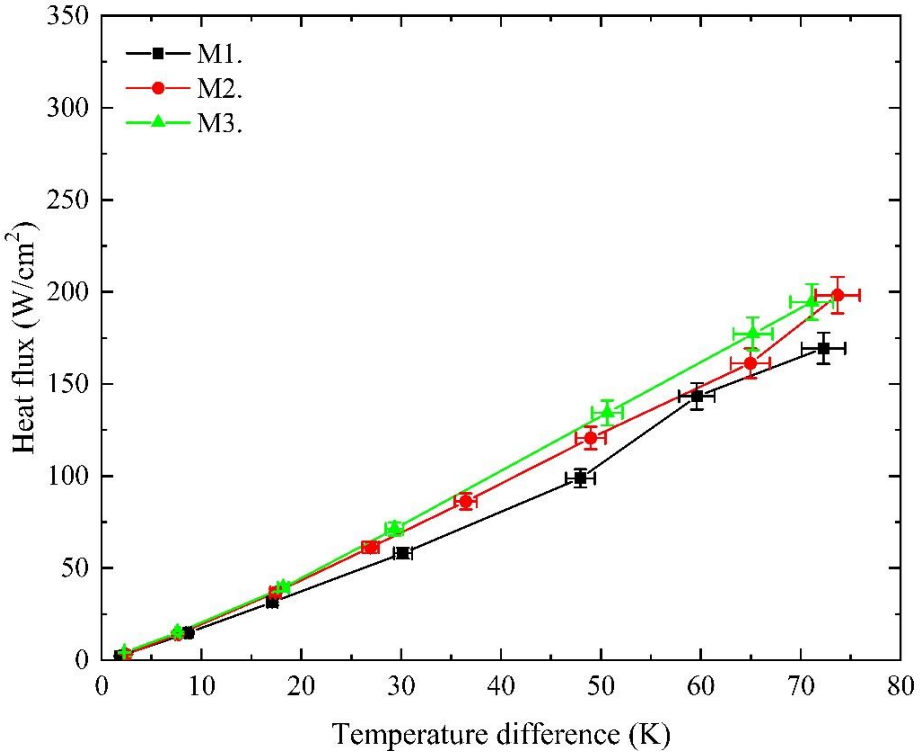

Figure 7.2 Heat flux curves at a volumetric flow rate of 115 mL/min.

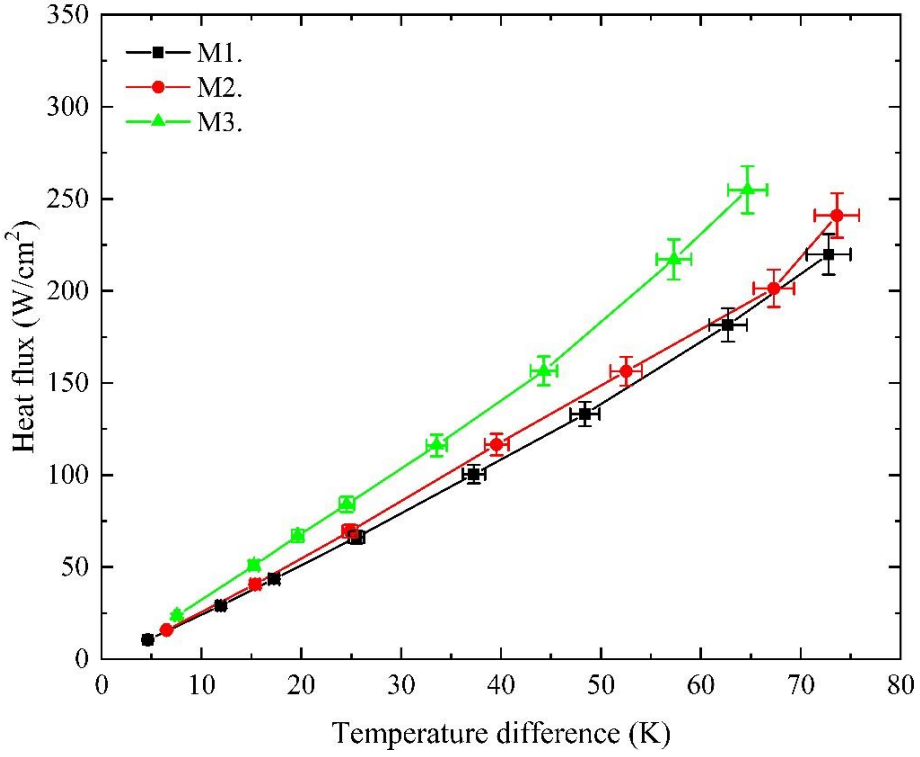

Figure 7.3 Heat flux curves at a volumetric flow rate of 153 mL/min.

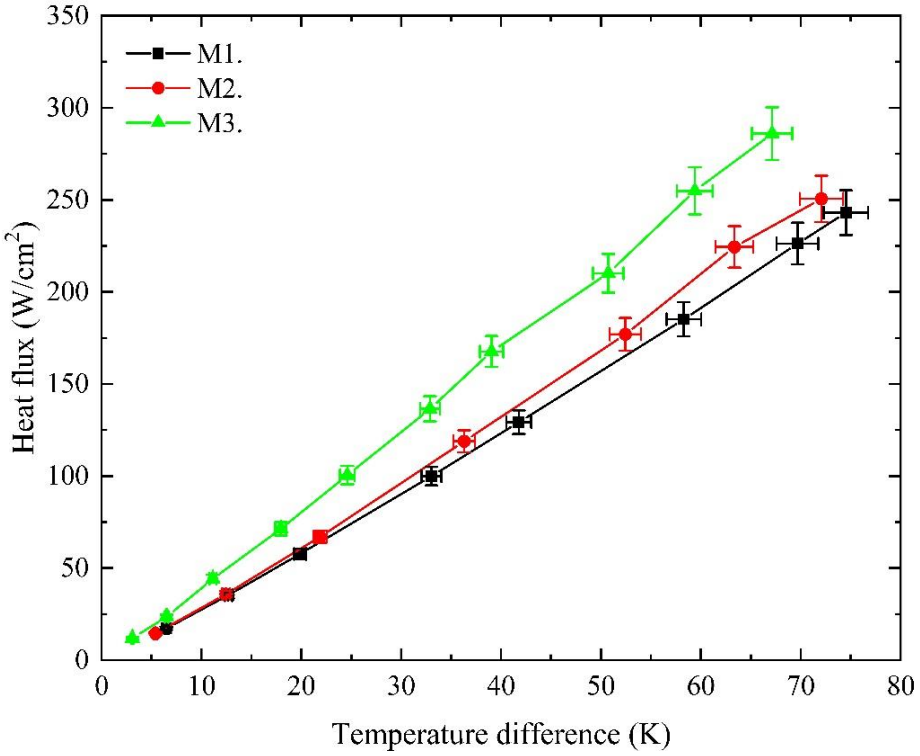

Figure 7.4 Heat flux curves at a volumetric flow rate of 180 mL/min.

Furthermore, the comparison between M2 and M3 showed that increasing the number of radial grooves improved the surface thermal performance, or heat removed, significantly. This means the radial flow has a substantial effect on a surface's thermal performance due to the increase in the contact area between the fluid and the target surface. Due to the activation of the radial flow and the resulting improvement of the mixing of fluid over the surface, fins on surfaces M2 and M3 worked as boundary layer disturbances, creating more turbulence on the surfaces. Moreover, the circular grooves in M2 and M3 surfaces worked as interconnectors between the radial grooves, which increase the mixing on the surface and reduced the surface temperature [75, 76]. Conversely, M1 had the lowest heat transfer performance among the enhanced surfaces because circular grooves stagnated some of the liquid, which led to a reduction in the liquid film velocity, temperature gradient within the liquid film, as well as added more thermal resistance.

From Figure 7.2 - Figure 7.4, it can be observed that increasing the volumetric flow rates enhanced the thermal performance of all surfaces with different ratios because, in the non-boiling regime, heat transfer characteristics depend primarily on forced convection induced by the momentum of droplets [82]. The ratio of enhancement depends on many parameters, such as surface geometry, heat flux, and the temperature difference between the surface temperature and the fluid inlet temperature. Increasing the volumetric flow rate increases the nozzle differential pressure, which is the primary influential parameter on spray cooling thermal performance [31]. In addition, increases in droplet number density and droplet velocity simultaneously decreased droplet diameter, which lead to an increase in the liquid surface area and improvements in the overall thermal performance [15, 22,23]. Increasing the volumetric flow rate improved the surface thermal performance until a certain limit; then the improvement decreases due to the increase in the thermal resistance, which mainly depends on the fluid film thickness. Additionally, the flow visualization, which was performed by using a Phantom 7.0 high-speed camera, showed that increasing the volumetric flow rate speeds up the droplet formation as shown Figure 5.4. Moreover, it was observed that the heat flux of a plain surface at low volumetric flow rate, as shown in chapter 5, increases non linearly alongside increasing the temperature difference between the surface and the working fluid; the same behavior reported by Zhang and Wang [52]. This relationship indicates that the velocity of the liquid film increases as the temperature difference increases due to the change in the thermophysical properties of the coolant, such as density, surface tension, and viscosity. Additionally, the liquid film becomes thinner as the temperature difference increases [82], which ultimately reduces the thermal resistance.

7.2.2 HEAT TRANSFER COEFFICIENT

Due to the unavailability of the surface temperature distribution of the enhanced surfaces of M1, M2, and M3, the following approach was used to calculate the average heat transfer coefficient [76, 77]:

$$Q_E = Q_F + Q_{ch} \tag{7.1}$$

As the fin is exposed to convection from all sides, the heat transferred through it was calculated via the following equation [73]:

$$Q_F = \sum_{i=1}^{n} M_i \frac{\sinh m_i L + \left({}^{h}/_{m_i k}\right) \cosh m_i L}{\cosh m_i L + \left({}^{h}/_{m_i k}\right) \sinh m_i L} \tag{7.2}$$

Where,

$$M_i \equiv \sqrt{h P_i k A_{C,i}}\ \ (T_s - T_{in})$$

$$m_i \equiv \sqrt{{}^{h P_i}/_{k A_{C,i}}}$$

Whereas, the heat transferred through the channels was calculated by using the following equation:

$$Q_{Ch} = h A_{Ch} (T_S - T_{in}) \tag{7.3}$$

The effective heat transfer coefficient (EHTC) for the modified surfaces was calculated by solving the above equations. The validity of this approach was verified by calculating the Biot number for the fins of enhanced surfaces based on the calculated average heat transfer coefficient. The comparison indicated that Biot number for enhanced surfaces was$\ll 0.1$, which means this approach is correct and valid.

Figure 7.5 - Figure 7.7 show the relationship between the effective heat transfer coefficient and the temperature difference of all enhanced surfaces at different volumetric flow rates. The results in the figures indicate that the effective heat transfer coefficient of

enhanced surfaces increases as the temperature difference increases because temperature difference depends proportionally on the heat flux due to the increase in the liquid film velocity, which is affected by the fluid thermophysical properties. Moreover, the results illustrated that the enhanced surfaces had lower effective heat transfer coefficients than a plain surface due to the reduction in liquid film velocity on enhanced surfaces [46]. Additionally, the increase in the wetted surface area and liquid film thickness over the enhanced surfaces, have an adverse effect on the heat transfer coefficient.

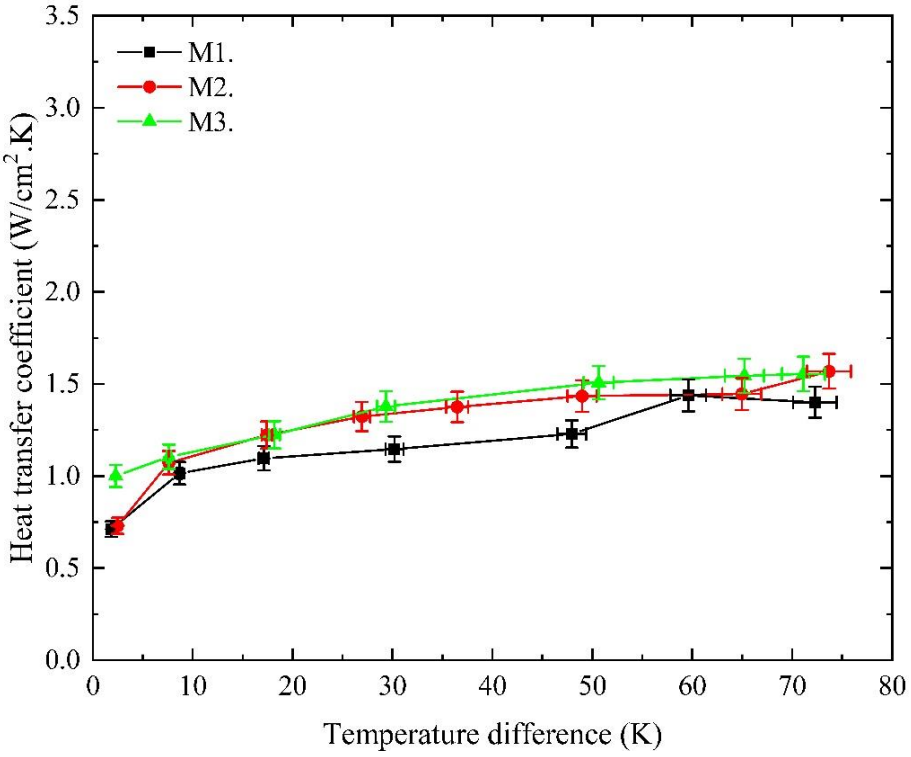

Figure 7.5 Average heat transfer coefficient of enhanced surfaces at a volumetric flow rate of 115 mL/min.

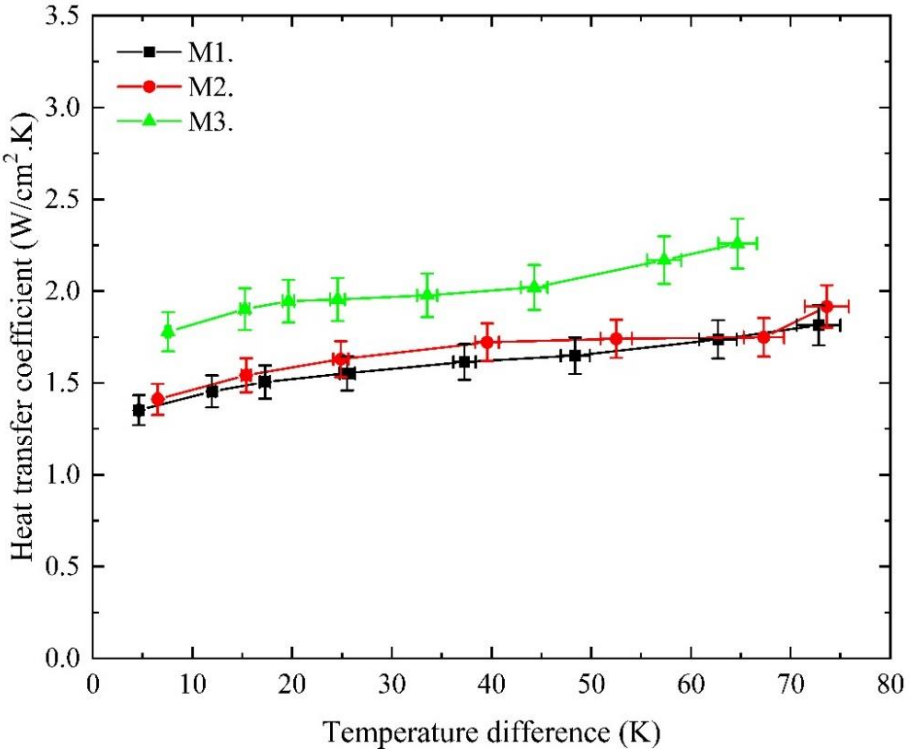

Figure 7.6 Average heat transfer coefficient of enhanced surfaces at a volumetric flow rate of 153 mL/min.

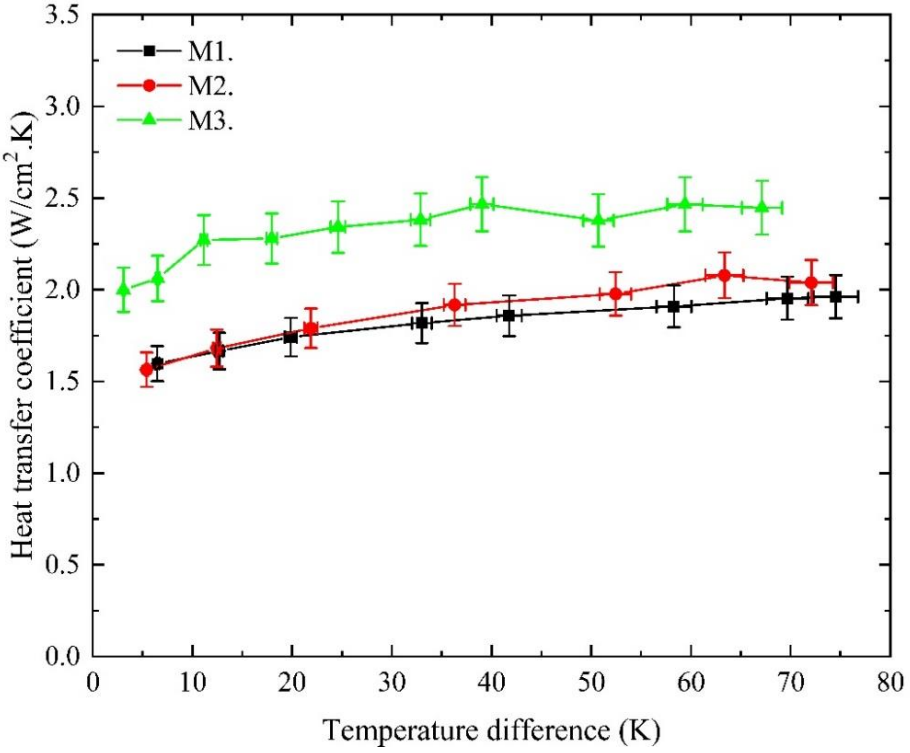

Figure 7.7 Average heat transfer coefficient of enhanced surfaces at a volumetric flow rate of 180 mL/min.

Modified surface M3 had the highest heat transfer coefficient among enhanced surfaces, followed by M2 and M1, respectively. This was the result of the effect of the radial flow, which increases the film velocity, liquid replacement rate, and provides the advantage of the momentum in the radial direction. However, the number of radial grooves did not have a significant impact on the effective heat transfer coefficient at a volumetric flow rate of 115 mL/min; however, it did have a significant effect at volumetric flow rates of 153 and 180 mL/min. M1 had the lowest heat transfer coefficient due to the increase in the thermal resistance and the decrease in the liquid film velocity. Other probable causes for these effects include the reduction in the water replacement rate and longer stagnation times for water in the channel, which reduced the temperature difference within the liquid film, and negatively affected the heat transfer characteristics. In order to replace the stagnated water promptly and improve the thermal performance of M1, more pumping power would be required. Thus, using surfaces modified with radial grooves in a spray cooling system is an economically efficient enhancement approach because it improves the spray cooling thermal performance without adding additional costs.

7.3 EFFECT OF NOZZLE-TO-SURFACE DISTANCE

The nozzle-to-surface distance was varied from 8 to 12 mm to study its effect on the thermal performance of enhanced surfaces. Figure 7.8 - Figure 7.10 show the effect of nozzle-to-surface distance on the thermal performance of a surface modified with circular grooves (M1) at different nozzle pressures. It was indicated that at a volumetric flow rate of 115 mL/min, the better heat transfer performance occurred at nozzle-to-surface distance of 10 mm followed by 12 and 8 mm. Increasing the nozzle-to-surface distance at volumetric flow rates of 153 and 180 mL/min decreased the heat flux slightly.

The decrease in the thermal performance results from the decrease in the droplet momentum, which leads to a reduction in the water replacement rate in channels and allows it to stagnate longer, ultimately increasing the thermal resistance on the target surface. Furthermore, increasing the distance between the nozzle and the target surface increases the number of channels filled with water due to the increase in the impingement zone. In the impingement zone, the liquid film has the lowest velocity and thickness.

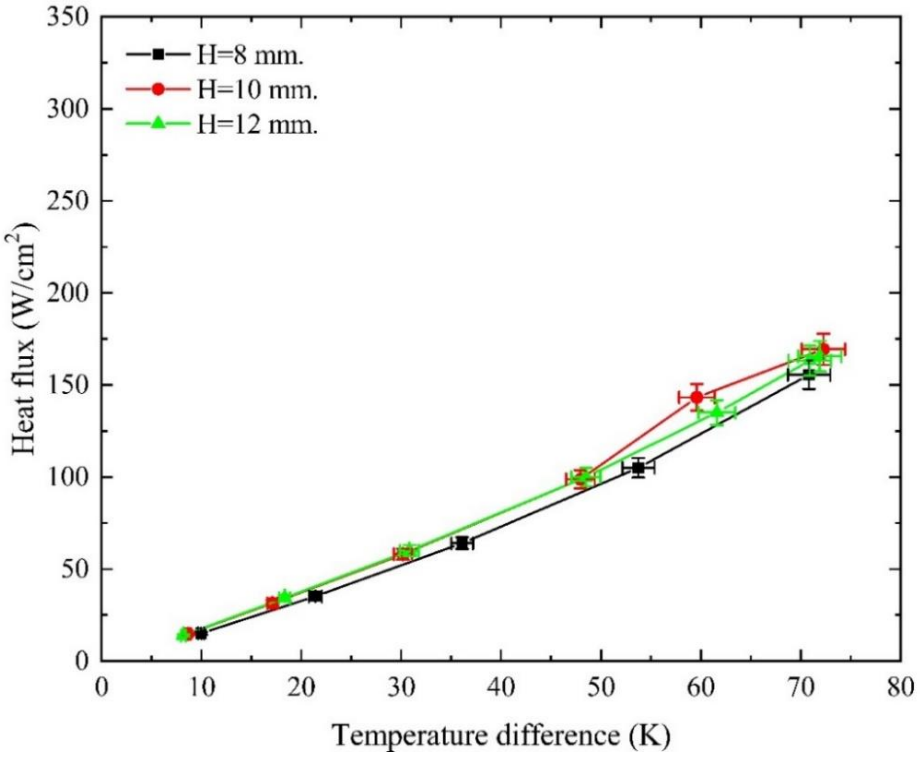

Figure 7.8 Effect of nozzle-to-surface distance on the thermal performance of M1 at a volumetric flow rate of 115 mL/min.

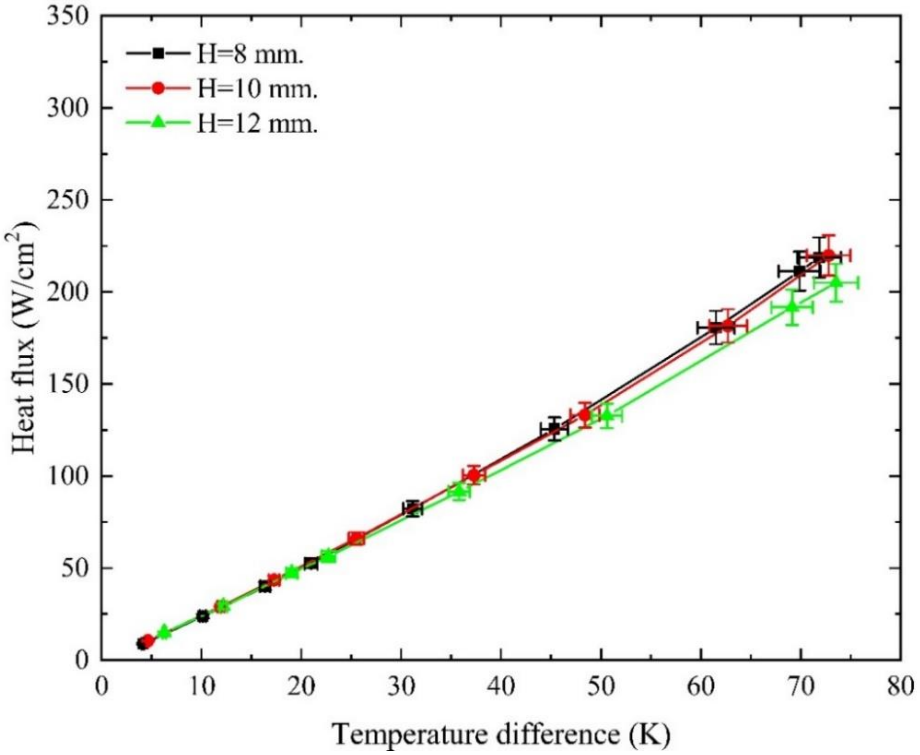

Figure 7.9 Effect of nozzle-to-surface distance on the thermal performance of M1 at a volumetric flow rate of 153 mL/min.

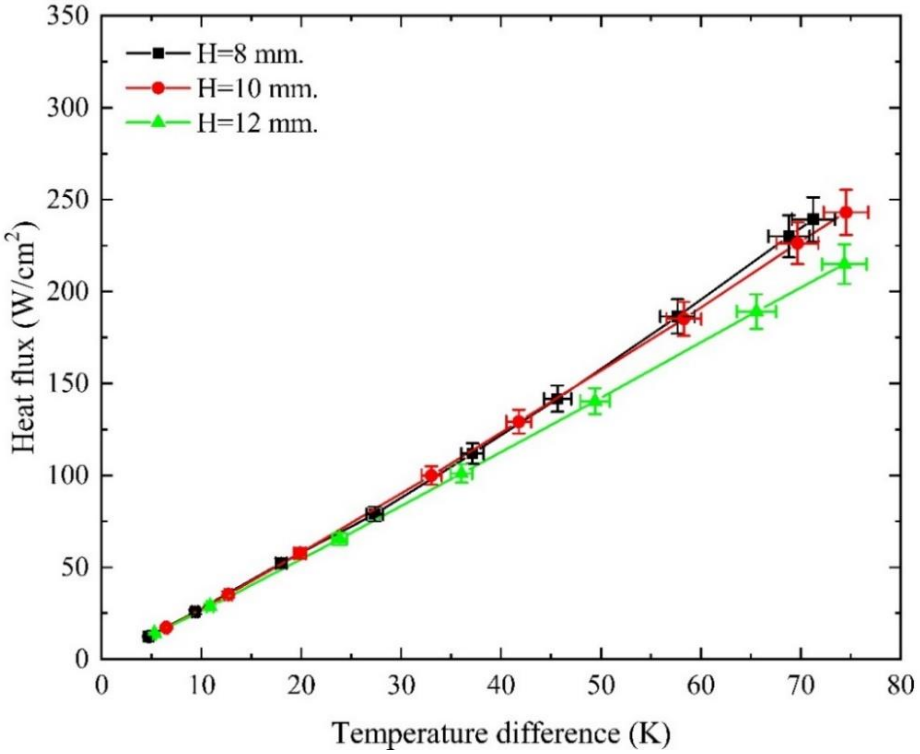

Figure 7.10 Effect of nozzle-to-surface distance on the thermal performance of M1 at a volumetric flow rate of 180 mL/min.

For M2, nozzle-to-surface distance has an inconsistent effect on heat transfer characteristics, as illustrated in Figure 7.11 - Figure 7.13. The figures indicate that the optimal heat transfer performance was obtained at a volumetric flow rate of 115 mL/min and a nozzle-to-surface distance of 12 mm, followed by 10 and 8 mm. Moreover, at volumetric flow rates of 153 and 180 mL/min, decreasing nozzle-to-surface distance increases the thermal performance of the enhanced surface M2. Decreasing nozzle-to-surface distance increases the turbulence intensity on the surface, as well as increases the drainage rate increase due to the existence of radial grooves. Also, increasing the volumetric flow rate leads to an increase in film velocity on the target surface, eventually reduces the convective thermal resistance, and finally improves the surface thermal performance.

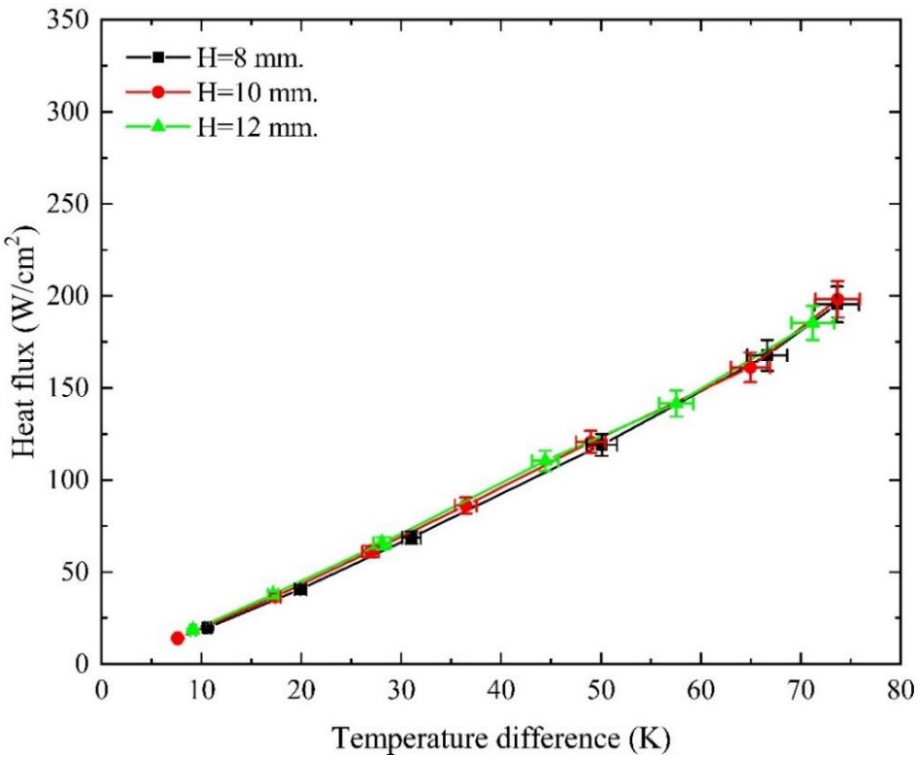

Figure 7.11 Effect of nozzle-to-surface distance on the thermal performance of M2 at a volumetric flow rate of 115 mL/min.

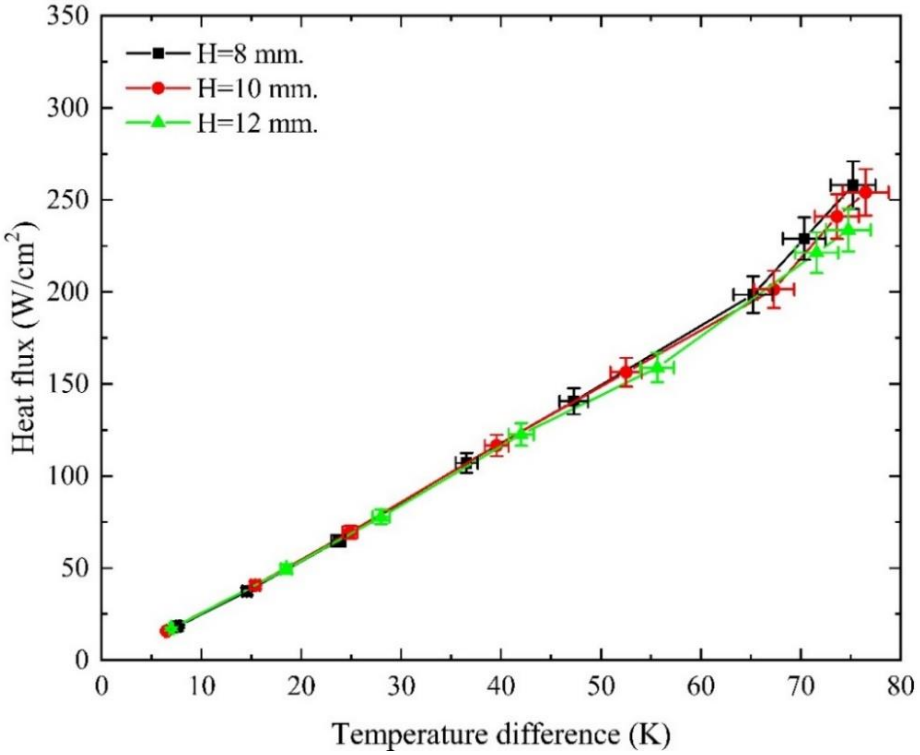

Figure 7.12 Effect of nozzle-to-surface distance on the thermal performance of M2 at a volumetric flow rate of 153 mL/min.

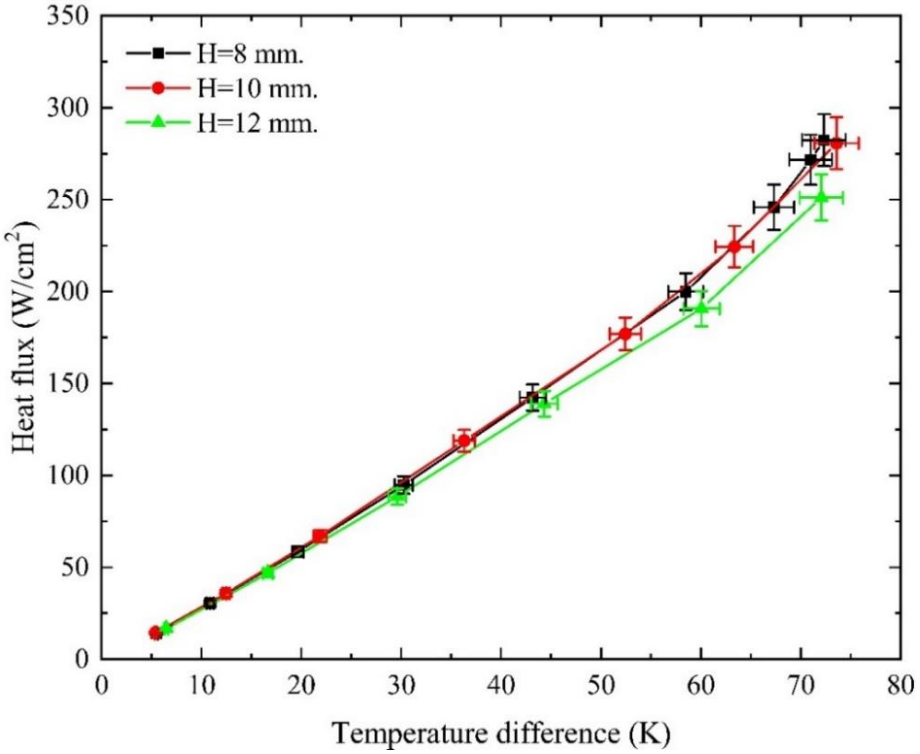

Figure 7.13 Effect of nozzle-to-surface distance on the thermal performance of M2 at a volumetric flow rate of 180 mL/min.

For M3, nozzle-to-surface distance has a slight effect on heat transfer characteristics at volumetric flow rates of 115 and 180 mL/min, as shown in Figure 7.14 and Figure 7.16, respectively. Increasing the distance between the nozzle and the target surface enhances heat transfer characteristics marginally, especially at high-temperature differences. Whereas, at a volumetric flow rate of 153 mL/min, increasing the nozzle-to-surface distance enhances the spray cooling thermal performance, as shown in Figure 7.15. The heat transfer enhancement results from the increase in the spray impingement area, which increases the liquid thin-film portion on the surface. Also, it increases the number of fins exposed to spray directly.

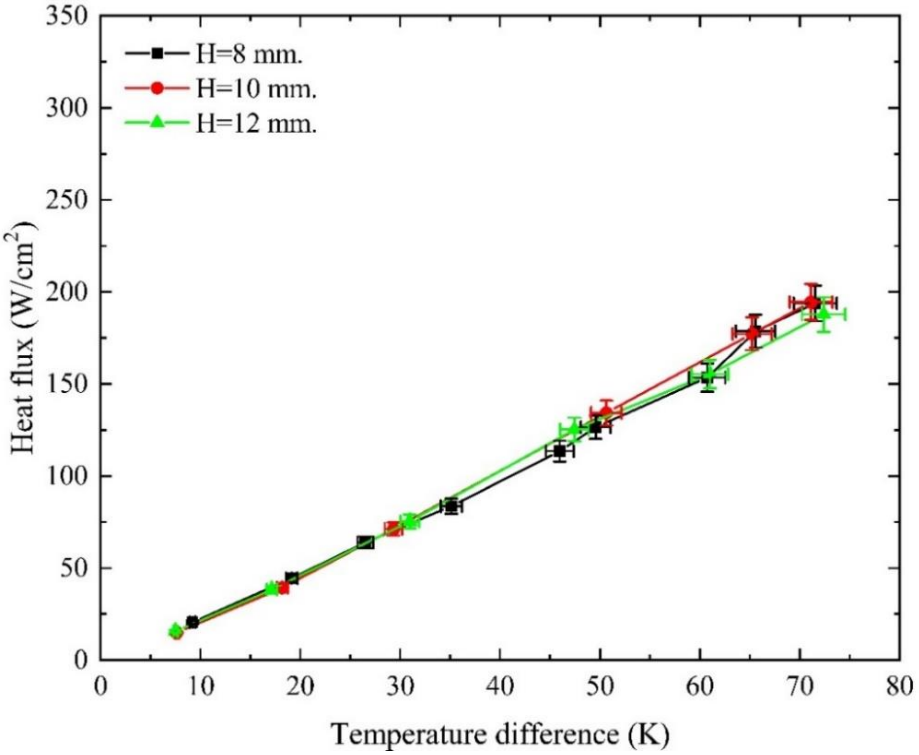

Figure 7.14 Effect of nozzle-to-surface distance on the thermal performance of M3 at a volumetric flow rate of 115 mL/min.

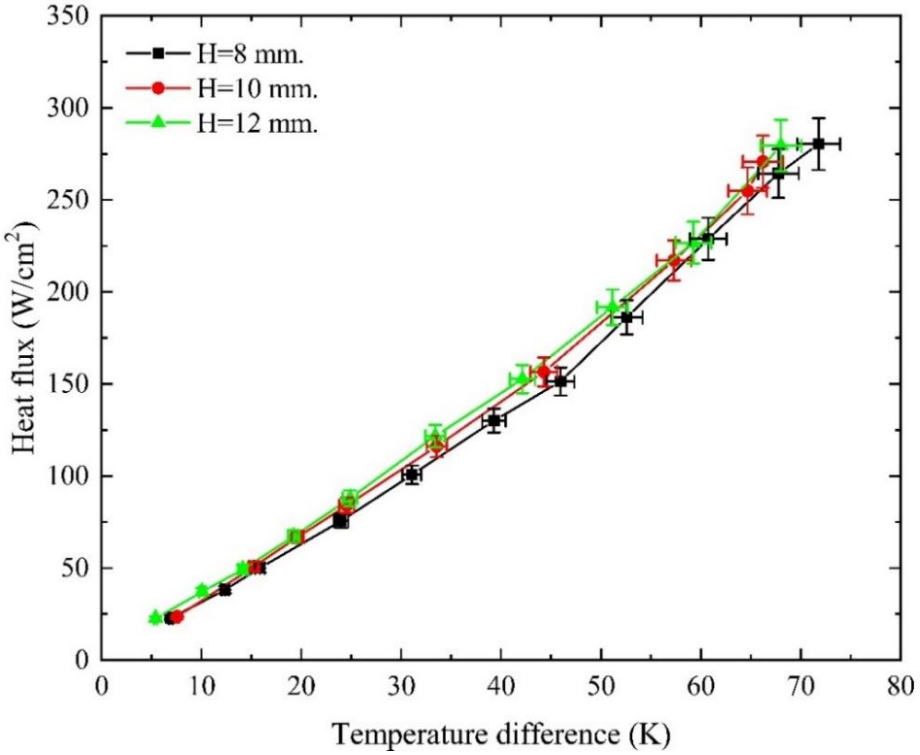

Figure 7.15 Effect of nozzle-to-surface distance on the thermal performance of M3 at a volumetric flow rate of 153 mL/min.

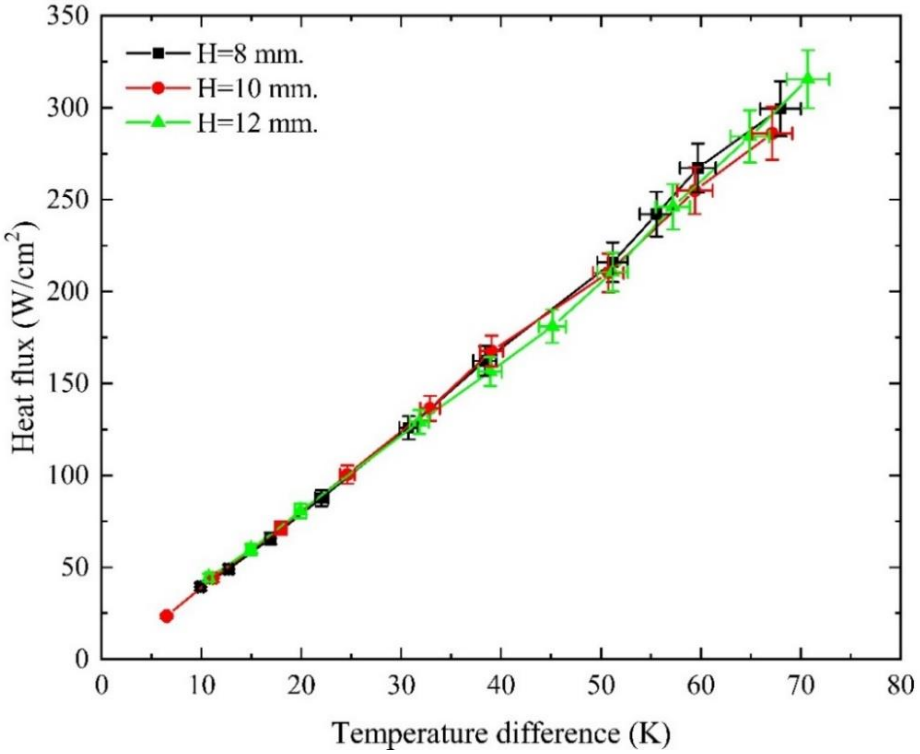

Figure 7.16 Effect of nozzle-to-surface distance on the thermal performance of M3 at a volumetric flow rate of 180 mL/min.

Figure 7.17 - Figure 7.25 show the influence of nozzle-to-surface distance on the average heat transfer coefficient of macro-structured surfaces at different volumetric flow rates. It is clear that at all nozzle-to-surface distances, the average heat transfer coefficient for all surfaces increases proportionally as both temperature difference and volumetric flow rate increase. Also, it was observed that for surface M1, increasing the nozzle-to-surface distance decreases the average heat transfer coefficient at a volumetric flow rate of 115 mL/min (as explained in Figure 7.17), while it increases as the nozzle-to-surface distance decreases at volumetric flow rates of 153 and 180 mL/min, as shown in Figure 7.18 and Figure 7.19 due to the increase in droplet flux and momentum, which reduces the amount of water stagnated in the circular grooves.

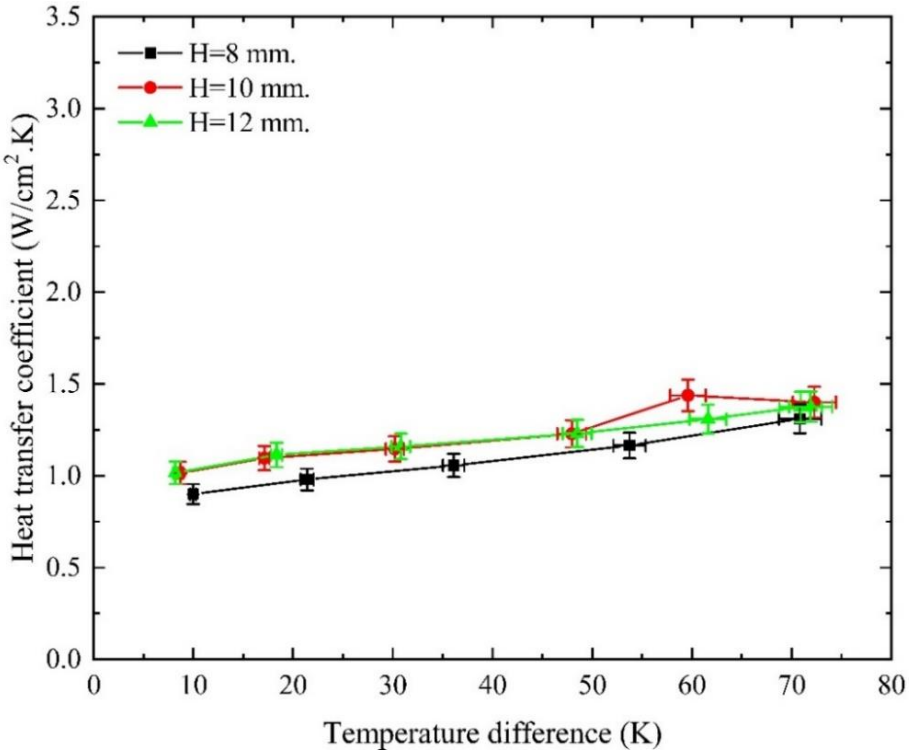

Figure 7.17 Effect of nozzle-to-surface distance on average heat transfer coefficient of M1 at a volumetric flow rate of 115 mL/min.

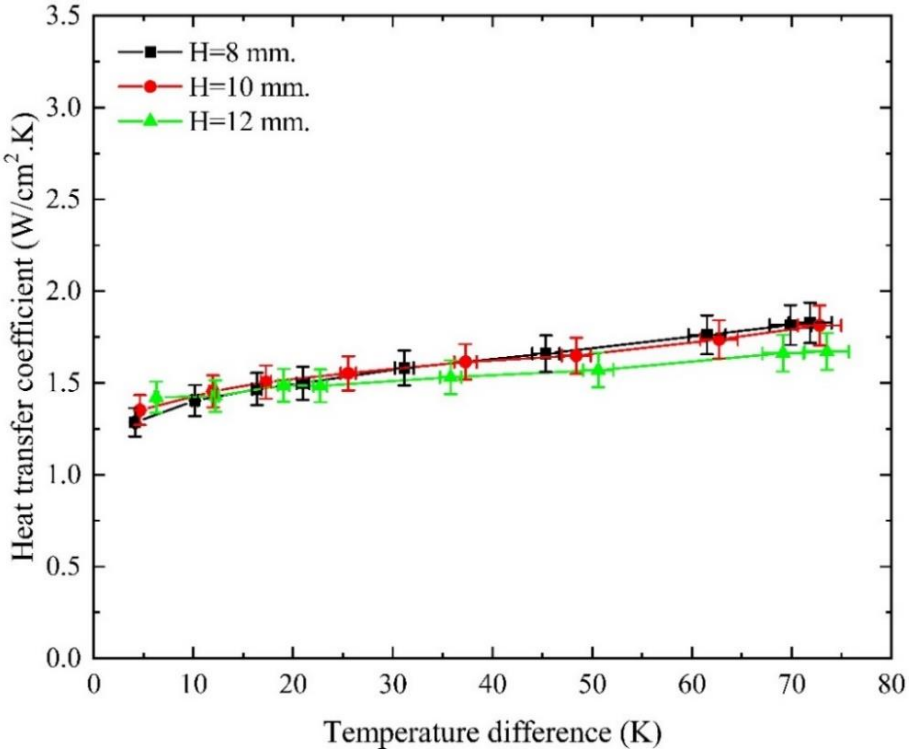

Figure 7.18 Effect of nozzle-to-surface distance on average heat transfer coefficient of M1 at a volumetric flow rate of 153 mL/min.

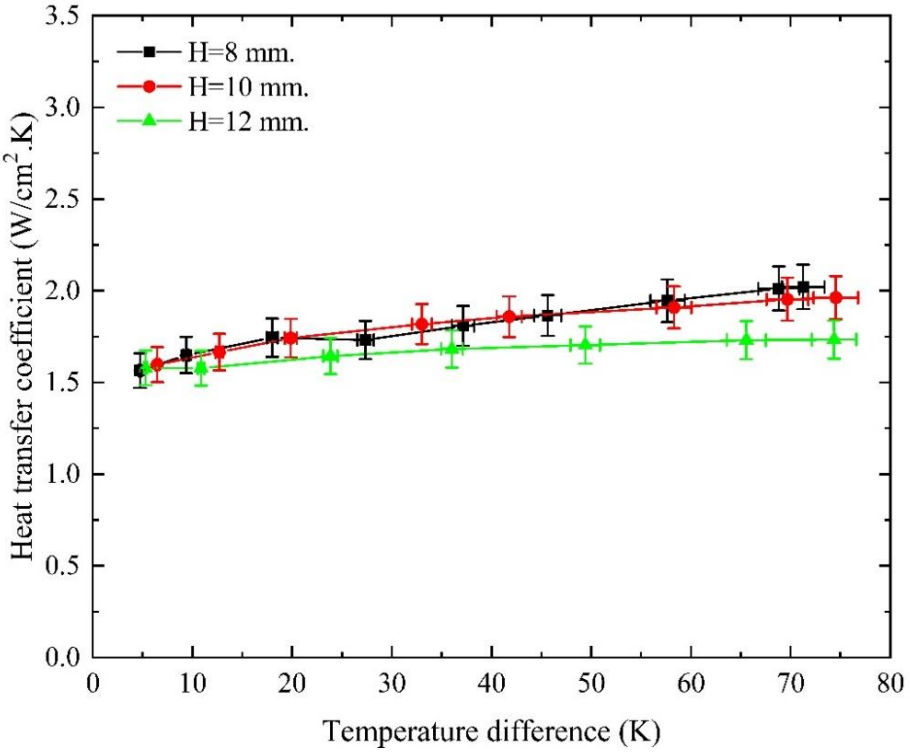

Figure 7.19 Effect of nozzle-to-surface distance on average heat transfer coefficient of M1 at a volumetric flow rate of 180 mL/min.

For surface M2, the highest average heat transfer coefficient occurred at a nozzle-to-surface distance of 10 mm for most volumetric flow rates (as illustrated in Figure 7.20 - Figure 7.22). The maximum average heat transfer coefficient variation between the highest and lowest nozzle-to-surface distances occurs at a volumetric flow rate of 180 mL/min, as shown in Figure 7.22. Nozzle-to-surface distance has a substantial influence on the average heat transfer coefficient of surface M3, especially at higher flow rates, as explained in Figure 7.24 and Figure 7.25.

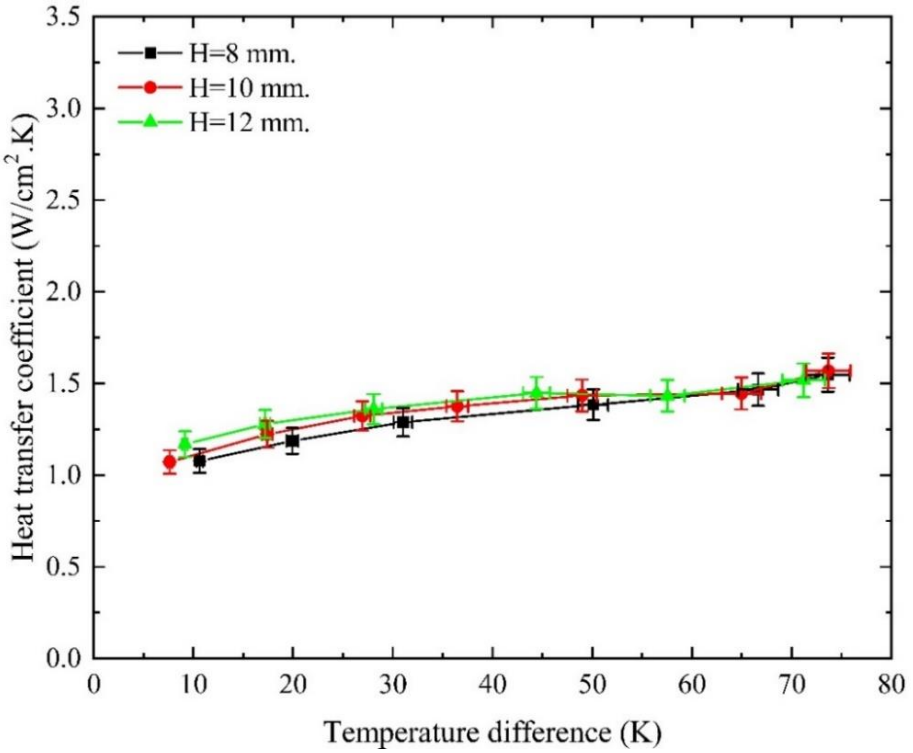

Figure 7.20 Effect of nozzle-to-surface distance on average heat transfer coefficient of M2 at a volumetric flow rate of 115 mL/min.

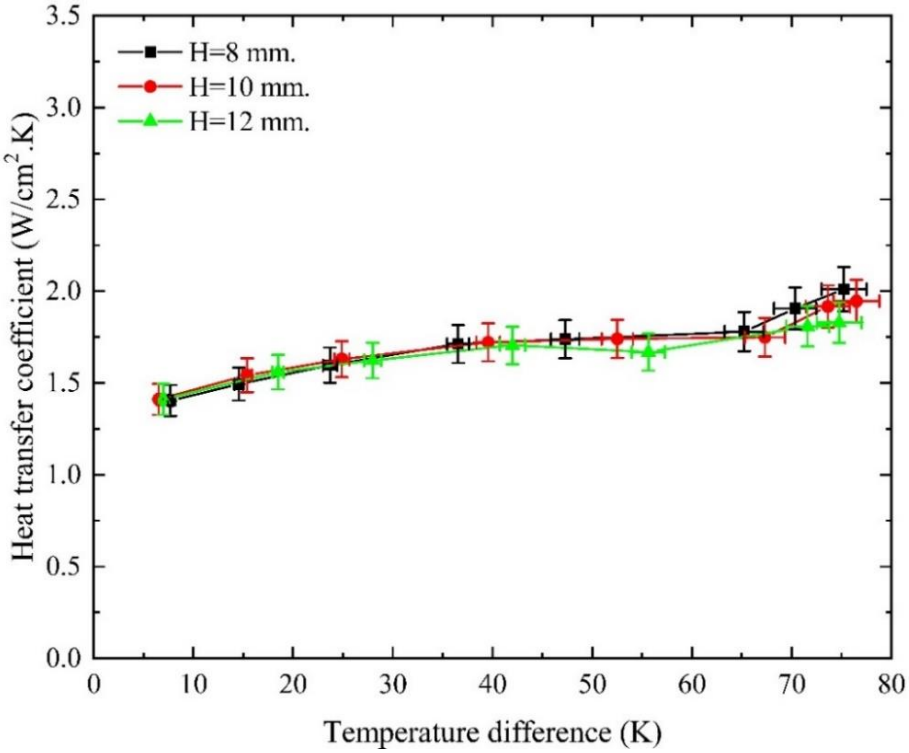

Figure 7.21 Effect of nozzle-to-surface distance on average heat transfer coefficient of M2 at a volumetric flow rate of 153 mL/min.

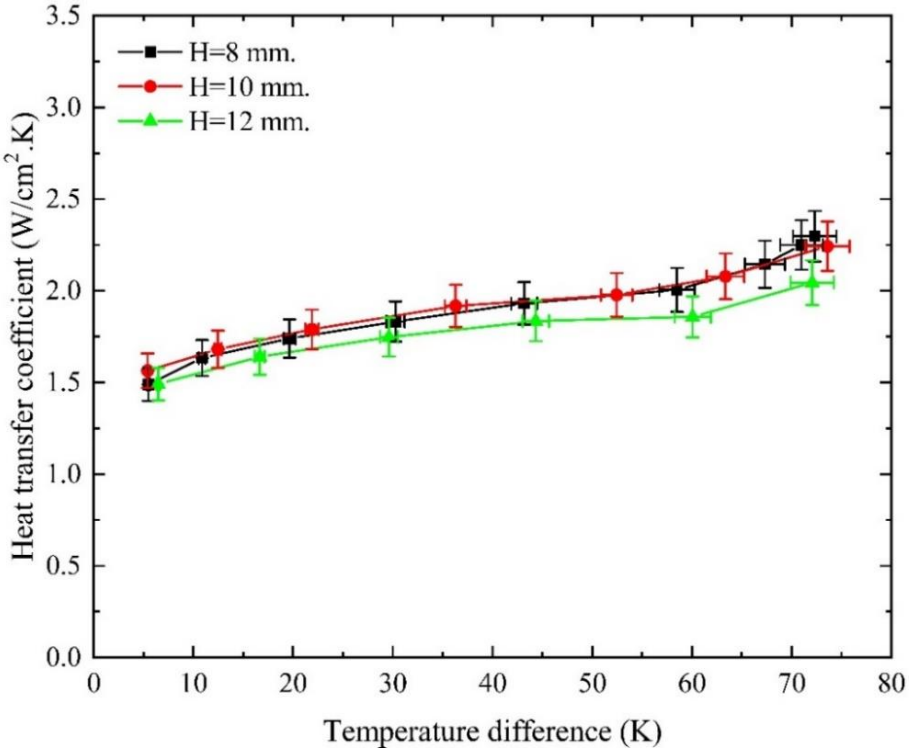

Figure 7.22 Effect of nozzle-to-surface distance on average heat transfer coefficient of M2 at a volumetric flow rate of 180 mL/min.

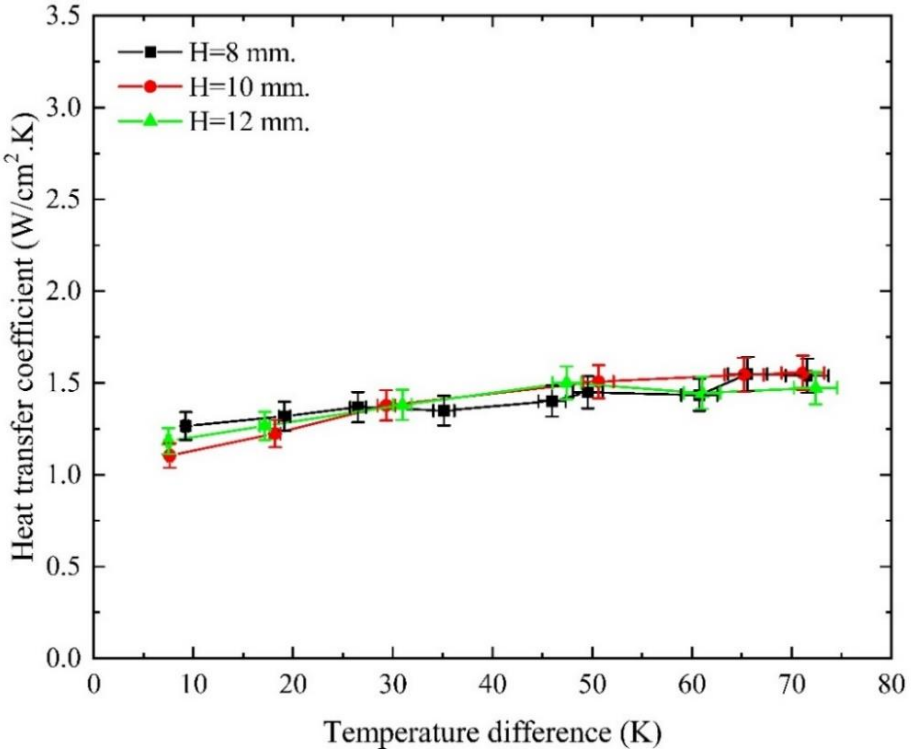

Figure 7.23 Effect of nozzle-to-surface distance on average heat transfer coefficient of M3 at a volumetric flow rate of 115 mL/min.

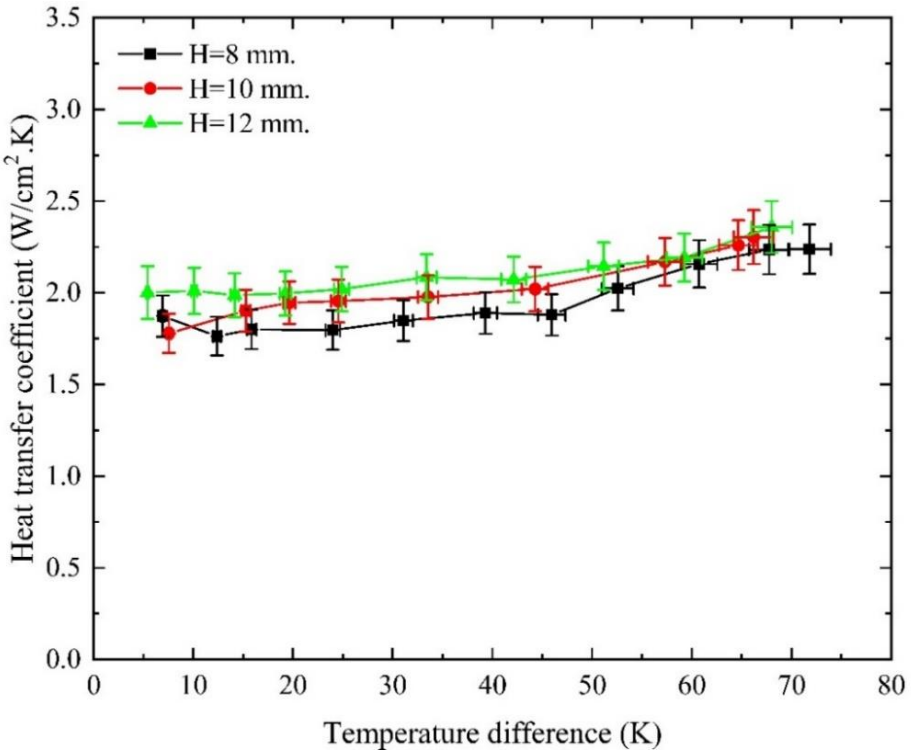

Figure 7.24 Effect of nozzle-to-surface distance on average heat transfer coefficient of M3 at a volumetric flow rate of 153 mL/min.

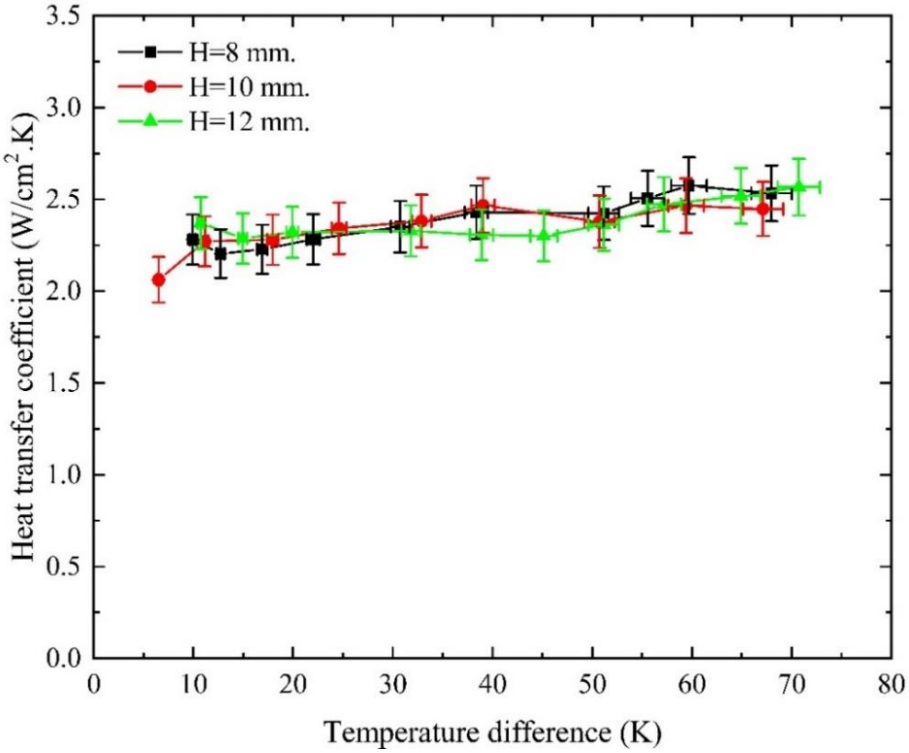

Figure 7.25 Effect of nozzle-to-surface distance on average heat transfer coefficient of M3 at a volumetric flow rate of 180 mL/min.

In conclusion, nozzle-to-surface distance has a minor effect on the average heat transfer coefficient of enhanced surfaces because the average heat transfer coefficient was calculated based on an assumption which states that the target surface has same base temperature and heat transfer coefficients in both spray and liquid film regions. Calculating the local heat transfer coefficient of a surface accurately requires knowing the temperature distribution of that surface. As mentioned before, finding the temperature distribution of a surface exposed to spray is difficult and requires advanced technology due to the droplets' density and splash rate.

7.4 ENHANCEMENT RATIO

In order to calculate the heat transfer enhancement ratio of macro-structured surfaces, the experimental data of the enhanced surfaces was fitted and correlated by using Origin 2019 software to find the most accurate mathematical relation between the heat flux and the temperature difference. Then the correlated data of the enhanced surfaces were compared at the same operating conditions with the data of a plain surface presented in [85]. Figure 7.26 - Figure 7.28 shows the enhancement ratio of surface M1 versus temperature difference at different volumetric flow rates and nozzle-to-surface distances. It was observed that at all volumetric flow rates, the highest enhancement ratio for surface M1 is achieved at temperature difference and nozzle-to-surface distance of 15 K and 10 mm, respectively. Moreover, the results indicate that the enhancement ratio of surface modified with only circular grooves depends strongly on the volumetric flow rate. Enhancement ratio of M1 at all volumetric flow rate increases as volumetric flow rate increases and temperature difference decreases. Figure 7.26 shows that at a nozzle-to-surface distance and volumetric flow rate of 8 mm and 115 mL/min, the enhanced surface has less thermal performance than a plain surface due to the increase in the temperature difference and the marginal increase in the convective thermal resistance.

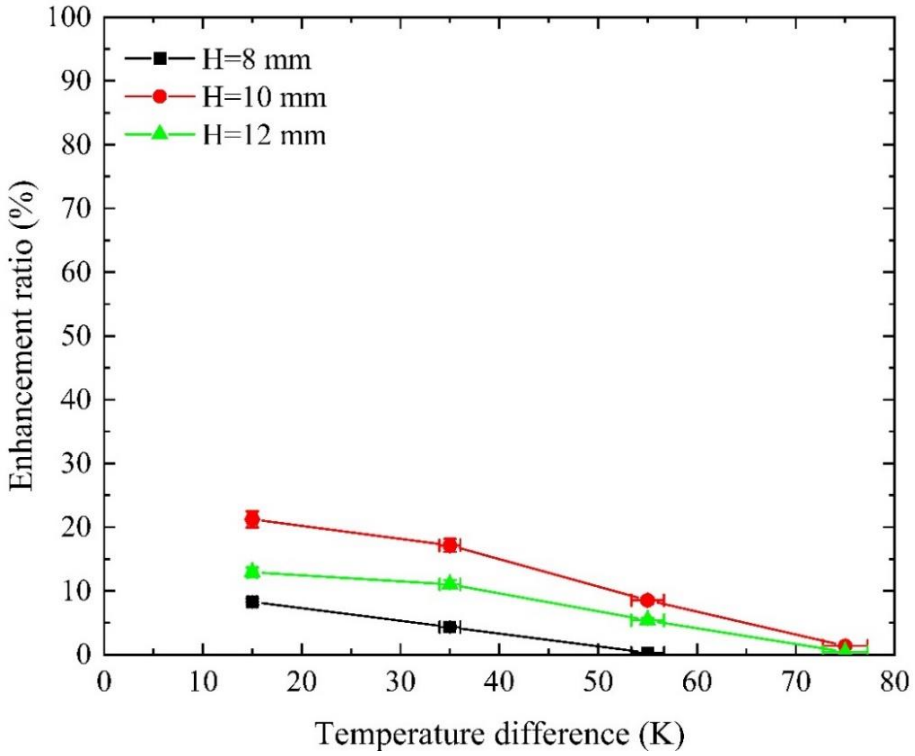

Figure 7.26 Enhancement ratio versus temperature difference for surface M1 at a volumetric flow rate of 115 mL/min and different nozzle-to-surface distances.

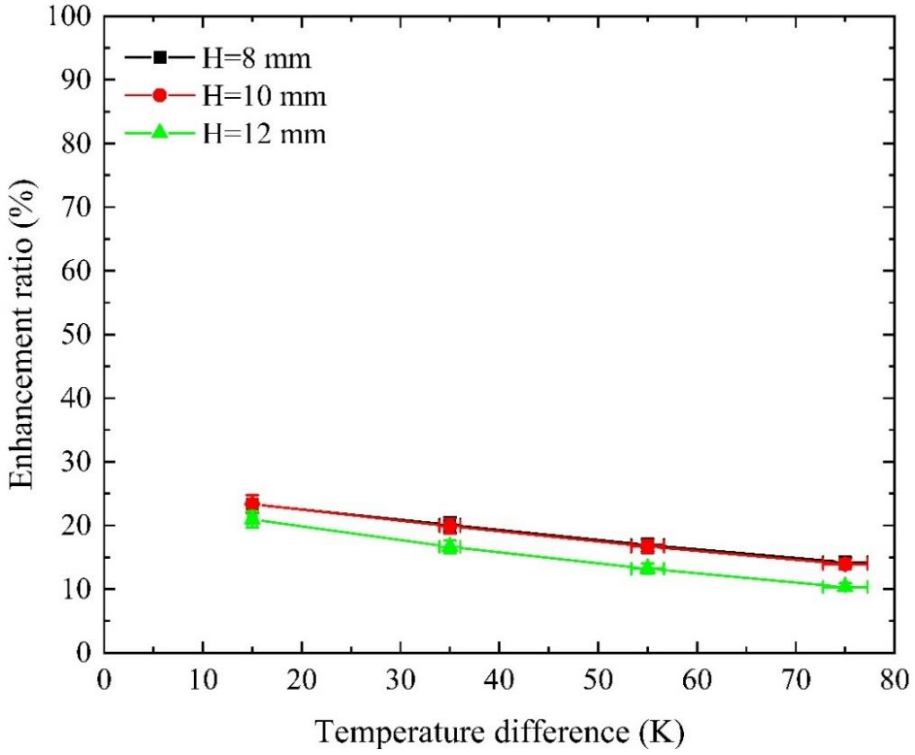

Figure 7.27 Enhancement ratio versus temperature difference for surface M1 at a volumetric flow rate of 153 mL/min and different nozzle-to-surface distances.

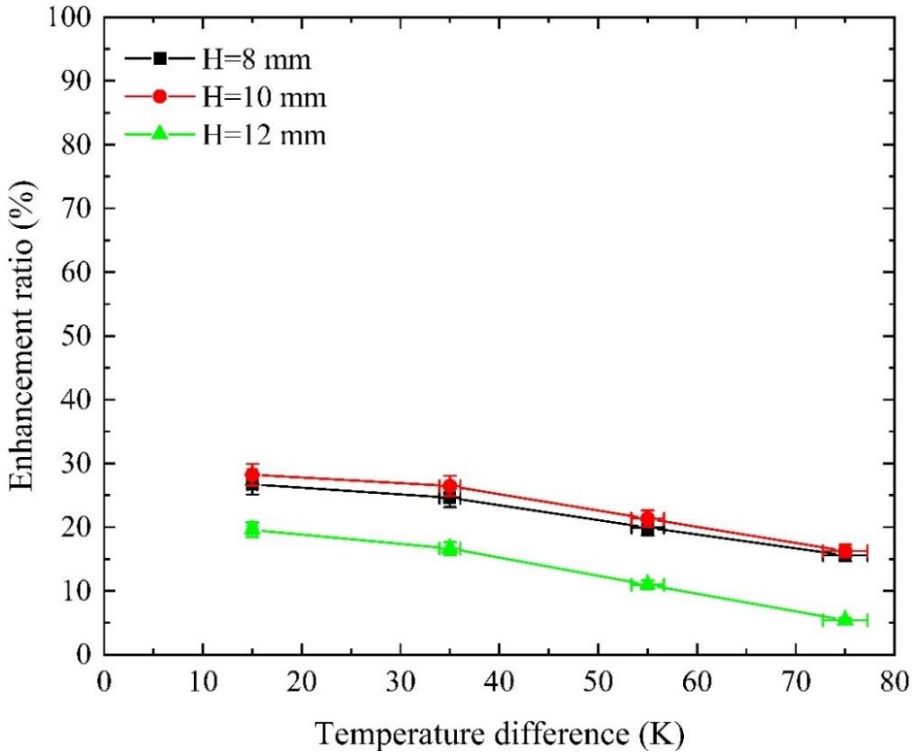

Figure 7.28 Enhancement ratio versus temperature difference for surface M1 at a volumetric flow rate of 180 mL/min and different nozzle-to-surface distances.

The enhancement ratios of M2, shown in Figure 7.29, illustrate that at a volumetric flow rate of 115 mL/min, the maximum enhancement ratio is achieved. It is 45% at a temperature difference and nozzle-to-surface distance of 15 K and 10 mm; it decreases as the temperature difference increases for the same reasons mentioned previously. Additionally, it was shown that the maximum enhancement ratios, at volumetric flow rates of 153 and 180 mL/min, are 30 and 35%, respectively, as shown in Figure 7.30 and Figure 7.31. Also, the enhancement ratio of surface M2 became independent of the temperature difference and almost became constant; it appears the enhanced surface reached its maximum efficiency at this point. Moreover, increasing the volumetric flow rate does not have a significant impact on thermal performance; nozzle-to-surface distance has a considerable effect on the enhancement ratio of this surface, especially at a volumetric flow rate of 180 mL/min, as shown in Figure 7.31.

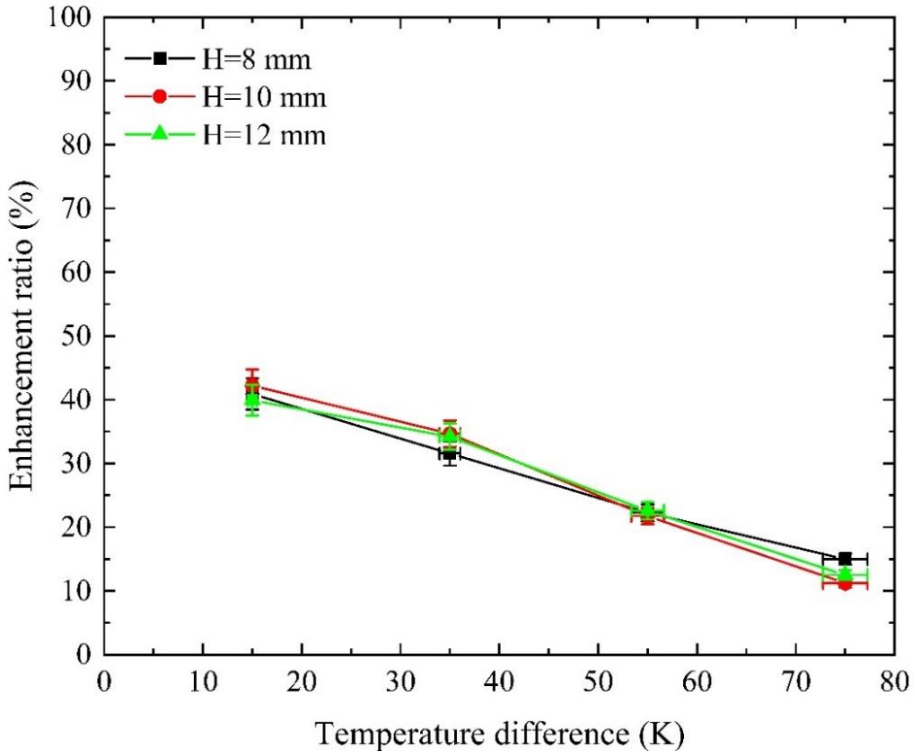

Figure 7.29 Enhancement ratio versus temperature difference for surface M2 at a volumetric flow rate of 115 mL/min and different nozzle-to-surface distances.

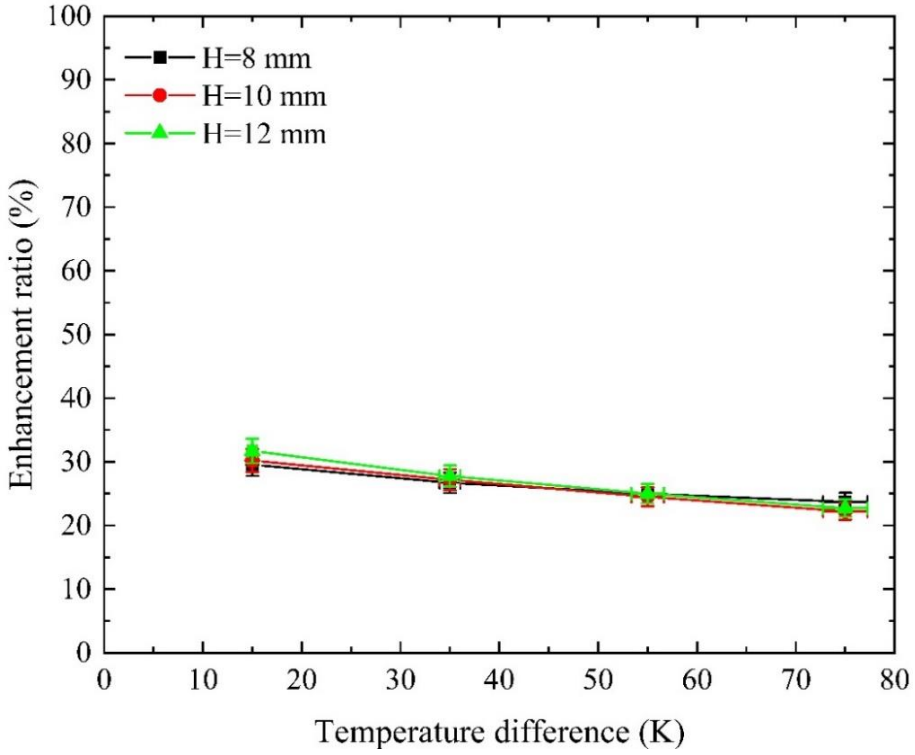

Figure 7.30 Enhancement ratio versus temperature difference for surface M2 at a volumetric flow rate of 153 mL/min and different nozzle-to-surface distances.

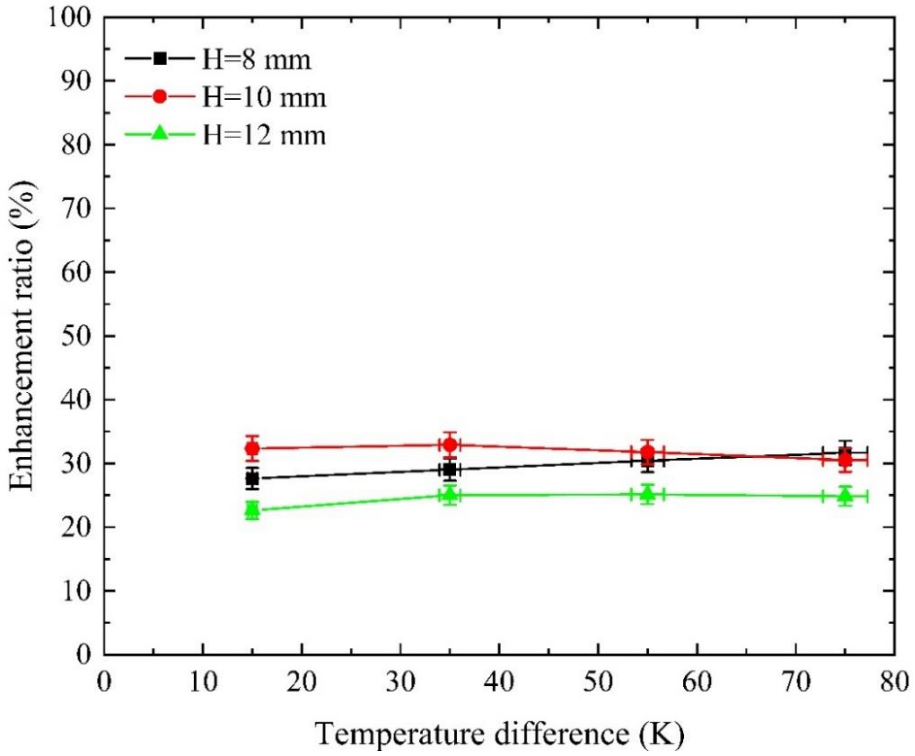

Figure 7.31 Enhancement ratio versus temperature difference for surface M2 at a volumetric flow rate of 180 mL/min and different nozzle-to-surface distances.

Figure 7.32 shows the enhancement ratio of surface M3 at different volumetric flow rates and nozzle-to-surface distances. At a volumetric flow rate of 115 mL/min, the maximum enhancement ratio is 60 % and occurred at a nozzle-to-surface distance of 8 mm. Also, at volumetric flow rates of 153 and 180 mL/min, the enhancement ratios of surface M3 are more affected by nozzle-to-surface distance because of the increase of fluid velocity over the target surface. The maximum enhancement ratios are 75 and 85%, and they occurred at a nozzle-to-surface distance of 10 mm, as shown in Figure 7.33 and Figure 7.34. Table 7.2 summarizes the average enhancement ratios within a temperature difference range of $15 \leq \mathrm{TD} \leq 75$, for modified surfaces at different experimental conditions.

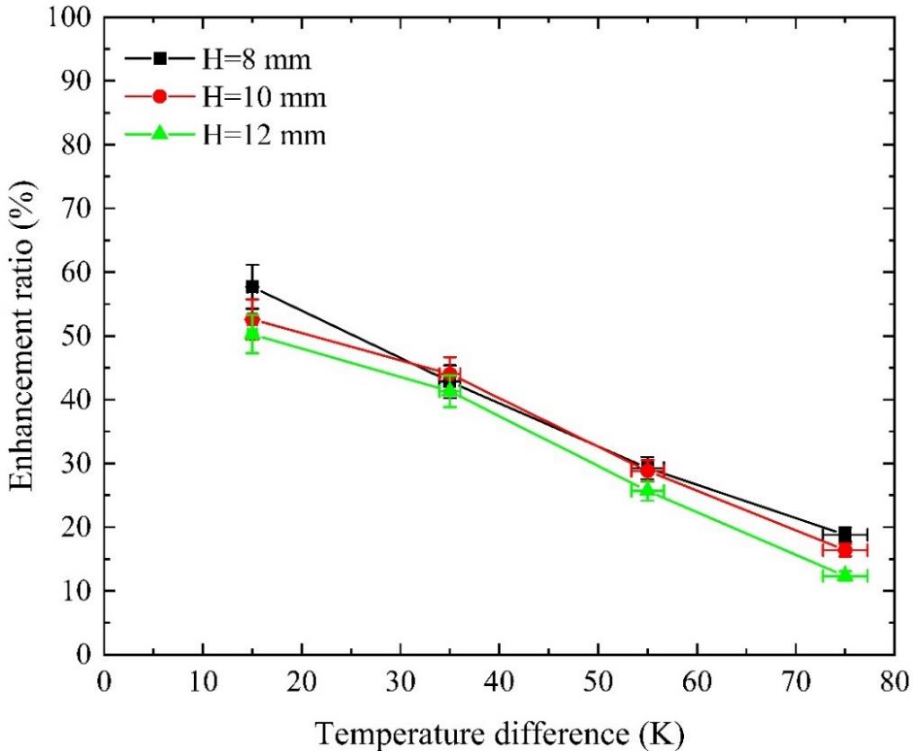

Figure 7.32 Enhancement ratio versus temperature difference for surface M3 at a volumetric flow rate of 115 mL/min and different nozzle-to-surface distances.

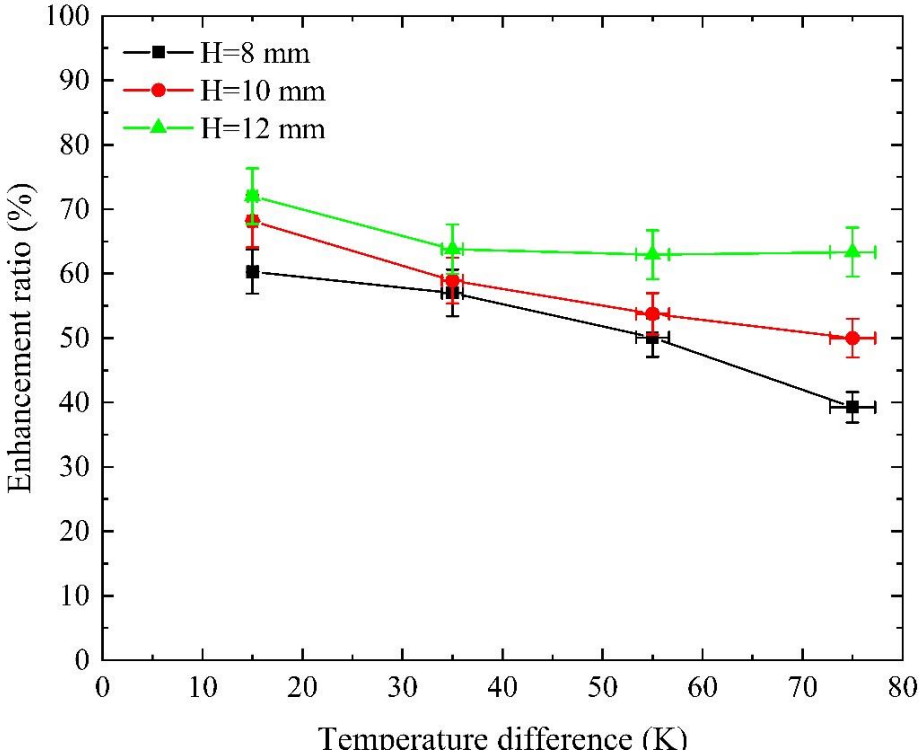

Figure 7.33 Enhancement ratio versus temperature difference for surface M3 at a volumetric flow rate of 153 mL/min and different nozzle-to-surface distances.

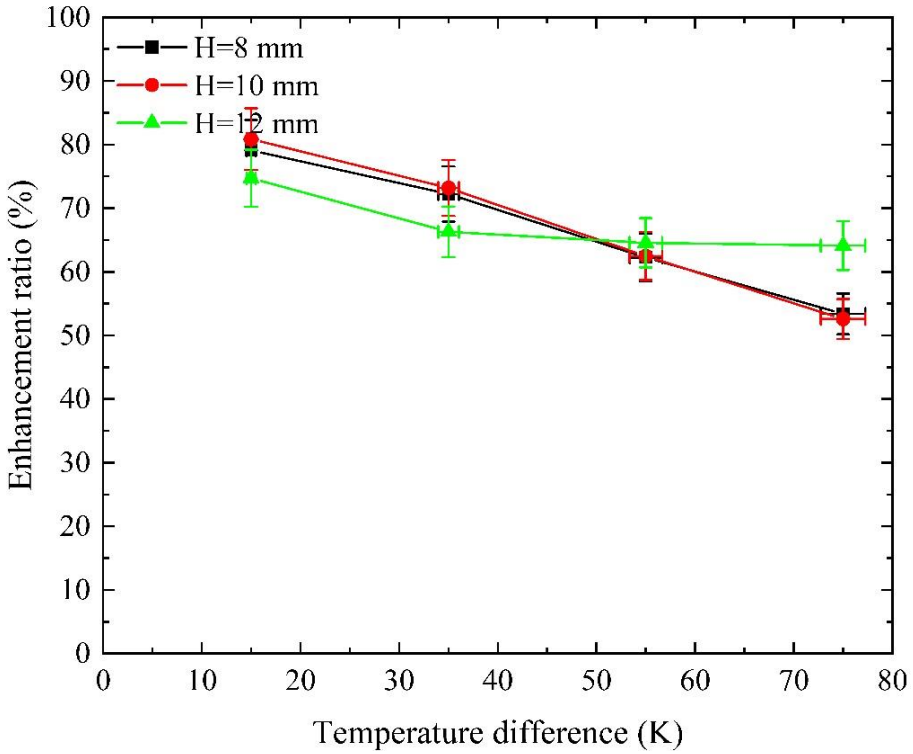

Figure 7.34 Enhancement ratio versus temperature difference for surface M3 at a volumetric flow rate of 180 mL/min and different nozzle-to-surface distances.

Table 7.2 Average enhancement ratios of modified surfaces at different operating conditions.

Nozzle-to-surface distance (mm)	Volumetric flow rate (mL/min.)								
	115			153			180		
	M1	M2	M3	M1	M2	M3	M1	M2	M3
8	2.5	27.42	37.14	18.65	26.23	51.57	21.7	29.68	66.74
10	12.06	27.45	35.46	18.46	26.02	57.7	23.06	31.88	67.47
12	7.43	27.3	32.4	15.2	26.79	65.5	13.16	24.4	67.42

Moreover, the thermal performance of surface M3 was compared with the thermal performance of a surface modified by Zhang and Wang [52] with only straight grooves and which had better thermal performance among their other modified surfaces.

The surfaces were compared based on the surface area and had the same nozzle-to-surface distance, volumetric flux, working fluid, and nozzle type (TG0.3). The comparison shows that the surface modified with circular and radial grooves M3 has higher thermal performance than the surface-enhanced with only straight grooves (No.5) by up to 34%, as shown in Figure 7.35. The enhancement in the thermal performance of surface M3 results from the change in the flow distribution over the target surface and the influence of the radial grooves and the circular grooves, which serve as inter-connectors between radial grooves.

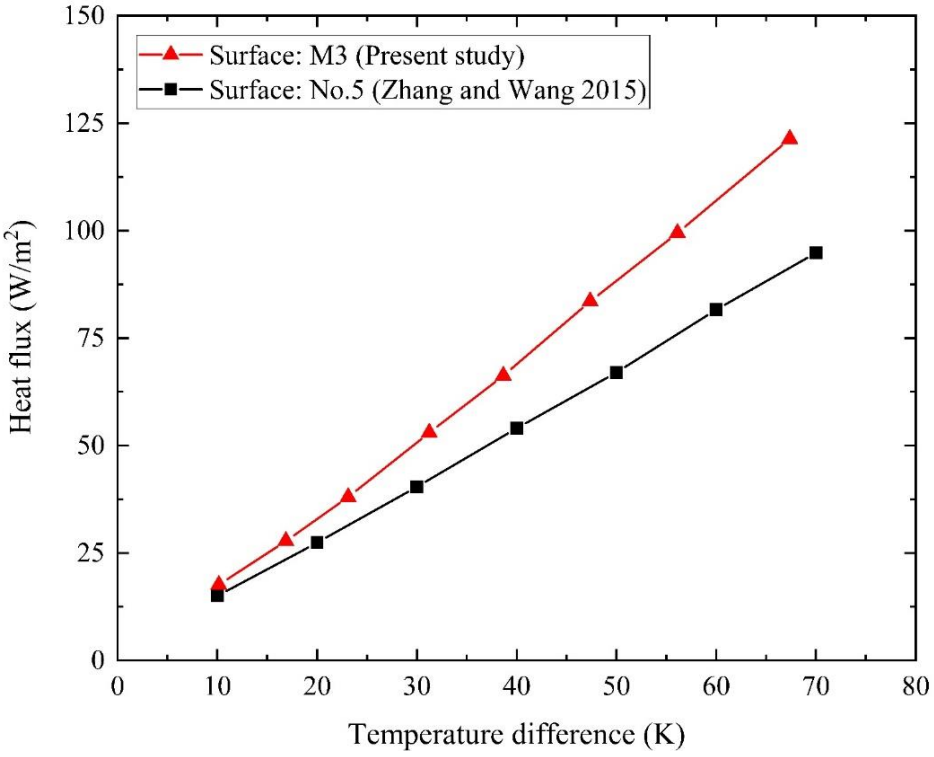

Figure 7.35 Comparison between the thermal performance of surface-modified with a combination of circular and radial grooves (M3) and surface modified with only straight grooves (No.5).

7.5 SUMMARY

Based on the analysis of the experimental results of enhanced surfaces and comparing them to the results of the plain surface (which shown in chapter 5), the following can be concluded:

1. M3 has the highest average enhancement ratio at all experimental conditions, followed by M2 and M1, respectively.
2. The thermal performance of all modified surfaces are enhanced as the volumetric flow rate increases at all nozzle-to-surface distances.
3. The highest enhancement ratio of most surfaces occurs at a temperature difference of 15 K due to the influence of the convective thermal resistance, which depends on the thermophysical properties of the working fluid.
4. The influence of nozzle-to-surface distance on the thermal performance of an enhanced surface depends on surface structure, volumetric flow rate, and temperature difference.
5. The surface modified with circular and radial grooves M3 has higher thermal performance than the surface enhanced by Zhang and Wang [52]with only straight grooves (No.5) by up to 34% at the same operating conditions.

CHAPTER 8

CONCLUSIONS, CONTRIBUTIONS, AND FUTURE WORK

This dissertation was developed to analyze, evaluate, and enhance the thermal performance of a spray cooling system. Spray cooling analysis and geometrical enhancements have been reviewed, investigated, and analyzed experimentally and numerically at different operating conditions. The conclusions, contributions, and suggestions for future work are discussed in the following sections.

8.1 CONCLUSIONS

Spray cooling experiments were conducted to test a flat surface at different operating conditions, such as volumetric flow rate, nozzle-to-surface distances, and heat fluxes. The results showed that the heat transfer performance enhances meaningfully by increasing the volumetric flow rate at all nozzle-to-surface distances. Nozzle-to surface-distance has a marginal effect on the thermal performance of the spray cooling system. Increasing volumetric flow rate increases consumed pumping power and reduces the overall spray cooling performance. Therefore, enhancing spray cooling performance actively is not a good economic enhancement option; as such, the results of the present research indicate that it is preferable to enhance spray cooling performance passively.

A three-dimensional multi-phase numerical model was developed to simulate the spray cooling heat transfer process. Similar operating experimental conditions were used for the numerical simulation to investigate the liquid film characteristics. The numerical results provide more insights about heat transfer mechanisms involved within the liquid

film in spray cooling. Also, it was noticed that a more uniform spatial distribution of liquid film and heat transfer coefficient can be achieved at a nozzle-to-surface distance and volumetric flow rate of 12 mm and 180 mL/min, respectively.

Spray cooling enhancement due to surface modification was studied experimentally with surfaces modified with a combination of circular and radial grooves. These surfaces were tested and compared with a flat surface under the same operating conditions. The results showed that surface modified with four circular and eight radial grooves enhances spray cooling thermal performance by up to 80%, followed by surfaces M2 and M1, which were enhanced by 36.3% and 28.7%, respectively.

8.2 CONTRIBUTIONS TO THE STATE OF THE ART

The main contributions to the state of the art are as follows:

1. The heat transfer characteristics, such as heat flux and heat transfer coefficient, are enhanced as the volumetric flow rate increases due to the increase in droplet flux and velocity, as well as the decrease in droplet size.
2. The chamber temperature has a negligible effect on droplet characteristics, such as size and break-up velocity.
3. The influence of nozzle-to-surface distance on spray cooling performance depends on the volumetric flow rate and temperature difference. Decreasing the distance between the nozzle and the target surface enhances the thermal performance of a plain surface as both the volumetric flow rate and temperature difference increase.
4. Enhancing the thermal performance of a spray cooling system is not a good economical option based on the performance evaluation criterion of spray cooling (PEC_{SC}) due to the increase in the consumed pumping power.

5. As the volumetric flow rate increases, a thinner and more uniform liquid film forms on the target surface, especially in the impingement zone (thin-film zone).
6. The spatial heat transfer coefficient in the impingement zone is more affected by the volumetric flow rate than the spatial heat transfer coefficient in the thick-film zone.
7. Increasing the volumetric flow rate increases the fluid velocity over the target surface at all nozzle-to-surface distances; the maximum fluid velocity occurs at the interface between the impingement and the thick-film zones.
8. At all volumetric flow rates, decreasing the distance between the nozzle and the target surface increases the spatial heat transfer coefficient in the impingement zone but decreases the average heat transfer coefficient over the target surface.
9. Increasing the nozzle-to-surface distance at all volumetric flow rates provides a thinner and more uniform fluid film over the surface and leads to reduction in the surface temperature, which ultimately enhances the spray cooling thermal performance.
10. Surface enhanced with combined circular and radial grooves (M3) has the highest average enhancement ratio at all experimental conditions, followed by M2 and M1, respectively.
11. The thermal performance of all modified surfaces enhances as the volumetric flow rate increases at all nozzle-to-surface distances.
12. The highest enhancement ratio of most surfaces occurs at a temperature difference of 15 K due to the influence of the convective thermal resistance, which depends on the thermophysical properties of the working fluid.

13. The influence of nozzle-to-surface distance on the thermal performance of an enhanced surface depends on many parameters, such as surface structure, volumetric flow rate, and temperature difference.
14. The surface modified with circular and radial grooves M3 has higher thermal performance than the surface enhanced by Zhang and Wang [52] with only straight grooves (No.5) by up to 34% at the same operating conditions.

8.3 SUGGESTIONS FOR FUTURE WORK

The present research was conducted at different operating conditions on the thermal performance of a spray cooling system utilizing deionized water. The experimental results showed that enhancing spray cooling performance through increasing the coolant volumetric flow rate is not a good economic enhancement option. Also, surfaces modified with a combination of circular and radial grooves has enhanced the spray cooling performance significantly. A nozzle with a larger orifice diameter can reduce the consumed pumping power significantly and the removed heat flux marginally, compared with a nozzle with a smaller orifice diameter for the same volumetric flow rate. Furthermore, the numerical results provided more insights about spatial distribution of heat transfer coefficient, liquid film thickness, velocity, and surface temperature within the liquid film on a flat surface at the same experimental operating conditions. Suggestions for future research are as follows:

1. Testing enhanced surfaces with different working fluids.
2. Conducting experimental investigations to enhance boiling and evaporation in spray cooling systems, based on the predicted results of the numerical model.
3. Testing hydrophobic surfaces in spray cooling systems.

REFERENCES

[1] P. Smakulski and S. Pietrowicz, “A review of the capabilities of high heat flux removal by porous materials, microchannels and spray cooling techniques,” *Appl. Therm. Eng.*, vol. 104, pp. 636–646, 2016.

[2] W. W. Zhang, W. L. Cheng, S. D. Shao, L. J. Jiang, and D. L. Hong, “Integrated thermal control and system assessment in plug-chip spray cooling enclosure,” *Appl. Therm. Eng.*, vol. 108, pp. 104–114, 2016.

[3] I. Mudawar, “Assessment of high-heat-flux thermal management schemes,” *IEEE Trans. Components Packag. Technol.*, vol. 24, no. 2, pp. 122–141, 2001.

[4] A. G. Pautsch and T. A. Shedd, “Spray impingement cooling with single- and multiple-nozzle arrays. Part I: Heat transfer data using FC-72,” *Int. J. Heat Mass Transf.*, vol. 48, no. 15, pp. 3167–3175, 2005.

[5] A. Jaikumar and S. G. Kandlikar, “Enhanced pool boiling for electronics cooling using porous fi n tops on open microchannels with FC-87,” *Appl. Therm. Eng.*, vol. 91, pp. 426–433, 2015.

[6] J. A. Khan, A. K. M. M. Monjur Morshed, and R. Fang, “Towards ultra-compact high heat flux microchannel heat sink,” *Procedia Eng.*, vol. 90, pp. 11–24, 2014.

[7] A. C. Kheirabadi and D. Groulx, “Cooling of server electronics: A design review of existing technology,” *Appl. Therm. Eng.*, vol. 105, pp. 622–638, 2016.

[8] S. Saha, R. Mahamud, J. Khan, and T. Farouk, “Simulation of sweating/evaporation boosted convective heat transfer under laminar flow condition,” *ASME 2017 Heat Transf. Summer Conf. HT 2017*, vol. 1, no. July, 2017.

[9] K. Ebrahimi, G. F. Jones, and A. S. Fleischer, “A review of data center cooling technology, operating conditions and the corresponding low-grade waste heat recovery opportunities,” *Renew. Sustain. Energy Rev.*, vol. 31, pp. 622–638, 2014.

[10] X. C. Tong, *Advanced Materials for Thermal Management of Electronic Packaging*. New York Heidelberg Dordrecht London: Springer, 2011.

[11] Saad K Oudah, Ruixian Fang, Amitav Tikadar, Karim Egab, Chen Li, Jamil Khan “The Effects of Hybrid Sandblasting on the Heat Transfer Performance in a Single-Phase Microchannel Heat Sink,” in *Proceedings of the ASME 2017 International Mechanical Engineering Congress and Exposition*, 2017, pp. 1–8.

[12] S. K. Oudah, A. Tikadar, R. Fang, K. Egab, and J. A. Khan, “Thermohydraulic Characteristics of a Knurled Microchannel Heat Sink in Single Phase Regime,” in *3rd Thermal and Fluids Engineering Conference (TFEC)*, 2018, pp. 1425–1436.

[13] Y. Wang, M. Liu, D. Liu, K. Xu, and Y. Chen, “Experimental study on the effects of spray inclination on water spray cooling performance in non-boiling regime,” *Exp. Therm. Fluid Sci.*, 2010.

[14] M. A. Ebadian and C. X. Lin, “A Review of High-Heat-Flux Heat Removal Technologies,” *J. Heat Transfer*, vol. 133, no. 11, p. 110801, 2011.

[15] A. Labergue, M. Gradeck, and F. Lemoine, “Comparative study of the cooling of a hot temperature surface using sprays and liquid jets,” *Int. J. Heat Mass Transf.*, 2015.

[16] I. Mudawar *et al.*, “Two-phase spray cooling of hybrid vehicle electronics,” *Therm. Thermomechanical Phenom. Electron. Syst. 2008. ITHERM 2008. 11th Intersoc. Conf.*, vol. 51, no. 9–10, pp. 2398–2410, 2008.

[17] M. Visaria and I. Mudawar, “Application of Two-Phase Spray Cooling for Thermal Management of Electronic Devices,” *IEEE Trans. Components Packag. Technol.*, vol. 32, no. 4, pp. 784–793, 2009.

[18] I. Mudawar, “Recent Advances in High-Flux, Two-Phase Thermal Management,” *J. Therm. Sci. Eng. Appl.*, vol. 5, no. 2, p. 021012, 2013.

[19] G. Liang and I. Mudawar, “Review of spray cooling - Part 2: High temperature boiling regimes and quenching applications,” *Int. J. Heat Mass Transf.*, vol. 115, pp. 1206–1222, 2017.

[20] G. Liang and I. Mudawar, “Review of spray cooling - Part 1: Single-phase and nucleate boiling regimes, and critical heat flux,” *Int. J. Heat Mass Transf.*, vol. 115, pp. 1174–1205, 2017.

[21] *Spraying Systems Co.* 2018.

[22] M. Ghodbane and J. P. Holman, “Experimental study of spray cooling with Freon-113,” *Int. J. Heat Mass Transf.*, vol. 34, no. 4–5, pp. 1163–1174, 1991.

[23] I. Mudawar *et al.*, “Optimizing and Predicting CHF in Spray Cooling of a Square Surface,” *J. Heat Transfer*, vol. 118, no. 3, p. 672, 1996.

[24] J. R. Rybicki and I. Mudawar, “Single-phase and two-phase cooling characteristics of upward-facing and downward-facing sprays,” *Int. J. Heat Mass Transf.*, vol. 49, no. 1–2, pp. 5–16, 2006.

[25] R.-H. Chen, L. C. Chow, and J. E. Navedo, “Effects of spray characteristics on critical heat flux in subcooled water spray cooling,” *Int. J. Heat Mass Transf.*, vol. 45, no. 19, pp. 4033–4043, 2002.

[26] R.-H. Chen, L. C. Chow, and J. E. Navedo, “Optimal spray characteristics in water spray cooling,” *Int. J. Heat Mass Transf.*, vol. 47, no. 23, pp. 5095–5099, 2004.

[27] W. L. Cheng, F. Y. Han, Q. N. Liu, and H. L. Fan, “Spray characteristics and spray cooling heat transfer in the non-boiling regime,” *Energy*, vol. 36, no. 5, pp. 3399–3405, 2011.

[28] Z. G. Yujia Tao , Xiulan Huai , Lei Wang, “Experimental characterization of heat transfer in non-boiling spray cooling with two nozzles,” *Appl. Therm. Eng.*, vol. 31, p. 1790e1797, 2011.

[29] J. L. Xie, Z. W. Gan, T. N. Wong, F. Duan, S. C. M. Yu, and Y. H. Wu, “Thermal effects on a pressure swirl nozzle in spray cooling,” *Int. J. Heat Mass Transf.*, 2014.

[30] Y. Hou, J. Liu, X. Su, Y. Qian, L. Liu, and X. Liu, “Experimental study on the characteristics of a closed loop R134-a spray cooling,” *Exp. Therm. Fluid Sci.*, vol. 61, pp. 194–200, 2015.

[31] N. Zhou, F. Chen, Y. Cao, M. Chen, and Y. Wang, “Experimental investigation on the performance of a water spray cooling system,” *Appl. Therm. Eng.*, vol. 112, pp. 1117–1128, 2017.

[32] X. Gao and R. Li, “Effects of nozzle positioning on single-phase spray cooling,” *Int. J. Heat Mass Transf.*, vol. 115, pp. 1247–1257, 2017.

[33] A. S. Salman and J. A. Khan, “The Effects of Spraying Parameters on Spray Cooling Heat Transfer Performance in the Non-Boiling Regime,” in *Proceedings of the ASME 2017 International Mechanical Engineering Congress and Exposition*, 2017, pp. 1–8.

[34] A. S. Salman, T. C. Paul, and J. A. Khan, “The Effects of Coverage Area on the Spray Cooling Heat Transfer Performance,” in *Proceeding of 3rd Thermal and Fluids Engineering Conference (TFEC)*, 2018, pp. 1345–1353.

[35] H. Y. Peiliang Yan, Hong Liu*, Chang Cai, Jiuliang Gao, “Numerical simulation on multiphase spray cooling,” in *1st International Global on Renewable Energy and Development (IGRED 2017)*, 2017, pp. 1–10.

[36] Y. Hou, Y. Tao, X. Huai, Y. Zou, and D. Sun, “Numerical simulation of multi-nozzle spray cooling heat transfer,” *Int. J. Therm. Sci.*, vol. 125, no. November 2017, pp. 81–88, 2018.

[37] H. Liu, C. Cai, Y. Yan, M. Jia, and B. Yin, “Numerical simulation and experimental investigation on spray cooling in the non-boiling region,” *Heat Mass Transf.*, 2018.

[38] M. Langari *et al.*, “Multiphase computational fluid dynamics–conjugate heat transfer for spray cooling in the non-boiling regime,” *J. Comput. Multiph. Flows*, vol. 10, no. 1, pp. 33–42, 2018.

[39] Z. Chen, Q. Xie, G. Chen, Y. Yu, and Z. Zhao, “Numerical Simulation of Single-Nozzle Large Scale Spray Cooling on Drum Wall,” *Therm. Sci.*, vol. 22, no. 1, pp. 359–370, 2018.

[40] E. A. Silk, J. Kim, and K. Kiger, “Investigation of Enhanced Surface Spray Cooling,” in *In: Proceedings of the ASME IMECE, Anaheim, CA.*, 2004, pp. 685–690.

[41] E. A. Silk, J. Kim, and K. Kiger, “Impact of Cubic Pin Finned Surface Structure Geometry Upon Spray Cooling Heat Transfer,” in *17–22, 2005, San Francisco*, 2005, pp. 1–9.

[42] E. A. Silk, J. Kim, and K. Kiger, “Enhanced Surface Spray Cooling With Embedded and Compound Extended surface Structures,” in *IEEE*, 2006, pp. 215–223.

[43] E. A. Silk, J. Kim, and K. Kiger, “Spray cooling of enhanced surfaces: Impact of structured surface geometry and spray axis inclination,” *Int. J. Heat Mass Transf.*, vol. 49, no. 25–26, pp. 4910–4920, 2006.

[44] J. S. Coursey, J. Kim, and K. T. Kiger, “Spray cooling of high aspect ratio open microchannels,” in *Proceedings of ITHERM 2006, San Diego, CA.*, 2006, vol. 20742, pp. 188–195.

[45] C. Sodtke and P. Stephan, “Spray cooling on micro structured surfaces,” *Int. J. Heat Mass Transf.*, vol. 50, no. 19–20, pp. 4089–4097, 2007.

[46] A. G. Ulson de Souza and J. R. Barbosa, “Spray cooling of plain and copper-foam enhanced surfaces,” *Exp. Therm. Fluid Sci.*, vol. 39, pp. 198–206, 2012.

[47] A. G. U. De Souza and J. R. B. Jr, “Experimental evaluation of spray cooling of R-134a on plain and enhanced surfaces ´ rimentale de la brumisation du R-134a sur des Evaluation expe ´ es surfaces planes et augmente,” *Int. J. Refrig.*, vol. 36, no. 2, pp. 527–533, 2012.

[48] Z. Zhang, J. Li, and P. X. Jiang, “Experimental investigation of spray cooling on flat and enhanced surfaces,” *Appl. Therm. Eng.*, vol. 51, no. 1–2, pp. 102–111, 2013.

[49] B. H. Yang, H. Wang, X. Zhu, Q. Liao, Y. D. Ding, and R. Chen, “Heat transfer enhancement of spray cooling with ammonia by microcavity surfaces,” *Appl. Therm. Eng.*, vol. 50, no. 1, pp. 245–250, 2013.

[50] Y. Hou, Y. Tao, and X. Huai, “The effects of micro-structured surfaces on multi-nozzle spray cooling,” *Appl. Therm. Eng.*, vol. 62, no. 2, pp. 613–621, 2014.

[51] H. Bostanci, D. P. Rini, J. P. Kizito, V. Singh, S. Seal, and L. C. Chow, “High heat flux spray cooling with ammonia : Investigation of enhanced surfaces for HTC,” *Int. J. Heat Mass Transf.*, vol. 75, pp. 718–725, 2014.

[52] W. Zhang and Z. Wang, “Heat transfer enhancement of spray cooling in straight-grooved surfaces in the non-boiling regime,” *Exp. Therm. Fluid Sci.*, vol. 69, pp. 38–44, 2015.

[53] N. Liu, L. Li, and Y. Tae, “Experimental study on heat transfer performance enhancement by micro-structured surfaces for inclination spray application,” *Int. J. Heat Mass Transf.*, vol. 133, pp. 631–640, 2019.

[54] Z. F. Zhou, Y. K. Lin, H. L. Tang, Y. Fang, B. Chen, and Y. C. Wang, “Heat transfer enhancement due to surface modification in the close-loop R410A flash evaporation spray cooling,” *Int. J. Heat Mass Transf.*, vol. 139, pp. 1047–1055, 2019.

[55] J. Kim, “Spray cooling heat transfer: The state of the art,” *Int. J. Heat Fluid Flow*, vol. 28, no. 4, pp. 753–767, 2007.

[56] B. Horacek, K. T. Kiger, and J. Kim, “Single nozzle spray cooling heat transfer mechanisms,” *Int. J. Heat Mass Transf.*, vol. 48, no. 8, pp. 1425–1438, 2005.

[57] A. S. Salman *et al.*, "Experimental investigation of the impact of geometrical surface modification on spray cooling heat transfer performance in the non-boiling regime," *Int. J. Heat Mass Transf.*, vol. 133, pp. 330–340, 2019.

[58] K. A. Estes and I. Mudawar, "Correlation of sauter mean diameter and critical heat flux for spray cooling of small surfaces," *Int. J. Heat Mass Transf.*, vol. 38, no. 16, pp. 2985–2996, 1995.

[59] M. Ciofalo, A. Caronia, M. Di Liberto, and S. Puleo, "The Nukiyama curve in water spray cooling: Its derivation from temperature-time histories and its dependence on the quantities that characterize drop impact," *Int. J. Heat Mass Transf.*, vol. 50, no. 25–26, pp. 4948–4966, 2007.

[60] G. Liang and I. Mudawar, "Review of mass and momentum interactions during drop impact on a liquid film," *Int. J. Heat Mass Transf.*, vol. 101, pp. 577–599, 2016.

[61] R. C. Hibbeler, *Engineering Mechanics Statics and Dynamics*, Seventh Ed. New Jersey: Prentice Hall, 1995.

[62] H. Wang, J. J. Wu, Q. Yang, X. Zhu, and Q. Liao, "Heat transfer enhancement of ammonia spray cooling by surface modification," *Int. J. Heat Mass Transf.*, vol. 101, pp. 60–68, 2016.

[63] M. Jafari, "Analysis of heat transfer in spray cooling systems using numerical simulations," University of Windsor, 2014.

[64] "STAR-CCM+ User Guide, Version 12.04010-R8, CD Adapco, 2018." .

[65] K. J. Choi and S. C. Yao, "Mechanisms of film boiling heat transfer of normally impacting spray," *Int. J. Heat Mass Transf.*, vol. 30, no. 2, pp. 311–318, 1987.

[66] W. L. Cheng, W. W. Zhang, H. Chen, and L. Hu, “Spray cooling and flash evaporation cooling: The current development and application,” *Renew. Sustain. Energy Rev.*, vol. 55, pp. 614–628, 2016.

[67] A. Bejan and A. D. Kraus, *Heat Transfer Handbook*. Hoboken, New Jersey: JOHN WILEY & SONS, INC., 2003.

[68] A. Faghri, Y. Zhang, and J. Howell, *Advanced Heat and Mass Transfer*. Columbia, MO, USA: Global Digital Press, 2010.

[69] M. Winter, “Heat Transfer Mechanisms during Spray Cooling of Electronic Devices,” Technische Universität Darmstadt; Darmstadt/Germany, 2015.

[70] J. Yang, L. C. Chow, and M. R. Pais, “Nucleate Boiling Heat Transfer in Spray Cooling,” *J. Heat Transfer*, vol. 118, pp. 668–671, 1996.

[71] E. Martínez-Galván, J. C. Ramos, R. Antón, and R. Khodabandeh, “Film Thickness and Heat Transfer Measurements in a Spray Cooling System With R134a,” *J. Electron. Packag.*, vol. 133, no. 1, p. 011002, 2011.

[72] C.-C. Hsieh and S.-C. Yao, “Evaporative heat transfer characteristics of a water spray on micro-structured silicon surfaces,” *Int. J. Heat Mass Transf.*, vol. 49, no. 5–6, pp. 962–974, 2006.

[73] F. P. Incropera and D. P. DeWitt, *Fundamentals of Heat and Mass Transfer*, Fourth Edi. JOHN WILEY & SONS, INC., 1996.

[74] J. P. Holman, *Experimental methods for engineers*, Eighth. New York: McGraw Hill, 2012.

[75] K. Oliphant, B. W. Webb, and M. Q. McQuay, “An experimental comparison of liquid jet array and spray impingement cooling in the non-boiling regime,” *Exp. Therm. Fluid Sci.*, vol. 18, no. 1, pp. 1–10, 1998.

[76] N. M. Abdulrazzaq, N. Anumbe, and J. Khan, “Experimental Investigation of the Performance of Refrigerant R134a Working in a Spray Cooling,” *3rd Therm. Fluids Eng. Conf.*, pp. 1355–1368, 2018.

[77] S. H. Q. Abdullah Alkhedhair*, Hal Gurgenci, Ingo Jahn, Zhiqiang Guan, “Numerical simulation of water spray for pre-cooling of inlet air in natural draft dry cooling towers,” *Appl. Therm. Eng.*, vol. 61, no. 2, pp. 416–424, 2013.

[78] A. Tikadar *et al.*, “Numerical investigation of heat transfer and pressure drop in nuclear fuel rod with three-dimensional surface roughness,” *Int. J. Heat Mass Transf.*, vol. 126, pp. 493–507, 2018.

[79] A. Tikadar, M. M. Hossain, and A. K. M. M. Morshed, “Numerical investigation of thermal performance of a water-cooled mini-channel heat sink for different chip arrangement,” *AIP Conf. Proc.*, vol. 1754, no. July, 2016.

[80] Amitav Tikadar, Saad K Oudah, Azzam S. Salman, A.K.M. M. Morshed, Titan C. Paul, Jamil Khan“Effect of Inter-Connector on Thermo-Hydraulic Characteristics of Parallel and Counter Flow Mini-Channel Heat Sink,” in *ASME 2018 International Mechanical Engineering Congress and Exposition*, 2018, p. V08BT10A036-V08BT10A036.

[81] A. Tikadar, S. K. Oudah, T. C. Paul, A. S. Salman, A. K. M. M. Morshed, and J. A. Khan, “Parametric study on thermal and hydraulic characteristics of inter-connected parallel and counter flow mini-channel heat sink,” *Appl. Therm. Eng.*, vol. 153, no. February, pp. 15–28, 2019.

[82] Z. Zhang, P. X. Jiang, X. L. Ouyang, J. N. Chen, and D. M. Christopher, “Experimental investigation of spray cooling on smooth and micro-structured surfaces,” *Int. J. Heat Mass Transf.*, vol. 76, pp. 366–375, 2014.

[83] L. G. H. and B. W. WEBB, “Air jet impingement heat transfer from modified surfaces,” *Int. J. Heat Mass Transf.*, vol. 36, no. 4, pp. 989–997, 1993.

[84] J. L. Xie *et al.*, “Study of heat transfer enhancement for structured surfaces in spray cooling,” *Appl. Therm. Eng.*, vol. 59, no. 1–2, pp. 464–472, 2013.

[85] A. S. Salman and J. A. Khan, “Experimental Investigation of Spray Cooling Heat Transfer on Circular Grooved Surface,” in *ASME 2017 Heat Transfer Summer Conference*, 2017, vol. 2, pp. 1–9.